

Aus dem Walter Brendel Zentrum für experimentelle Medizin
der Ludwig-Maximilians-Universität München
Institut für Kardiovaskuläre Physiologie und Pathophysiologie

Komm. Vorstand: Prof. Dr. med. dent. Reinhard Hickel
Ehem. Vorstand: Prof. Dr. Ulrich Pohl

Functional characterization of parvins regarding their
regulation of endothelial cell behavior during angiogenesis



Dissertation

zum Erwerb des Doktorgrades der Humanbiologie
an der Medizinischen Fakultät der
Ludwig-Maximilians-Universität zu München

vorgelegt von

Bettina Pitter

aus Großpold

2018

Mit Genehmigung der Medizinischen Fakultät
der Universität München

Berichterstatter: Prof. Dr. med. Ulrich Pohl

Mitberichterstatter: PD Dr. Bruno C. Huber

PD Dr. Gerald Schmid

Mitbetreuung durch den
promovierten Mitarbeiter: Dr. Eloi Montanez

Dekan: Prof. Dr. med. dent. Reinhard HICKEL

Tag der mündlichen Prüfung: 18.09.2018

Eidesstattliche Versicherung

München, den 04.10.2017

Ich, Bettina Pitter, erkläre hiermit an Eides statt, dass ich die vorliegende Dissertationsschrift mit dem Thema:

**Functional characterization of parvins regarding their regulation of endothelial cell
behavior during angiogenesis**

selbstständig verfasst, mich außer der angegebenen keiner weiteren Hilfsmittel bedient und alle Erkenntnisse, die aus dem Schrifttum ganz oder annähernd übernommen sind, als solche kenntlich gemacht und nach ihrer Herkunft unter Bezeichnung der Fundstelle einzeln nachgewiesen habe.

Ich erkläre des Weiteren, dass die hier vorgelegte Dissertationsschrift nicht in gleicher oder ähnlicher Form bei einer anderen Stelle zur Erlangung eines akademischen Grades eingereicht wurde.

Bettina Pitter

Für Peter

Summary

The expansion of the blood vessel network, known as angiogenesis, is a critical process that occurs in response to an insufficient tissue supply of oxygen during development, tissue growth, and tissue regeneration. Angiogenesis also contributes to the progression of many diseases including diabetic retinopathy, tumor growth and metastasis. Moreover, neurodegenerative diseases, such as amyotrophic lateral sclerosis (ALS), are associated with vascular dysfunction. The causative contribution of vascular system-associated defects to neurodegenerative disorders, however, remains unclear.

Angiogenesis involves coordinated endothelial cell (EC) specification, adhesion, migration, and proliferation, and the regulation of these processes includes physical interactions of ECs to the extracellular matrix (ECM) mediated by the integrins. Upon ECM binding, integrins recruit adaptor and signalling proteins to their cytoplasmic domains and form the focal adhesions (FAs), through which they relay signals into the cells. As such, integrins regulate EC specification, vessel elongation, lumen formation, cell-cell junction integrity, and vessel stability. The molecular mechanisms and intracellular signalling pathways that contribute to these integrin-mediated processes are, however, only partially understood.

Parvins are actin-binding proteins that localize to FAs and facilitate the interaction of integrins with the actin cytoskeleton and the coupling of the integrin signaling to the receptor tyrosine kinase (RTK) signaling. The parvin family consists of three members: α -parvin (α -pv), β -parvin (β -pv), and γ -parvin (γ -pv), and ECs express only α -pv and β -pv. Parvins are central regulators of vascular development. Deletion of the α -pv gene in mice results in embryonic lethality associated with cardiovascular defects and signs of impaired angiogenesis including defective coverage of vessels by vascular smooth muscle cells (vSMCs), vascular rupture and abnormal heart development. While it is well established that ECs are instrumental in angiogenesis, the relevance for α -pv and β -pv on EC function during angiogenesis is, however, unknown and remains to be explored.

In this thesis, the role of α -pv and β -pv in ECs and their importance during angiogenesis in physiological and pathological conditions have been investigated. To meet these goals, we used an interdisciplinary approach, which includes mouse genetic tools including tissue-specific gene targeting approaches, cell culture models, molecular biology assays and high-resolution fluorescence microscopy.

To study the function of α -pv in ECs *in vivo*, we generated mice with ECs lacking α -pv by crossing mice carrying a *loxP*-flanked α -pv gene (α -pv^{fl/fl}) with mice expressing the Cre recombinase under the *Tie-2* promoter (*Tie2-Cre*) (referred to herein as α -pv ^{Δ EC}). α -pv ^{Δ EC} mice died during embryonic development starting at embryonic day (E) 15.5. The lethality of α -pv ^{Δ EC} embryos was associated with hemorrhages and an altered vascular network. α -pv ^{Δ EC} embryos displayed a tortuous and instable vasculature compared to control embryos. These defects were associated with impaired endothelial cell-cell junction integrity. *In vitro*, α -pv depleted ECs displayed defective actin cytoskeleton organization, decreased formation of integrin-based cell-ECM adhesion structures, impaired lamellipodia formation and reduced Rac1 activity. Consequently, migration, cell-cell junction integrity, and monolayer formation were impaired in the absence of α -pv. To investigate the role of endothelial α -pv in pathological angiogenesis, we used the mouse glioma neovascularization model. The analysis showed that depletion of endothelial α -pv leads to reduced tumor vessel density and tumor size.

Although, mice lacking β -pv (β -pv^{-/-}) are viable, fertile and do not show any obvious embryonic phenotype, it could be that β -pv partially compensates endothelial α -pv deficiency during early embryonic stages. To test this hypothesis, we generated mice with ECs lacking both α -pv and β -pv (referred to herein as α -pv ^{Δ EC}; β -pv^{-/-} mice) by intercrossing α -pv^{fl/+}; *Tie2-Cre* mice with α -pv^{fl/fl}; β -pv^{-/-} mice. We showed that α -pv ^{Δ EC}; β -pv^{-/-} mice exhibited hemorrhages in the head and trunk and died between E11.5 and E12.5. Paralleling sites of hemorrhage, α -pv ^{Δ EC}; β -pv^{-/-} embryos displayed selective central nervous system (CNS)-specific vascular patterning defects, with markedly decreased angiogenic sprouting into the brain and the spinal cord, reduced vascular density, enlargement of vessel diameter, glomeruloid vascular malformations, and impaired pericyte (PE) coverage of the vessels. Together, these findings indicate for the first time that β -pv partially compensates the loss of

endothelial α -pv and that parvins are critical for the vascularization of the CNS during embryonic development. Our data also suggest that parvins might play a central role in blood-brain barrier (BBB) formation and maintenance.

Besides motor neuron degeneration and muscle atrophy, ALS patients show EC damage, PE degeneration and disrupted barrier function, leading to the classification of ALS as a neurovascular disease. The majority of ALS patients share a common neuropathology characterized by cytoplasmic deposition of TDP-43 positive protein inclusions. TDP-43 is a DNA/RNA-binding protein that regulates the expression of several genes. Interestingly, depletion of TDP-43 in zebrafish leads to shortened motor neurons, muscle degeneration, vascular miss-patterning, and death. However, the role of TDP-43 in ECs and whether endothelial TDP-43 regulates angiogenesis and is implicated in the vascular defects observed in ALS patients, is unknown, and remain to be determined.

During my thesis and in collaboration with the group of Dr. Bettina Schmid at the German Centre for Neurodegenerative Diseases (DZNE) in Munich, we studied the role of TDP-43 in ECs in mice. To do this, we used mice with ECs genetically deficient of TDP-43 (herein referred as TDP-43^{i Δ EC} mice) that were generated by crossing TDP-43^{fl/fl} mice with mice expressing Cre recombinase under the control of the tamoxifen-inducible VE-cadherin (VEcad) promoter (Cadh5(PAC)-CreERT2), and analyzed postnatal retinal vascularization over time. Our results showed for the first time, that endothelial TDP-43 controls sprouting angiogenesis by regulating polarity and migration of ECs.

Using new endothelial-specific gene targeting mouse models we have uncovered novel and essential functions of parvins and TDP-43 in the formation of blood vessels, opening new experimental opportunities to gain further insights into the molecular control of EC biology, in both, health and disease.

Zusammenfassung

Das Wachsen des Blutgefäßsystems, die Angiogenese, ist ein wichtiger Prozess, der bei mangelnder Versorgung von Gewebe mit Sauerstoff während der Entwicklung, im Wachstum und bei Gewebshheilung stattfindet. Die Angiogenese spielt auch bei der Pathogenese vieler Krankheiten eine Rolle, wie etwa bei der Diabetischen Retinopathie, Tumorwachstum und der Metastasierung. Des Weiteren sind neurodegenerative Krankheiten, wie etwa die Amyotrophe Lateralsklerose (ALS), mit Gefäßfehlbildungen assoziiert. Der Einfluss von Gefäß-assoziierten Schäden auf neurodegenerative Funktionsstörungen ist jedoch noch unklar.

Die Angiogenese beinhaltet koordinierte Endothelzell (EZ)- Spezifizierung, Adhäsion, Migration und Proliferation, und die Regulation dieser Prozesse schließt die physische Interaktion von EZ mit der Extrazellulären Matrix (EZM) durch die Integrine ein. Bei Bindung an die EZM rekrutieren Integrine Adaptor- und Signalproteine an ihr cytoplasmatisches Ende und bilden somit fokale Adhäsionspunkte (FA), durch welche sie Signale in die Zellen übertragen. Auf diesem Weg regulieren Integrine EZ Spezifikation, Gefäßwachstum, Lumenformierung, Zellkontakte und Gefäßstabilität. Die molekularen Mechanismen und intrazellulären Signalkaskaden, die wichtig für diese Integrin-basierenden Prozesse sind, sind jedoch nur teilweise bekannt.

Die Parvine sind Aktin-bindende Proteine, welche an FA lokalisieren und die Interaktionen von Integrinen mit dem Zytoskelett und die Verknüpfung der Integrinsignalwege mit den Rezeptortyrosinkinase (RTK) Signalwegen regulieren. Die Familie der Parvine besteht aus drei Mitgliedern: α -parvin (α -pv), β -parvin (β -pv), und γ -parvin (γ -pv) und EZ exprimieren nur α -pv und β -pv. Parvine sind wichtige Moleküle bei der Regulation der Gefäßentwicklung. Die Deletion des α -pv-Gens in Mäusen führt zum Tod im Embryonalstadium wegen kardiovaskulärer Defekte und Anzeichen von fehlerhafter Angiogenese, einschließlich gestörter Anlagerung von Glattmuskelzellen an Gefäßwände, Gefäßrisse und abnormaler Herzentwicklung. Es ist wohl bekannt, dass EZ eine wichtige Rolle in der Angiogenese spielen, die Bedeutung von α -pv und β -pv für EZ-Funktionen während der Angiogenese ist jedoch nicht bekannt und muss noch untersucht werden.

Diese Arbeit hatte zum Ziel, die Funktionen von α -pv und β -pv während physiologischer und pathologischer Angiogenese-Prozesse zu untersuchen. Um dies zu erreichen, wurden interdisziplinäre Methoden angewandt, unter anderem genetisch veränderte Mauslinien und gewebs-spezifische Gendeletationsmethoden, Zellkulturmethoden, molekularbiologische Untersuchungen und hochauflösende Fluoreszenzmikroskopie.

Um die Funktion von α -pv *in vivo* zu untersuchen, wurden Mäuse generiert, deren EZ kein α -pv exprimieren, indem Mäusen mit dem *loxP*-flankierten α -pv Gen (α -pv^{fl/fl}) mit Mäusen verpaart wurden, die die Cre Rekombinase unter dem *Tie2*-Promotor exprimieren (von nun an α -pv ^{Δ EC} genannt). Dies führte zum Tod im späten Embryonalstadium beginnend am Embryonaltag (E) 15.5 und ging einher mit Blutungen und veränderten Gefäßstrukturen. α -pv ^{Δ EC} Embryonen wiesen turbulente und instabile Gefäße im Vergleich zu Kontrollgefäßen auf. Diese Defekte gingen einher mit unstabilen Zell-Zell Verbindungen. *In vitro* zeigten Zellen ohne α -pv ein abnormales Zytoskelett, defekte Formung von Integrin-basierenden Adhäsionsstrukturen, abnormale Formung von Lamellipodien und verminderte Rac1 Aktivität auf. Daraus ergaben sich Defekte in Migration, Zell-Zell Kontakten und Formung eines Zellrasens in EZ ohne α -pv. Um die Rolle von endothelialem α -pv in der pathologischen Angiogenese zu untersuchen, wurde das Glioma Neovaskularisationsmodell verwendet. Die Ergebnisse zeigten, dass endotheliales α -pv eine Rolle in Tumor Vaskularisation spielt. Das Fehlen von α -pv führte zu verminderter Tumorgefäßdichte und Tumorgroße.

Obwohl Mäuse ohne β -pv (β -pv^{-/-}) vital und fruchtbar sind und zudem keinen offensichtlichen embryonalen Phänotypen aufweisen, könnte es sein, dass β -pv teilweise in der frühen Embryonalentwicklung die endotheliale Deletion von α -pv kompensiert. Um diese Hypothese zu testen, wurden Mäuse generiert, deren EZ weder α -pv noch β -pv exprimieren (von nun an α -pv ^{Δ EC}; β -pv^{-/-} genannt). Dies wurde durch die Verpaarung von α -pv^{fl/+}; *Tie2*-Cre Mäusen mit α -pv^{fl/fl}; β -pv^{-/-} Mäusen erreicht. Hier zeigten wir, dass α -pv ^{Δ EC}; β -pv^{-/-} Embryonen zwischen E11.5 und E12.5 starben und Blutungen im Kopf und Körper aufwiesen. Zudem hatten α -pv ^{Δ EC}; β -pv^{-/-} Embryonen eine stark geschädigte Vaskularisation des zentralen Nervensystems (ZNS), die sich durch reduziertes Einwachsen von Blutgefäßen in das Gehirn und das Rückenmark, reduzierte Gefäßdichte, größere Gefäßdurchmesser, Bläschenstrukturen und mangelhafte Anlagerung von Perizyten an Gefäßwände

auszeichneten. Diese Ergebnisse deuten erstmals darauf hin, dass β -pv teilweise den endothelialen Verlust von α -pv während der Embryogenese kompensiert und dass Parvine für die Vaskularisierung des ZNS von großer Bedeutung ist. Unsere Daten zeigten auch, dass Parvine möglicherweise eine wichtige Rolle in der Bildung und der Aufrechterhaltung der Blut-Hirn-Schranke spielen.

Neben der Degeneration von Motoneuronen und Muskelschwund, wurde bei ALS-Patienten EZ Schaden, Perizyten-Degeneration und eine fehlerhafte Blut-Hirn-Schranke festgestellt, was dazu führt ALS als neurovaskuläre Erkrankung einzustufen. Die meisten ALS-Patienten haben eine neuropathologische Eigenschaft gemeinsam: die zytoplasmatische Ablagerung von TDP-43-positiven Proteineinlagerungen. TDP-43 ist ein DNS/RNS-bindendes Protein, das die Expression vieler Gene reguliert. Es ist interessant, dass die Deletion von TDP-43 in Zebrafischen zu verkürzten Motoneuronen, Muskelschwund, fehlerhaften Gefäßmustern und schließlich zum Tod führt. Die Rolle von TDP-43 in EZ ist jedoch nicht geklärt, und ob endotheliales TDP-43 in Angiogeneseprozessen mitwirkt und in die vaskulären Defekte, die bei ALS Patienten beobachtet wurden, involviert ist, muss noch untersucht werden.

Während meiner Arbeit und in Kollaboration mit der Gruppe von Dr. Bettina Schmid am Deutschen Zentrum Neurodegenerativer Erkrankungen (DZNE) in München, habe ich die Rolle von TDP-43 in EZ in Mäusen untersucht. Dafür wurden Mäuse verwendet, deren EZ kein TDP-43 haben (von nun an TDP-43^{iAEC} genannt), und diese wurden generiert, indem TDP-43^{fl/fl} Mäuse mit Mäusen gekreuzt wurden, die die Tamoxifen-induzierbare Cre Rekombinase unter dem VE-cadherin (VEcad)-Promotor (Cadh5(PAC)-CreERT2) exprimieren. Mithilfe der TDP-43^{iAEC} Mäuse wurde die postnatale Retinavaskularisation zu verschiedenen Zeitpunkten analysiert. Unsere Ergebnisse zeigten erstmals, dass endotheliales TDP-43 die Sprossung in der Angiogenese durch Regulation von EZ- Polarisation und Migration beeinflusst.

Mit neuen Mausmodellen zur endothel-spezifischen Gendeletion gelang es uns neue Funktionen von Parvinen und TDP-43 in der Gefäßformation aufzuzeigen, und hiermit wurde der Weg für neue experimentelle Möglichkeiten geebnet, weiterführende Einblicke in die molekulare Regulation der EZ-Biologie in Gesundheit und Krankheit zu erlangen.

Table of contents

Summary	V
Zusammenfassung	VIII
1 Introduction.....	1
1.1 The development of the vascular system	1
1.2 EC-extracellular matrix (ECM) interaction.....	4
1.2.1 The integrins	4
1.2.2 Formation of integrin-mediated adhesion structures.....	5
1.2.3 Integrins in angiogenesis	7
1.2.4 The ILK/PINCH/parvin complex in integrin signaling.....	8
1.2.4.1 Assembly of the IPP complex	8
1.2.5 The IPP complex <i>in vivo</i>	11
1.3 Endothelial cell-cell junction integrity.....	14
1.3.1 Cell-cell junctions.....	14
1.3.2 The function of JAIL in cell-cell junction integrity	15
1.4 Angiogenesis and disease	17

Table of contents

1.4.1	Tumor angiogenesis.....	17
1.4.2	ALS and Tar DNA binding protein of 43 kDa (TDP-43, TARDBP).....	18
1.5	Aim of the thesis.....	22
2	Materials and Methods.....	23
2.1	Materials.....	23
2.1.1	Antibodies.....	23
2.1.2	Secondary antibodies	24
2.1.3	Cell culture reagents.....	25
2.1.4	Chemical inhibitors.....	25
2.1.5	Chemicals and reagents.....	25
2.1.6	Kits	27
2.1.7	Disposables/Consumables.....	28
2.1.8	Oligonucleotides.....	28
2.1.9	siRNA (Sigma-Aldrich).....	29
2.1.10	Equipment	29
2.1.11	Microscopes.....	30
2.1.12	Hardware and software.....	31
2.2	Methods.....	32
2.2.1	Animals	32
2.2.1.1	Breeding schemes	32

Table of contents

2.2.1.1.1	Constitutive KO Cre line.....	32
2.2.1.1.2	Inducible KO Cre line.....	32
2.2.2	Mouse models to study angiogenesis	33
2.2.2.1	The mouse embryo hindbrain.....	33
2.2.2.2	The postnatal mouse retina	34
2.2.2.3	Tumor angiogenesis in glioblastoma.....	35
2.2.3	Histological analysis.....	36
2.2.3.1	Preparation of paraffin sections	36
2.2.3.2	Preparation of cryo sections	36
2.2.3.3	Hematoxylin/Eosin (H&E) staining.....	36
2.2.4	Immunological analysis	37
2.2.4.1	Whole embryo and tissue immunohistochemistry.....	37
2.2.4.2	Hindbrain immunohistochemistry	38
2.2.4.3	Whole retina immunohistochemistry	38
2.2.4.4	Immunohistochemistry of cryo and paraffin sections	39
2.2.4.5	Immunofluorescent staining of cells.....	40
2.2.4.6	Proliferation assay.....	40
2.2.5	Biochemical methods	41
2.2.5.1	Preparation of protein lysates.....	41
2.2.5.1.1	Protein lysates from mouse lungs and brains	41

Table of contents

2.2.5.1.2	Protein lysates from adherent cells.....	41
2.2.5.2	Protein quantification assay.....	41
2.2.5.3	SDS-polyacrylamide-gel electrophoresis (SDS-PAGE).....	42
2.2.5.4	Western blotting and immunodetection.....	42
2.2.5.5	Protein pull-down assay.....	43
2.2.6	Molecular biological methods.....	43
2.2.6.1	Extraction of DNA.....	43
2.2.6.2	Polymerase chain reaction (PCR).....	44
2.2.6.2.1	PCR reactions.....	44
2.2.6.2.2	PCR programs.....	45
2.2.6.3	Agarose gel electrophoresis.....	46
2.2.6.4	Lipofectamin transfection.....	46
2.2.7	Cell culture.....	47
2.2.7.1	Culture of HUVECs.....	47
2.2.7.2	Migration assay.....	48
2.2.7.3	Transendothelial cell resistance (TEER).....	48
2.2.7.4	Isolation of mouse ECs.....	48
2.2.8	Statistical analysis.....	49
3	Results.....	50
3.1	Role of parvins in ECs during angiogenesis.....	50

3.1.1	Analysis of α -pv functions in ECs	51
3.1.1.1	Deletion of α -pv in ECs in mice leads to embryonic lethality associated with hemorrhages.....	51
3.1.1.2	Altered vascular morphology in α -pv ^{ΔEC} mice	52
3.1.1.3	Normal mural cell coverage of vessels in α -pv ^{ΔEC} embryos	53
3.1.1.4	Loss of endothelial α -pv impairs cell-cell junction integrity	54
3.1.1.5	α -pv localizes to FXs, FAs and JAIL in ECs <i>in vitro</i>	55
3.1.1.6	Depletion of α -pv in HUVECs.....	57
3.1.1.7	α -pv depleted ECs show reduced FX formation and impaired lamellipodia	58
3.1.1.8	Depletion of α -pv in ECs leads to decreased Rac1 activity and cell migration	60
3.1.1.9	Depletion of α -pv in ECs impairs cell-cell junction formation and monolayer integrity	60
3.1.1.10	α -pv localizes at JAIL and is crucial for JAIL formation.....	63
3.1.2	Analysis of α -pv and β -pv functions in ECs.....	65
3.1.2.1	Mice with ECs lacking α -pv and β -pv are embryonically lethal and display abnormal vessel morphology	65
3.1.2.2	α -pv and β -pv are crucial for hindbrain vascularization	67
3.1.2.3	α -pv ^{ΔEC} ; β -pv ^{-/-} embryos showed reduced spinal cord vascularization.....	69
3.1.2.4	Impaired vessel maturation in α -pv ^{ΔEC} ; β -pv ^{-/-} embryos.....	72
3.1.2.5	Altered cell morphology of ECs in α -pv ^{ΔEC} ; β -pv ^{-/-} embryos	76

Table of contents

3.1.3	Reduced tumor angiogenesis in absence of α -pv	79
3.2	Role of TDP-43 in ECs during angiogenesis	81
4	Discussion	86
4.1	α -pv regulates vessel integrity and is crucial for cell-cell junction integrity.....	86
4.2	Impaired integrin-mediated parvin signaling results in severe vascular malformations	90
4.3	TDP-43 depletion in ECs causes vascular defects.....	93
5	References.....	95
6	Index of figures and tables	110
7	List of Abbreviations.....	113
8	Publications	117
9	Danksagung	1

1 Introduction

1.1 The development of the vascular system

The vascular system consists of a hierarchically organized network of blood vessels that can be divided into arteries, veins, and capillaries. The blood vessels are formed by an inner layer of endothelial cells (ECs) enclosed by vascular mural cells, comprising vascular smooth muscle cells (vSMC) and pericytes (PE), which, among other functions, provide stability to the vessel. While arteries and veins are surrounded by vSMC and PE, capillaries which link arteries and veins, have no smooth muscle but are associated with PE^{1,2}. The main function of the vascular system is to assure an adequate distribution of fluids, nutrients, gases, circulating cells, hormones, and metabolites to all cells of the body, thereby being essential for embryo development, organogenesis, organ function, tissue homeostasis, and immune response³. Pathologic changes of the function or structure of the vascular system also contribute to the progression of many diseases including cancer, diabetic retinopathy, arthritis, psoriasis, and neurodegenerative disorders^{4,5}. During the last years important insights into the molecular mechanisms that regulate angiogenesis have been achieved, however, therapeutic efforts to control vessel growth still remain (pre)clinical in most cases⁶⁻⁸. The work of this thesis aims to contribute to a better understanding of the mechanisms that control angiogenesis, which could pave the way for future treatment of vascular disorders.

Fehler! Verwenden Sie die Registerkarte 'Start', um Überschrift 1;Ü 1 dem Text zuzuweisen, der hier angezeigt werden soll.

The vascular system develops by two different morphogenetic processes; by vasculogenesis, i.e. the *de novo* formation of blood vessels by mesoderm-derived endothelial precursor cells (angioblasts)² and by angiogenesis, i.e. the formation of new vessels from preexisting ones. Hypoxic tissues can induce angiogenesis by producing proangiogenic factors, such as vascular endothelial growth factor-A (VEGF-A) and chemokines that activate the endothelium⁹. Angiogenesis is a complex process that involves EC-matrix adhesion, and EC polarization, migration, and proliferation, and requires that activated ECs escape from the quiescent vessel. The process how ECs escape the quiescent vessel depends on proteolytic degradation of the basal membrane (BM), containing collagen IV (Col-IV), laminin, and proteoglycans. This can be facilitated by matrix metalloproteases (MMPs), such as membrane type-1-MMP (MT1-MMP). Activated ECs also can form EC-matrix structures, such as podosomes, that locally degrade BM components^{10,11}.

Angiogenesis is initiated by a temporary spatial differentiation of ECs into tip and stalk cells, a behavior that is mainly induced by VEGF-A, and regulated by delta-like 4 (Dll4)/Notch signaling. Tip and stalk cells can be distinguished by their morphology, their gene expression signature, and their position in the developing vessel sprout. Tip cells lead the new sprout, are highly migratory, and project long filopodia that search the environment for proangiogenic factors^{12,13}. Tip cells express high levels of EC-specific molecule 1 (ESM1), Dll4, and platelet-derived growth factor (PDGF)¹⁴. The stalk cells follow the tip cells and elongate the sprout by proliferation. Stalk cells also secrete the components of the BM, adopt apical/basal polarity to form the lumen, and establish tight cell-cell junctions with neighboring ECs to stabilize the sprout⁹ (Figure 1).

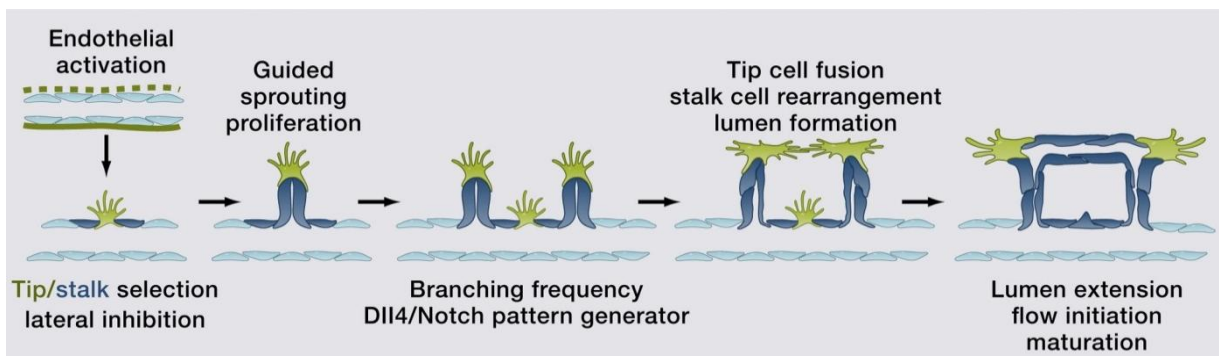


Figure 1. Schematic Steps of vessel formation. (1) Endothelial activation and tip/stalk cell selection. (2) Tip cell guidance and stalk cell proliferation. (3) Coordination of branching frequency. (4) Anastomosis and lumen formation (5) Perfusion and vessel maturation (modified after⁶).

Fehler! Verwenden Sie die Registerkarte 'Start', um Überschrift 1;Ü 1 dem Text zuzuweisen, der hier angezeigt werden soll.

Tip/stalk cell specification is tightly regulated by the relative protein expression of VEGF receptor 2 (VEGFR2) and Dll4 between ECs¹⁵⁻¹⁸. ECs with higher levels of VEGFR2 and Dll4 become tip cells. The binding of VEGF-A to VEGFR2 on these cells promotes the expression of Dll4 and the activation of Notch signaling in the adjacent ECs, which then become stalk cells^{9,18}. The binding of Dll4 to Notch triggers the release of the Notch intracellular domain (NICD), which regulates the expression of many genes including the down-regulation of VEGFR2^{19,20,21,22}. Therefore, the activity and relative protein levels of the VEGFR2 is regulated by the Dll4/Notch signaling, thereby creating a positive feedback loop between these two signaling pathways^{23,24}. This model of tip/stalk cells selection is highly dynamic and stochastic, allowing the rapid switch between tip and stalk specification and vice versa¹⁶. The importance of these signaling pathways in angiogenesis was shown using genetic studies in mice in which deletion of Dll4, Notch, VEGF-A or VEGFR2 leads to embryonic lethality due to severe defects in blood vessel formation²⁵⁻²⁸.

When two tip cells from different sprouts touch, they establish cell-cell junctions allowing the fusion of the sprouts in a process called anastomosis²⁹. Next, mural cells are recruited to stabilize the newly formed vessels and facilitate their maturation^{1,30-32}. Finally, vessel regression and pruning processes regulated by the blood flow remodel the new vascular network to achieve an optimal perfusion of the tissue. As soon as the formation of a mature vascular network is completed, the vessels remain in a quiescent state until new stimuli activate the endothelium⁶.

1.2 EC-extracellular matrix (ECM) interaction

1.2.1 The integrins

The adhesion of ECs to the ECM, mediated by the integrins, is essential for angiogenesis and function of the vessels^{33,34}. Integrins are the main cell-ECM receptors. Integrins are transmembrane heterodimeric glycoprotein receptors that consist of an α and a β subunit, with a large extracellular domain, a single transmembrane domain, and a short intracellular domain^{35,36}. In mammals there exist 18 α and 8 β subunits that can form 24 different integrins^{36,37}. Integrins can be clustered in four major classes: collagen-binding, laminin-binding, arginine-glycine-aspartate (RGD)-binding, and leukocyte-specific integrins³⁸⁻⁴⁰ (Figure 2).

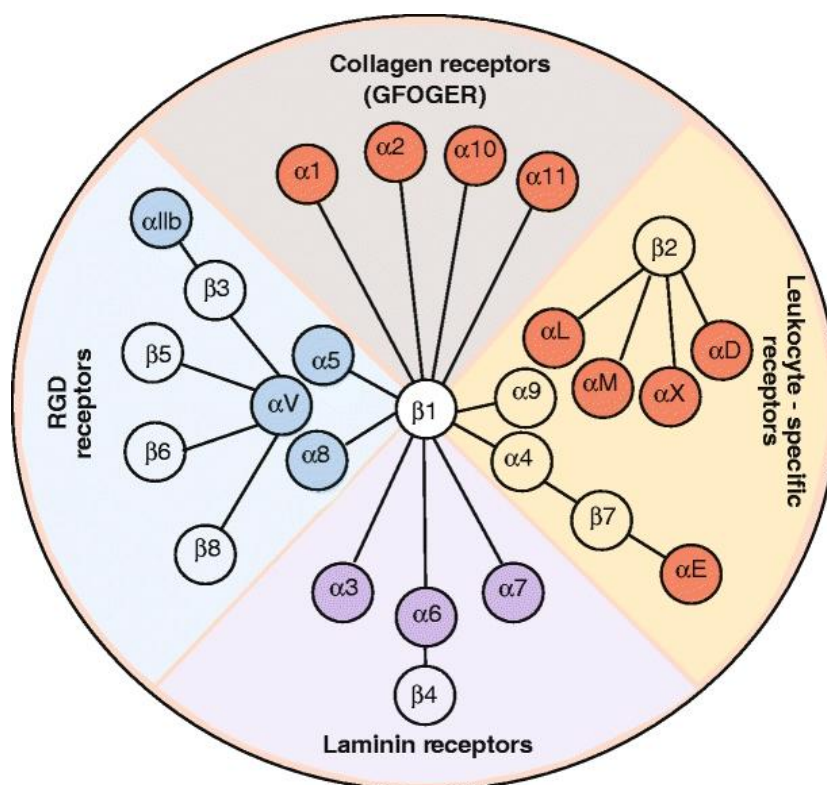


Figure 2. Integrin family in mammals. The integrins can be grouped in four groups: (1) collagen-binding (GFOGER), (2) laminin-binding, (3) arginine-glycine-aspartate (RGD)-binding, and (4) leukocyte-specific integrins (modified after³⁹).

Integrins can exist in two different conformations; an active and an inactive conformation. Integrin activation is triggered by signals from the inside of the cell (inside-out signaling),

Fehler! Verwenden Sie die Registerkarte 'Start', um Überschrift 1;Ü 1 dem Text zuzuweisen, der hier angezeigt werden soll.

that induce conformational changes, which increase their affinity to their ligands⁴¹. Integrins lack enzymatic activity. Therefore, they recruit intracellular signaling and adaptor molecules to their cytoplasmic tail to form the focal adhesions (FAs) and transduce the signals from the ECM into the cell (outside-in signaling). Integrin-mediated signals control many cellular processes including cell polarization, migration, proliferation, and survival^{35,36}.

1.2.2 Formation of integrin-mediated adhesion structures

Cell-ECM adhesion is initiated by the formation of the nascent adhesions and the focal contacts (FXs) at the periphery of the cell. Then, some of the FXs mature and form the FAs, which anchor the stress fibers to the integrins. Some of the FAs further mature into fibrillar adhesions (FB), which are mostly found at the center of the cell associated to thin actin cables and bind to fibronectin (FN)⁴² (Figure 3).

Cell spreading, filopodia and lamellipodia formation, and migration require dynamic regulation of the organization of the actin cytoskeleton^{43,44}. Different types of actin structures are found in cells; (1) branched network of short and thin fibers at the lamellipodia (2) thick unbranched contractile stress fibers and (3) cortical actin rings at the cell periphery^{45,46}. An overview of the different types of actin structures is shown in Figure 3.

Fehler! Verwenden Sie die Registerkarte 'Start', um Überschrift 1;Ü 1 dem Text zuzuweisen, der hier angezeigt werden soll.

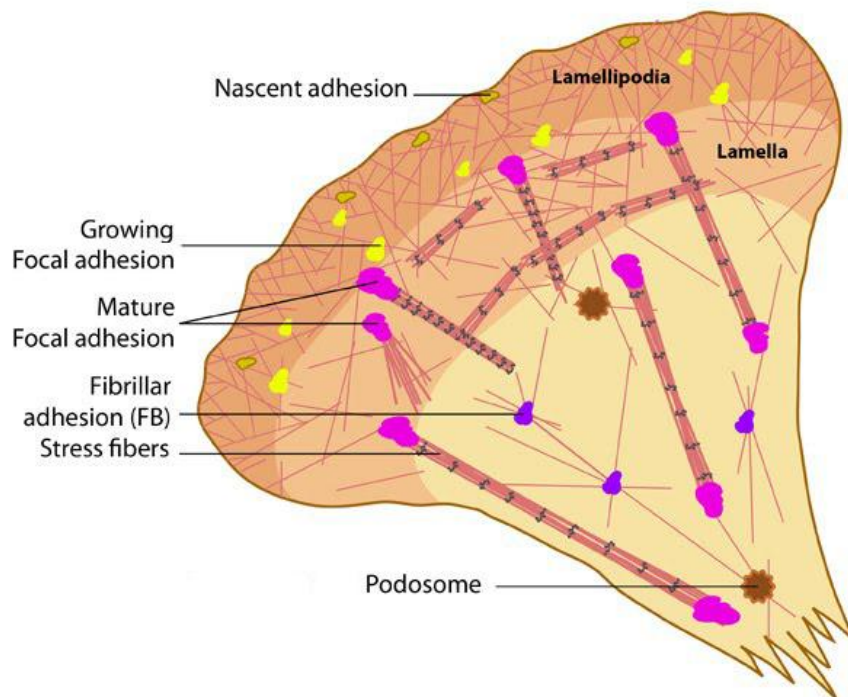


Figure 3. Overview of integrin-mediated cell-ECM adhesion structures and actin cytoskeleton organization in a migrating cell. Nascent adhesions and FXs are located at the cell periphery, and FAs and FBs are found at the center of the cell. Different types of actin structures occur in the cell: branched actin network at the lamella and lamellipodia, and stress fibers at the center of the cell (modified after⁴⁷).

Integrin-mediated signaling regulates the actin cytoskeleton through the small Rho GTPases, which can interact with several effectors and lead to assembly or disassembly of filamentous (F)-actin⁴⁸. Around 20 small Rho proteins have been identified of which Rho-A, Rac1, and Cdc42 are the most studied. While Rho-A regulates stress fiber formation, Rac1 controls lamellipodia projection, and Cdc42 is involved in filopodia formation^{48,49}. The activity of Rho-A, Rac1 and Cdc42 is regulated by guanine-nucleotide-exchange factors (GEFs) and GTPase-activating proteins (GAPs)⁵⁰ (Figure 4).

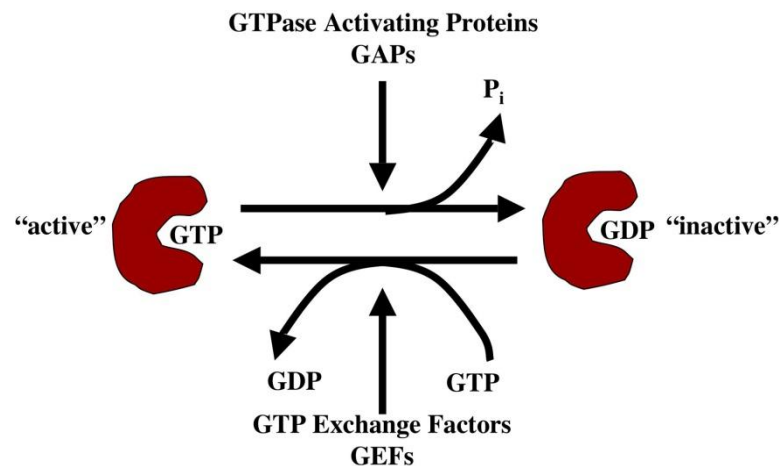


Figure 4. Regulation of GTPases activity. By hydrolyzing GTP to GDP, the proteins become inactivated. GAPs favor the inactive state, while GEFs exchange GDP with GTP resulting in an active state. GAP: GTPase-activating protein, GEF: guanine-nucleotide-exchange factor, GDP: Guanosine diphosphate, GTP: Guanosine triphosphate (modified after⁵⁰).

1.2.3 Integrins in angiogenesis

Integrins control EC adhesion, proliferation, survival, differentiation, and migration, thereby being essential for vascular development⁵¹⁻⁵³. ECs express many different integrins, including $\alpha 1\beta 1$ and $\alpha 2\beta 1$ (collagen receptors), $\alpha 3\beta 1$, $\alpha 6\beta 1$, and $\alpha 6\beta 4$ (laminin receptors), $\alpha 4\beta 1$ and $\alpha 5\beta 1$ (FN receptors), as well as $\alpha v\beta 3$ and $\alpha v\beta 5$ (receptors for FN and other ligands). Genetic studies in mice have shown that integrins are not required for vasculogenesis, but they are fundamental for angiogenesis^{54,55} (reviewed in³⁷).

Deletion of $\beta 1$ integrin in mice leads to embryonic lethality at the peri-implantation stage, precluding its analysis in angiogenesis^{35,55,56}. Endothelial-specific deletion of $\beta 1$ integrin ($\beta 1^{\Delta EC}$) results in embryonic lethality around embryonic day (E) 10.5 associated with defective formation of the EC monolayer in large blood vessels and the heart, and disorganized vascular patterning in the yolk sac (YS)^{57,58}. $\beta 1$ integrin is crucial for ligand-specific adhesion to laminin, Col-I, Col-IV, and migration, and is therefore important in sprout elongation^{57,59}. Postnatally induced deletion of endothelial $\beta 1$ integrin in the retina reveals that $\beta 1$ integrins also regulate tip/stalk cell selection via Dll4/Notch signaling⁶⁰. $\beta 1$ integrin is also required for apical/basal polarity and cell-cell junction integrity, thereby regulating lumen formation and vessel stability^{61,59}. $\beta 1$ integrin-mediated regulation of cell-cell junctions occurs via VE-cadherin (VEcad) trafficking and actin cytoskeleton

Fehler! Verwenden Sie die Registerkarte 'Start', um Überschrift 1;Ü 1 dem Text zuzuweisen, der hier angezeigt werden soll.

remodeling^{62,63}. Genetic studies of integrin subunits show that there is redundancy between the different integrins during angiogenesis *in vivo*, for instance loss of $\alpha 5\beta 1$ integrin is compensated by $\alpha \nu\beta 3$ integrin signaling^{52,64,65}. Altogether these studies show the importance of integrin signaling in blood vessel development.

$\beta 3$ and $\beta 5$ integrin are not needed for embryonic vascular development, however, it has been shown that the crosstalk between $\beta 3$ and $\beta 5$ integrin signaling and VEGF-A/VEGFR signaling is required for barrier function and tumor angiogenesis^{66,67}.

1.2.4 The ILK/PINCH/parvin complex in integrin signaling

During the last two decades, a complex of proteins consisting of integrin linked kinase (ILK), particularly interesting Cys-His-rich protein (PINCH) and parvins, the so called IPP complex, has emerged as a main regulator of the integrin signaling (Figure 5). The IPP complex controls spreading, migration, proliferation, and survival of the cells, and its biological importance has been demonstrated using *in vivo* genetic studies in different species³⁵.

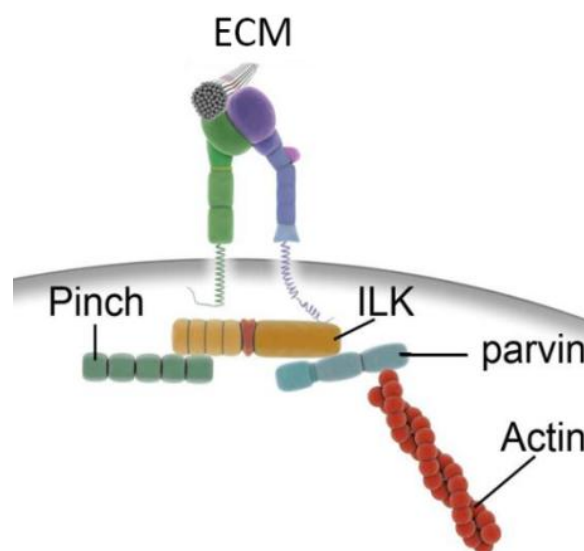


Figure 5. Schematic composition of the IPP-complex. The IPP complex is composed of ILK, PINCH, and parvin that binds to F-actin. The IPP complex interacts with integrins via ILK and through the actin via parvins (modified after⁶⁸).

1.2.4.1 Assembly of the IPP complex

The formation of the IPP complex occurs in the cytosol prior to its recruitment to the

Fehler! Verwenden Sie die Registerkarte 'Start', um Überschrift 1;Ü 1 dem Text zuzuweisen, der hier angezeigt werden soll.

cytoplasmic tail of integrins⁶⁹. After its formation, the complex interacts with paxillin (Pax) which facilitates its recruitment to the cytoplasmic tail of integrins⁷⁰⁻⁷². Depletion of one component of the complex leads to degradation of the other components by a proteasome-mediated process^{35,68,69} (Figure 6).

ILK is the first member of the complex that was identified. ILK consists of three domains. The N-terminal domain contains five ankyrin repeats and mediates protein-protein interaction. The C-terminal domain shares significant homology in the sequences of serin/threonin protein kinases, although its kinase activity is not clear. A pleckstrin homology (PH) domain is located between these two domains³⁵. ILK is the central component of the complex. ILK interacts with PINCH through the N-terminal domain and with parvins via its C-terminal domain⁷³. ILK also directly binds to kindlins, which then link the IPP complex to $\beta 1$ and $\beta 3$ integrins^{70,74}.

PINCH is a family of adaptor proteins consisting of PINCH-1 and PINCH-2⁷⁵. They are composed of five LIM domains and a nuclear localization site (NLS) motif. PINCH-1 and PINCH-2 are both ubiquitously expressed and their expression patterns overlap in many tissues⁷⁶⁻⁷⁸. The PINCH isoforms bind to the receptor tyrosin kinases (RTK) through the NCK2, thereby coupling integrin signaling to growth factor signaling.

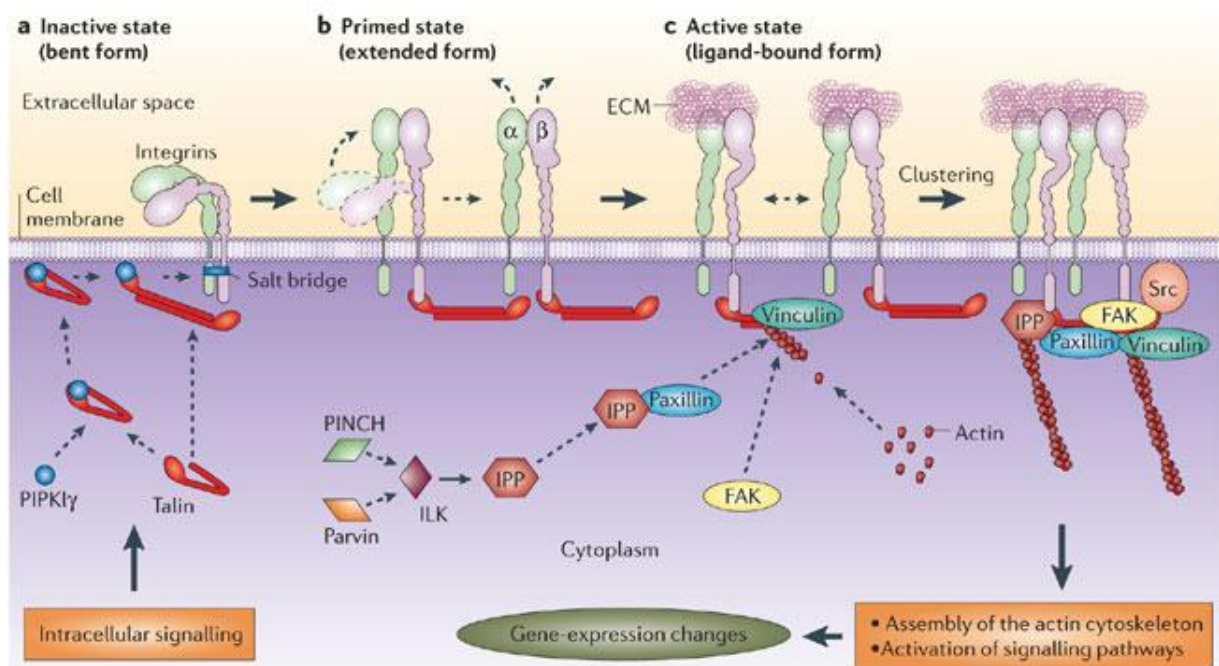


Figure 6. Recruitment of the IPP complex to FAs. Integrins are present on the cell surface in an inactive state (a) and upon binding of talin, integrins transform to the prime state (b) and bind ECM ligands in their active state

Fehler! Verwenden Sie die Registerkarte 'Start', um Überschrift 1;Ü 1 dem Text zuzuweisen, der hier angezeigt werden soll.

(c). The IPP complex is formed in the cytoplasm and by interaction with Pax, it is recruited to FAs. Vinculin (Vinc) and focal adhesion kinase (FAK) are sequentially recruited to nascent FXs. FA maturation involves integrin clustering and the formation of an adhesome, which binds to F-actin (modified after³⁵).

The parvins are a family of actin-binding proteins that consists of three members; α -parvin (α -pv), β -parvin (β -pv), and γ -parvin (γ -pv), containing 373, 364 and 331 amino acids, respectively. The hallmark of the structure of the parvins is the presence of two in tandem calponin homology (CH) domains that can bind directly to the F-actin. α -pv and β -pv also contain a NLS, however, their localization and function in the nucleus is unknown. While α -pv and β -pv are ubiquitously expressed, γ -pv expression is restricted to the hematopoietic system. ECs express α -pv and β -pv. Furthermore, splicing variations of β -pv termed s-PARVB and ss-PARVB have been described^{35,79} (Figure 7).

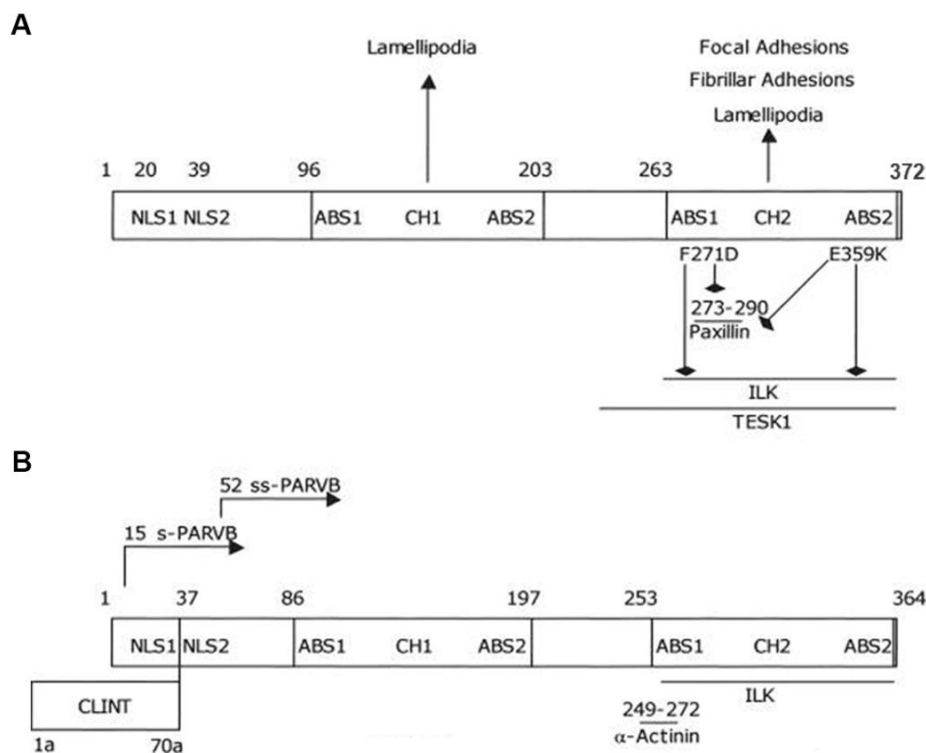


Figure 7. Structural features of (A) α -pv and (B) β -pv and their binding sites. Splicing variations of β -pv are termed s-PARVB and ss-PARVB. Numbers indicate amino acid positions. Arrows indicate effects of point mutations (modified after⁷⁹).

Parvins interact with ILK via their CH2 domain at the C-terminus⁸⁰. α -pv and β -pv have also different binding partners. α -pv can bind to HIC5 (isoform of Pax) and testicular protein kinase 1 (Test-1), whereas β -pv can interact with α -actinin and α -PIX, a GEF that can regulate the small Rho GTPases^{79,80,81}. An important interaction partner of α -pv is Pax, a main regulator of cell-ECM adhesion structure formation and maturation^{82,83}. α -pv can regulate

Fehler! Verwenden Sie die Registerkarte 'Start', um Überschrift 1;Ü 1 dem Text zuzuweisen, der hier angezeigt werden soll.

cell spreading via TESK1, which controls F-actin polymerization through cofilin phosphorylation^{84,85}. Finally, parvins can also influence actin cytoskeleton organization by modulating the activity of the small Rho GTPases⁷⁹. α -pv regulates cell spreading and contraction via Rac1, and RhoA/Rho-kinase (ROCK)-mediated signaling^{86,87}, whereas β -pv effects the actin cytoskeleton via Rac1 and Cdc42⁸⁸. The functions of parvins can also be modulated by their phosphorylation. α -pv can be phosphorylated at its N-terminus, which contains phosphorylation consensus for proline-directed serin/threonin kinases, including ERK and Cdc2^{89,90}. This phosphorylation enhances the interaction of α -pv with ILK and is important for cell spreading⁹¹. Moreover, it has been reported that the phosphorylation of β -pv by ILK also promotes cell spreading⁷¹.

1.2.5 The IPP complex *in vivo*

The functions of the IPP complex and its components were studied in several organisms, such as *C.elegans*, *D.melanogaster*, zebrafish, and mice. The results have revealed that, additionally to their role as part of the IPP complex, each component has discrete functions³⁵. The depletion of ILK in *C.elegans* results in embryonic lethality associated with muscle attachment defects, its depletion in *D.melanogaster* is also embryonically lethal and leads to actin detachment from the muscle membrane^{92,93}. The same defects can be observed in PINCH-1 depletion in these organisms^{77,94,95}. Absence of α -pv in *C.elegans* also causes vascular muscle attachment defects due to impaired assembly of integrin adhesion complexes⁹⁶. These studies point to the essential role of the IPP complex in integrin-mediated cell-ECM adhesion. Studies in mice show that ILK and PINCH also participate in cell-cell junction formation in keratinocytes and endoderm cells⁷⁸.

Like loss of expression of β 1 integrin in mice, deletion of ILK and PINCH-1 lead to embryonic lethality at the peri-implantation stage^{97,98}. Interestingly, loss of PINCH-2 does not show any embryonic phenotype, most likely due to compensation by PINCH-1⁹⁹. Studies with embryoid bodies (EBs) provide evidence that ILK and PINCH-1 regulate epiblast polarization and cavity formation. PINCH-1^{-/-} EBs also show cell-cell junction defects and increased apoptosis in endoderm cells^{78,100}. Cell-cell junction defects are associated with loss of E-cadherin staining at the adherens junctions (AJs), however, how PINCH-1 molecularly regulates cell-cell

Fehler! Verwenden Sie die Registerkarte 'Start', um Überschrift 1;Ü 1 dem Text zuzuweisen, der hier angezeigt werden soll.

junction integrity is not known. Further studies show that PINCH-1 regulates endoderm cell survival via modulating JNK signaling⁹⁵. Depletion of α -pv in mice leads to embryonic lethality between E10.5 and E14.5, suggesting a partial compensation via β -pv. However, this remains to be proved. Lethality of α -pv^{-/-} embryos is associated with hemorrhages, aneurysms, and severe heart defects, which implicate impaired vessel remodeling and vessel rupture. Furthermore, depletion of α -pv perturbs the coverage of vessels with vSMCs and impairs vessel maturation¹⁰¹. This is caused by the upregulation of RhoA/ROCK signaling pathway that leads to an increase of myosin light chain phosphorylation, hypercontraction of vSMCs, and migration defects towards PDGF¹⁰¹. Mice depleted of β -pv (β -pv^{-/-}) are viable and do not show any obvious embryonic phenotype³⁵. Finally, loss of γ -pv in mice does not show any defect in hematopoiesis¹⁰². An overview of gene deletion impacts is shown in Figure 8.

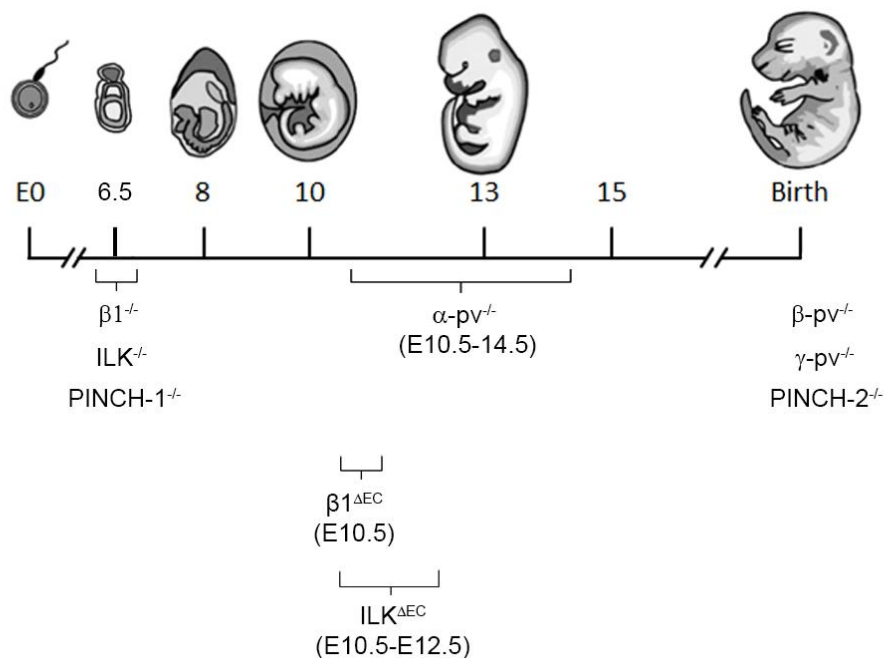


Figure 8. Impact of gene deletions of the integrin signaling cascade on embryonic lethality in mice. Loss of endothelial $\beta 1$ integrin ($\beta 1^{\Delta EC}$), endothelial ILK ($ILK^{\Delta EC}$), and complete α -pv (α -pv^{-/-}), but not complete β -pv (β -pv^{-/-}) result in embryonic lethality. But their time points of death and the embryonic phenotypes show distinct differences, which suggests unique underlying mechanisms for each molecule (modified after⁵⁴).

To overcome embryonic lethality associated to the loss of the IPP complex members, several conditional KO mice have been created. Endothelial-specific deletion of ILK ($ILK^{\Delta EC}$) in mice results in embryonic lethality at around E10.5 associated with impaired vascular development¹⁰³. Cardiovascular defects and vessel patterning have been observed in zebrafish lacking ILK^{103,104}. Moreover, deletion of ILK in vSMC shows that ILK is also required

Fehler! Verwenden Sie die Registerkarte 'Start', um Überschrift 1;Ü 1 dem Text zuzuweisen, der hier angezeigt werden soll.

for mural cell recruitment to the vessel wall¹⁰⁵. Finally, keratinocyte-specific deletion of ILK indicates that ILK is also necessary for AJs formation^{106,107}. Similar cell-cell junction defects have been reported by the loss of PINCH-1 in keratinocytes⁷⁸.

The complex phenotype of α -pv^{-/-} embryos makes it difficult to analyze the role of parvins in angiogenesis. Therefore, in order to analyze parvins in angiogenesis, we generated different mice with ECs lacking either α -pv or α -pv and β -pv parvins. Postnatal deletion of α -pv in ECs showed retinal hypo-vascularization, associated with reduced sprouting and increased vessel regression¹⁰⁸.

However, the role of α -pv in the regulation of EC behavior during embryonic development and the capacity of β -pv to compensate for the loss of α -pv in ECs is unknown. This was the the main aim of my thesis.

1.3 Endothelial cell-cell junction integrity

1.3.1 Cell-cell junctions

Vessel formation and maintenance not only depend on EC-ECM interactions, but also on the cell-cell junctions between neighboring ECs, which are critical for tissue perfusion and barrier function. Endothelial cell-cell junctions also have to be dynamically regulated in order to facilitate leukocyte extravasation, which is important in certain conditions, e.g. during inflammation¹⁰⁹. Defects of endothelial cell-cell junctions lead to angiogenic defects, altered permeability, and they have been associated to human diseases, such as cerebral cavernous malformations (CCMs), and hemorrhagic stroke¹¹⁰⁻¹¹².

Endothelial cell-cell junctions can be divided into AJs, tight junctions (TJs), and gap junctions. While AJs and TJs play a main role in barrier function, gap junctions mediate cell-to-cell communication¹¹³. The central component of AJs is the VEcad, which establishes homophilic interactions at the plasma membrane with neighboring ECs^{114,115}. The cytoplasmic domain of VEcad interacts with β -catenin (β -cat), p120, and plakoglobin, which can bind to α -actinin, Vinc, and eplin, thereby linking the AJs to the actin cytoskeleton^{109,114,116,117} (Figure 9). The connection between the AJs and the actin allows junction maturation and the fast and dynamic remodeling of the junctions. Stable AJs are continuous and are aligned to cortical actin, whereas dynamic AJs are discontinuous being connected to actin stress fibers. Furthermore, ECs can form reticular junctions that assemble overlapping cell areas. AJs modulate actin cytoskeleton organization via Rac1 and Cdc42¹¹⁸. AJ remodeling can also be regulated by the phosphorylation and internalization of VEcad^{110,119}. Moreover, VEcad transmits intracellular signals that regulate contact inhibition of cell growth, protection from apoptosis, and vascular permeability. By interacting with VEGFR2, VEcad is regulating its downstream signaling. Both, VEcad and β -cat are required to bind VEGFR2, thereby retaining VEGFR2 at the plasma membrane, where it is dephosphorylated and its signaling regulated¹²⁰. An overview of the AJ architecture is shown in Figure 9. Claudins are the core of TJs, which are transmembrane molecules crucial for junction integrity^{121,122}. TJs control the movement of ions and solutes and limit the free passing of lipids and proteins between the

Fehler! Verwenden Sie die Registerkarte 'Start', um Überschrift 1;Ü 1 dem Text zuzuweisen, der hier angezeigt werden soll.

apical and basolateral cell surface¹¹⁴. TJs are essential for the barrier function in the vessel of the CNS (see 1.4.2).

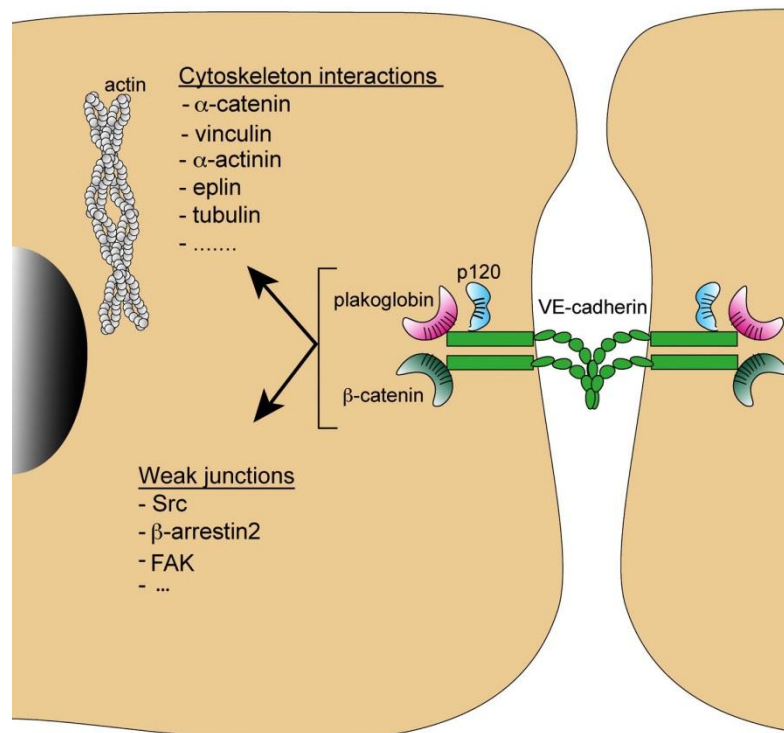


Figure 9. Architecture of AJs in ECs. VEcad is a transmembrane protein that binds p120, plakoglobin, and β -cat at the cytoplasmic tail and transmits signals for actin rearrangement involving e.g. α -catenin, and Vinc, and junction dynamics via Src or FAK (modified after¹⁰⁹).

1.3.2 The function of JAIL in cell-cell junction integrity

EC junctions require dynamic reaction abilities in response to stimulation to mediate adaptive functions, e.g. in inflammation, chemokine or growth factor stimulation. These responses are supported by increased actin cytoskeleton dynamics, mediated by rapid assembly and disassembly of actin filaments, which depend on many actin-binding and actin-regulating proteins¹²³.

Recently, the actin-regulating molecule, actin-related protein-2/3 (Arp-2/3) was reported to play a central role in junction formation and maintenance and being functionally involved in the VEcad complex¹¹⁶. The ARP-2/3 complex, regulated by N-VASP and WAVE, is a central regulator of actin polymerization and organization of actin filaments and is crucial for actin branching and therefore lamellipodia protrusion¹²⁴. The complex includes Vinc, which

Fehler! Verwenden Sie die Registerkarte 'Start', um Überschrift 1;Ü 1 dem Text zuzuweisen, der hier angezeigt werden soll.

facilitates the anchoring of the actin polymerization machinery to integrin-mediated adhesion at the lamellipodium via talin¹²⁵. Lamellipodia formation is not only important for initial junction formation, but plays also a role in cell junction dynamics and barrier maintenance^{126,127}. Lamellipodia-like structures particularly appear in subconfluent cell cultures conditions, in which interrupted VEcad patterning at cell-cell junctions and intercellular gaps can be observed¹²⁸. Junction-associated intermittent lamellipodia (JAIL) are small lamellipodia-like protrusions that occur at EC junctions and overlap VEcad-free spots in immature AJs in order to ensure monolayer integrity. It has been shown that Arp-2/3 is promoting JAIL formation¹²⁶. These small lamellipodia-like protrusions are actin-dependent structures and drive VEcad dynamics to facilitate the formation of new VEcad adhesion sites that are fused into EC junction upon JAIL retraction¹²⁹ (Figure 10).

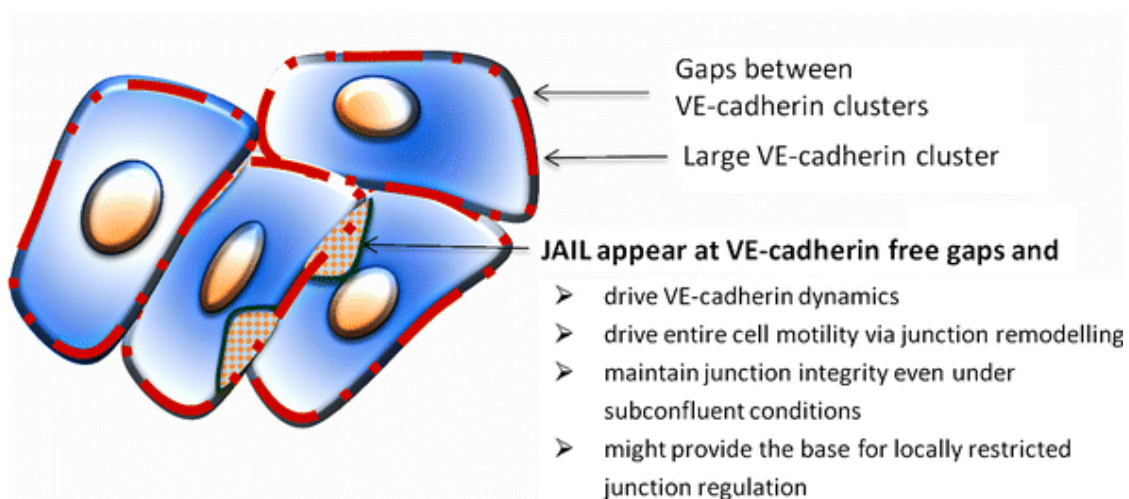


Figure 10. Schematic illustration of JAIL formation at EC junctions under subconfluent conditions. JAIL are actin-related lamellipodia-like structures that occur at VEcad-free gaps at cell-cell junctions and drive VEcad dynamics in order to facilitate monolayer integrity (modified after¹²⁹).

1.4 Angiogenesis and disease

Angiogenesis is a fundamental physiological process in development and homeostasis, but also contributes to the progression of many diseases including diabetic retinopathy, inflammation, tumor growth and metastasis¹³⁰. Moreover, neurodegenerative disorders, such as amyotrophic lateral sclerosis (ALS), are associated with vascular dysfunction¹³¹. The causative contribution of vascular system-associated defects related to vessel growth and vessel function to neurodegenerative diseases is, however, not clear.

1.4.1 Tumor angiogenesis

Tumor growth and tumor metastasis requires blood and lymphatic vessels that invade the tumor in order to allow access for nutrients. Tumors are vascularized through angiogenesis from existing vessels or by enrollment of circulating bone marrow-derived endothelial progenitor cells^{130,132,133}. Tumors induce angiogenesis by the release of many proangiogenic factors, such as VEGF¹³⁴⁻¹³⁶ (Figure 11).

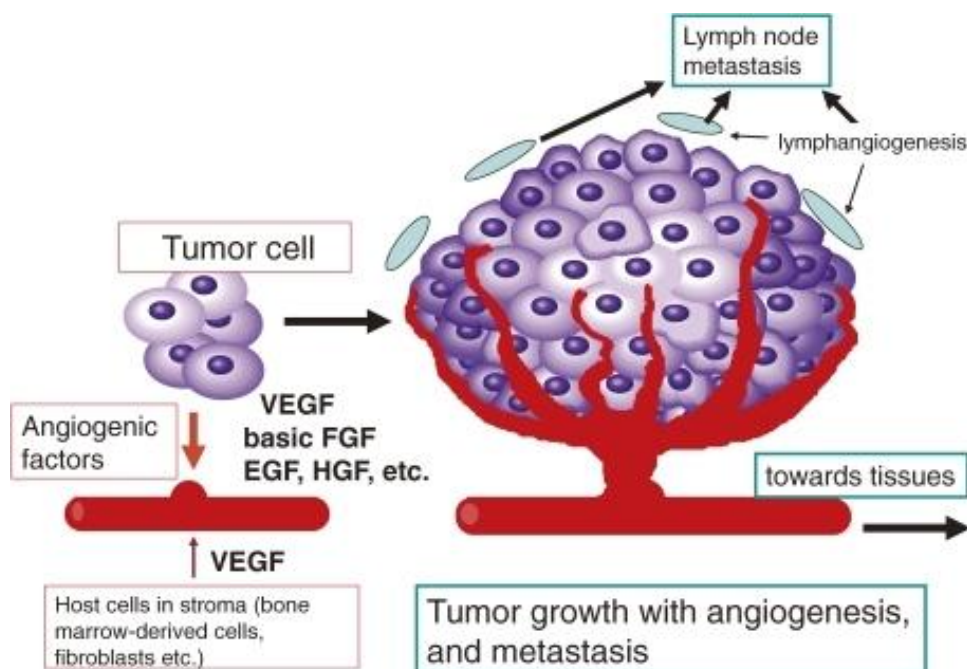


Figure 11. Angiogenesis in tumor growth. Tumors, macrophages, and fibroblast in tumor-microenvironments secrete angiogenic factors, such as VEGF. Newly formed blood vessels mediate tumor growth and metastasis towards other tissues and lymph nodes. EGF: epidermal growth factor; FGF: fibroblast growth factor; HGF: hematopoietic growth factor (modified after^{137,138}).

Fehler! Verwenden Sie die Registerkarte 'Start', um Überschrift 1;Ü 1 dem Text zuzuweisen, der hier angezeigt werden soll.

Basic and clinical studies showed that suppression of tumor angiogenesis can influence tumor growth and metastasis¹³⁹. Due to the main role of integrins in physiological angiogenesis, targeting integrin-mediated signaling in tumor angiogenesis has become promising in cancer therapy. Further understanding of the molecular mechanisms involved in tumor angiogenesis are needed to bridge basic studies with cancer therapy^{133,140}.

Gliomas, the most common tumors in the brain, are highly vascularized. Patients diagnosed with gliomas die in less than a year after first diagnosis. Until now, there is no available successful treatment¹⁴¹. The highly aggressive and invasive characteristics of most glioma cells make complete surgical treatment very complicated. Moreover, radiotherapy is also not very successful due to radio resistance of the tumor cells. In order to improve glioma treatment, a variety of glioma mouse models have been established¹⁴²⁻¹⁴⁵.

1.4.2 ALS and Tar DNA binding protein of 43 kDa (TDP-43, TARDBP)

The mammalian CNS has high energy demands and requires the continuous supply of oxygen. Therefore, its proper function requires full integrity of a complex vascular network. Upon increased neuronal activity, the neurovascular coupling leads to an increase in local blood flow, matching the increased demand by an adequate amount of oxygen and nutrient delivery while also leading to the removal of metabolites. The functional unit regulating the hemodynamic response is the neurovascular unit (NVU), which consist of ECs, PE, astrocytes and neurons^{146,147} (Figure 12). Thus, defects in these non-neuronal cells can lead to defective neurovascular coupling, impairing neuronal functions and eventually resulting in neuronal death. Therefore, defects in the NVU are thought to contribute to neurodegeneration¹⁴⁸.

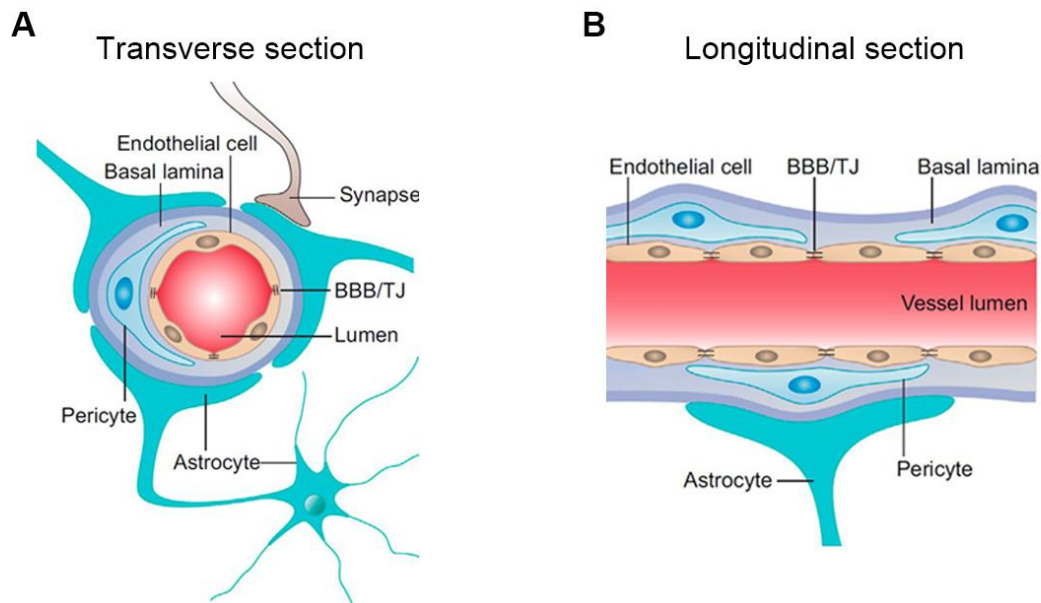


Figure 12. Organization of the NVU. (A) Transverse and (B) longitudinal sections of CNS vessels. ECs and PE are ensheathed by a common basal lamina that is composed of the endothelial and the parenchymal BM. The blood-brain barrier (BBB) is formed by microvascular ECs that are connected via complex TJ, thereby inhibiting paracellular diffusion of water soluble molecules (modified after¹⁴⁹).

The wall of blood vessels in the brain represents a specialized structure called the blood-brain-barrier (BBB), which limits the flow of molecules and ions from the blood to the brain, thereby being critical for brain homeostasis and protection of the brain from circulating toxins and pathogens. The BBB is an integral part of the NVU and its development and maintenance are regulated by dynamic interactions between ECs, PE and astrocytes. The molecular cross-talk between these cell types is not completely understood, but is among others, regulated by integrins and their ligands¹⁵⁰⁻¹⁵² (Figure 12). Perturbations in BBB integrity and function are found in many neurological disorders, such as ALS, Alzheimer's disease (AD), multiple sclerosis (MS), and Parkinson's disease¹⁵³. ALS is one of the most common neurodegenerative disorders characterized by the progressive degeneration of motor neurons in the brain and spinal cord, leading to muscle atrophy, paralysis, and death¹⁵⁴. Despite its high prevalence and broad incidence, the molecular mechanisms underlying ALS remain unclear. The majority of the ALS patients share a common neuropathology characterized by cytoplasmic deposition of TDP-43 positive protein inclusions. TDP-43, which is normally observed in the nucleus, is detected in pathological inclusions in the cytoplasm and nucleus of both neurons and glial cells of ALS patients (Figure 13, A). TDP-43 is a highly conserved and ubiquitously expressed DNA/RNA-binding protein that contains two RNA recognition motifs (RRM) and a glycine-rich C-terminal region (GRR),

Fehler! Verwenden Sie die Registerkarte 'Start', um Überschrift 1;Ü 1 dem Text zuzuweisen, der hier angezeigt werden soll.

characteristic of the heterogeneous nuclear ribonucleoproteins (hnRNP) class of proteins¹⁵⁵ (Figure 13, B). The physiological function of TDP-43 is still unclear, but it has been implicated in several steps of gene expression regulation including transcription, RNA splicing, RNA transport, and translation, thereby influencing many cellular processes. Signaling pathways regulated by TDP-43 include cell-matrix adhesion, cell-cell adhesion, axon guidance and body fat metabolism¹⁵⁶. Among cell-matrix adhesion proteins, TDP-43 regulates expression of FN, laminin, filamin, and β -pv¹⁵⁶. TDP-43 interaction with DNA is known to downregulate transcription. Furthermore, TDP-43 is able to regulate its own RNA levels in a negative feedback loop, which is thought to be important in pathogenesis^{157,158}.

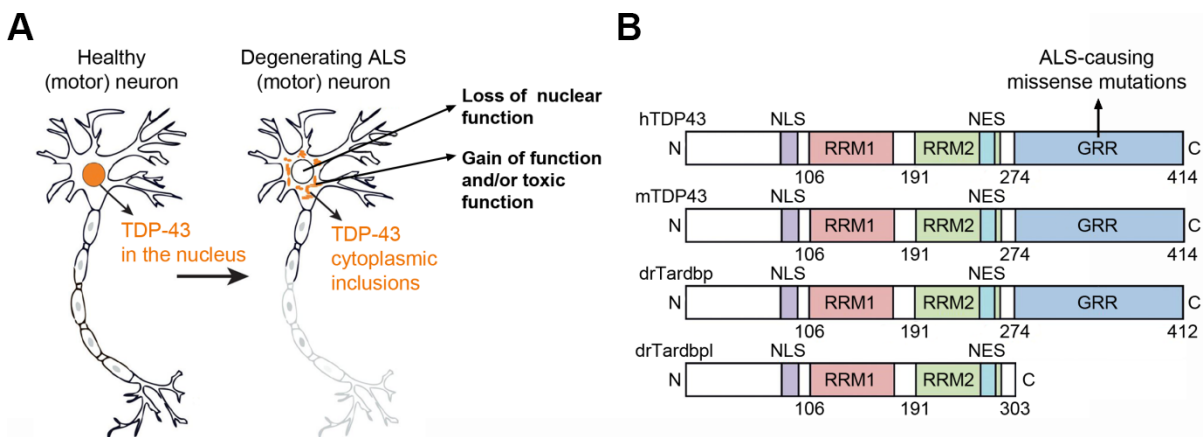


Figure 13. TDP-43 and ALS. (A) TDP-43 redistributes from the neuronal nucleus to the cytoplasm in ALS patients with TDP-43 proteinopathy. Three possible mechanisms that explain TDP-43-mediated neurodegeneration: toxic gain of function, gain of cytoplasmic function, and loss of nuclear function. (B) Schematic representations of the TDP-43 orthologs in humans (hTDP-43), mouse (mTDP-43) and zebrafish (drTardbp and drTardbpl) are shown. TDP-43 proteins share highly conserved RNA-binding domains (RRM1 and RRM2), nuclear localization signal (NLS), nuclear export signal (NES), and glycine rich region (GRR). The numbers represent amino acids (modified after¹⁵⁴).

The identification of pathogenic mutations in the TARDBP encoding gene in ALS patients mechanistically link neurodegeneration to the occurrence of TDP-43 inclusions¹⁵⁹ (Figure 13, B). However, whether neurotoxicity of the TDP-43 inclusions or reduced TDP-43 function upon nuclear clearance is responsible for ALS is unknown and remains under debate (Figure 13, A). To investigate the link between TDP-43 and ALS pathogenesis, several TDP-43 KO models have been generated. Deletion of TDP-43 in mice and zebrafish leads to early embryonic lethality, which preclude the analysis of ALS. TDP-43 deficient zebrafish embryos (herein *tardbp*^{-/-}; *tardbpl*^{-/-} zebrafish embryos) display shortened motor neurons and muscle degeneration¹³¹ (Figure 14).

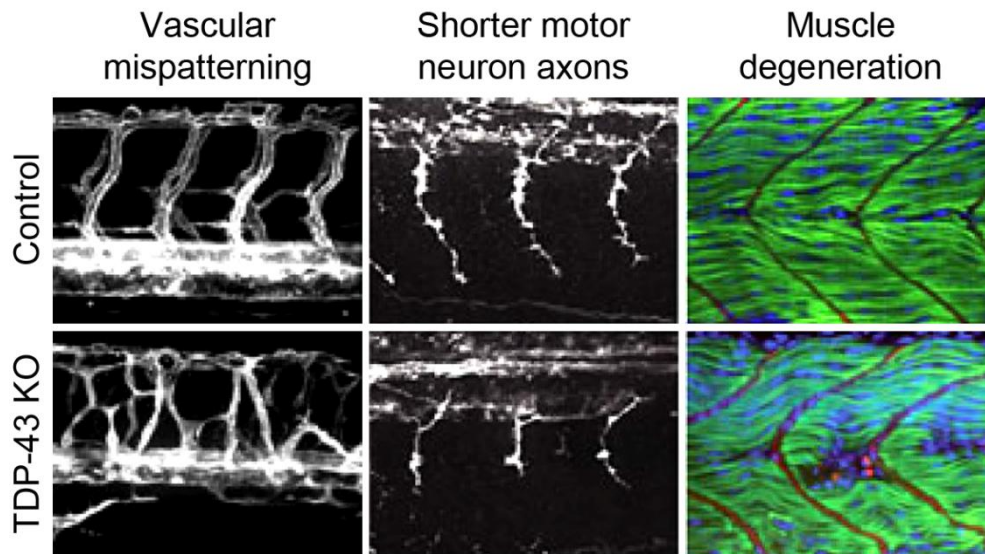


Figure 14. TDP-43 KO phenotypes in zebrafish embryos. Double homozygous loss of TDP-43 orthologues (*tardbp*; *tardbpl*) in zebrafish leads to vascular mispatterning, shorter spinal cord motor neuron axons and muscle degeneration (modified after¹³¹).

Besides motor neuron degeneration and muscle atrophy, ALS patients show impairment of all components of the NVU including EC damage, PE degeneration, astrocyte end-feet capillary dissociation and disrupted barrier function, leading to the classification of the ALS as a neurovascular disease. Interestingly, lethality of *tardbp*^{-/-};*tardbpl*^{-/-} zebrafish embryos is associated with reduced vessel perfusion and vascular miss-patterning, indicating that TDP-43 is required for proper vessel function¹³¹ (Figure 14). Vascular malfunction and disruption of the barrier function has also been found in mouse models of ALS prior to motor neuron degeneration and neurovascular inflammatory response¹⁶⁰. Altogether, these results suggest that endothelial damage, impaired barrier function, and chronic vascular insufficiency might play a central role in the initiation and progression of ALS, preceding neuronal loss. However, whether vascular dysfunction indeed contributes to the human disease remains to be proven. The role of TDP-43 in ECs and its relevance in vascular development and BBB function are unknown and remain to be studied.

1.5 Aim of the thesis

Hypothesis I

Integrin-mediated signaling is essential for vessel growth and vessel stability. How integrins regulate these processes at the molecular level is, however, not completely understood. Parvins are actin-binding proteins that facilitate the interaction of integrins with the actin cytoskeleton and are key regulators of integrin function. We hypothesize that endothelial α -pv and β -pv are critical for EC function and angiogenesis.

This thesis aims at:

- Generate mice with ECs lacking α -pv and β -pv (α -pv ^{Δ EC}; β -pv^{-/-}).
- Unravel the cellular and molecular mechanisms underlying vascular development in mice with ECs lacking α -pv and mice with ECs lacking α -pv and β -pv.
- Determine the role of endothelial α -pv in tumor angiogenesis and tumor growth.

Hypothesis II

Loss of TDP-43 in zebrafish leads to vascular miss-patterning, suggesting an important role of TDP-43 in EC function. The role of TDP-43 in ECs is, however, not known. We hypothesize that TDP-43 controls EC behavior and it is critical for angiogenesis.

This thesis aims at:

- Generate mice with tamoxifen-inducible endothelial-specific depletion of TDP-43 (TDP-43^{i Δ EC}).
- Analyze the vascular phenotype in the retina in TDP-43^{i Δ EC} mice.

2 Materials and Methods

2.1 Materials

2.1.1 Antibodies

BrdU Pure, 347580	Immunofluorescence (IF): 1:50	BD Bioscience
β -catenin, C2206	IF: 1:200	Sigma-Aldrich
CD31, 553370	IF: 1:100	BD Pharmingen
Collagen IV, 2150-1470	IF: 1:50	Bio-Rad
Endocan/Esm1, AF199	IF: 1:200	R&D Systems
Endomucin, MAB2624	IF: 1:200	Millipore
Erg1/2/3, sc-353	IF: 1:100	Santa Cruz
Fibronectin, F3648	IF:1:100	Sigma-Aldrich
GAPDH, MAB374	Western Blot (WB): 1:5000	Millipore
Glut-1, 07-1401	IF: 1:200	Merck
ICAM-2, 553326	IF: 1:200	BD Pharmingen
Isolectin B4 488 conjugated, 121411	IF: 1:200	Invitrogen
Isolectin B4 647 conjugated, I32450	IF: 1:200	Invitrogen
Laminin α 4, 377b serum antibody	IF: 1:10000	<i>kindly provided by Lydia Sorokin</i>
NG2, AB5320	IF: 1:100	Chemicon
α -parvin, 4026	IF: 1:100, WB: 1:1000	Cell signaling

Fehler! Verwenden Sie die Registerkarte 'Start', um Überschrift 1;Ü 1 dem Text zuzuweisen, der hier angezeigt werden soll.

phospho- (p)-paxillin, 2541S	IF: 1:50, WB: 1:1000	Cell Signaling
p-histone 3, 06-570	IF:1:200	Millipore
Paxillin, 610051	WB: 1:1000	BD Biosciences
Phalloidin Cy3 conjugated, A22283	IF: 1:200	Invitrogen
Podocalyxin, AF1556	IF: 1:200	R&D Systems
Rac1, 1862341	WB: 1:1000	Thermo Scientific
α -SMA Cy3 conjugated, A2547	IF: 1:100	Sigma-Aldrich
To-Pro3 Cy5 conjugated, T160.1	IF: 1:1000	Invitrogen
VE-cadherin human, 14-1449-82	IF: 1:100	eBioscience
VE-cadherin mouse, 14-1442-82	IF: 1:100	eBioscience
Vinculin, V9131	IF: 1:200	Sigma-Aldrich
von-Willebrand-Factor, A008229-2	IF: 1:200	Dako

2.1.2 Secondary antibodies

Alexa Flour 488 anti-rat, A21070	IF: 1:200	Invitrogen
Alexa Flour 488 anti-rabbit, A21206	IF: 1:200	Invitrogen
Alexa Flour 546 anti-mouse, A10036	IF: 1:200	Invitrogen
Alexa Flour 546 anti-rabbit A10040	IF: 1:200	Invitrogen
Alexa Flour 546 anti-rat, A11081	IF: 1:200	Invitrogen
Alexa Flour 546 anti-goat, A11056	IF: 1:200	Invitrogen
Alexa Flour 633 anti-rabbit, A21070	IF: 1:200	Invitrogen
Alexa Flour 633 anti-rat, A21094	IF: 1:200	Invitrogen
Alexa Flour 633 anti-mouse, A21052	IF: 1:200	Invitrogen
Peroxidase conj. anti-rabbit, 401393	WB:1:5000	Calbiochem
Peroxidase conj. anti-mouse, 401253	WB:1:5000	Calbiochem
Peroxidase conj. anti-mouse, 401515	WB:1:5000	Calbiochem

Fehler! Verwenden Sie die Registerkarte 'Start', um Überschrift 1;Ü 1 dem Text zuzuweisen, der hier angezeigt werden soll.

2.1.3 Cell culture reagents

Collagenase 2, LS004176	Cell Systems
Collagenase 4, LS004188	Cell Systems
Desoxyribonuclease, LS002139	Cell Systems
Dulbecco's modified eagle's medium (DMEM), 21969-035	Gibco
Endothelial Cell growth medium, C22010	Promocell
Fetal Calf Serum (FCS), S0615	Biochrom
HUVECs, C-12203	Promocell
Medium 199, 3110-022	Gibco
Opti-MEM, 11058-021	Gibco
PELO, PB-MH-100-2190-6	Biotech
Penicillin/Streptomycin (P/S), P0781-100ml	Sigma-Aldrich
Trypsin/EDTA, P10-024100	PAN Biotech

2.1.4 Chemical inhibitors

Complete Protease inhibitor, 04693116001	Roche
Phosphatase inhibitor 100 mM NaF, S6776	Sigma-Aldrich
Phosphatase inhibitor Na_3VO_4 , S-6508	Sigma-Aldrich

2.1.5 Chemicals and reagents

Aqua ad injectabilia, 111208061	Braun
Acrylamid, A1672	AppliChem
Agarose, 35-1020	peqlab
Albumin Fraction V, A1391	AppliChem
APS, 7727-54-0	Sigma-Aldrich

Fehler! Verwenden Sie die Registerkarte 'Start', um Überschrift 1;Ü 1 dem Text zuzuweisen, der hier angezeigt werden soll.

Bromophenol blue, 18040	Fluka
BrdU, B23151	Invitrogen
Calcein, C3100MP	Life Technologies
Dimethylsulfoxid (DMSO), D2650	Sigma-Aldrich
Direct PCR-tail, 31-101-T	PEQLAB Biotechnology
Sheep anti-rat Dyna beads, 11035	Life Technologies
EDTA, 0310	Fluka
Eosin G 0.5%, X883.2	Carl Roth GmbH & Co KG
Ethanol (100% (vol/vol)), 9065.4	Carl Roth GmbH & Co KG
Fluoromount, 0100-01	SouthernBiotech
Formamide, F9037	Sigma
Gelatin, 4070	Merck
GelRed, 41003	Biotium
GeneRuler™ DNA ladder 1kbp, SM313	Thermo Scientific
Glutaraldehyde, 16210	Electron Microscopy Sciences
Glycine, A1067	AppliChem
Glycerol, G6279	Sigma-Aldrich
Hematoxylin solution acidic, T865.2	Carl Roth GmbH & Co KG
Hydrochloric acid (HCl 37%(wt/vol)), 141020.1212	AppliChem
Lipofectamin, 11668-027	Life Technologies
Loading Dye 10x, 1032517	Qiagen
Magnesium chloride, 1005482	Qiagen
β-Mercaptoethanol, A1108	AppliChem
Methanol, 8388.5	Carl Roth GmbH & Co KG
Mounting medium, Roti Histokitt T160-1	Carl Roth GmbH & Co KG
Nonfat-dried milk, A0830	Sigma-Aldrich

Fehler! Verwenden Sie die Registerkarte 'Start', um Überschrift 1;Ü 1 dem Text zuzuweisen, der hier angezeigt werden soll.

Phosphate-buffered saline (PBS)	<i>provided by the pharmacy of "Klinikum Großhadern"</i>
Peanut oil, P2144-1L	Sigma-Aldrich
Paraformaldehyde (PFA), A0877	AppliChem
Poly-L-Lysine, L7240	Biochrom
Proteinase K, 04-1075	peqlab
Protein PageRuler™, 26616	Thermo Scientific
SDS, A1112	AppliChem
Sodium chloride (NaCl), 141659.1211	AppliChem
Sodium desoxycholat, A1531	AppliChem
Sucrose, S-0389	Sigma-Aldrich
Tamoxifen, T5648-1G	Sigma-Aldrich
TEMED, A1148	AppliChem
Tissue-Tek® O.C.T.™, 4583	Sakura
Tris, A2264	AppliChem
Trypsin/EDTA, P10-024100	PAN Biotech
TritonX 100, A4975	AppliChem
Xylol, A2476.5000	AppliChem

2.1.6 Kits

BCA Protein Assay, Reagent A 23228, Reagent B 1859078	Thermo Scientific
Chemiluminescence detection Kit, A3417 1200A/A3417 1200B	AppliChem
Rac1 pull-down Kit, 16118	Thermo Scientific
Taq all inclusive, 01-1001	peqlab

Fehler! Verwenden Sie die Registerkarte 'Start', um Überschrift 1;Ü 1 dem Text zuzuweisen, der hier angezeigt werden soll.

2.1.7 Disposables/Consumables

Angiogenesis System for EC migration, 354144	BD Bioscience
Cell scraper, 353086	Falcon
Coverslips, H 875	Carl Roth GmbH & Co KG
Delimiting Pen, S2002	Dako
60, 100 mm dishes, 353003, 353004	BD Falcon
E-plate 16, 2801032	ACEA Bioscience Inc.
FluoroBlock inserts, 351152	BD Bioscience
Injection needle 30G x ½", 304000	BD Becton Dickinson
Microcentrifuge tubes, 72.690.001, 0030.120.094	Sarstedt/Eppendorf
Nitrocellulose membrane, 39-1010	peqlab
5, 10, 25 ml pipettes, 4497/4488/4489	Corning
6-well plate, 353224	BD Falcon
24-well plate, 353226	BD Falcon
96-well plates, 9017	Costar
8-well slides ibiTreat, 80826	ibidi
slides ibiTreat 0.4 Luer, 80176	ibidi
40 µm cell strainer, 352340	BD Falcon
SuperFrost® slides, 8073/1	ThermoScientific ISO
Tissue embedding mold, 18986	polyscience
15, 50 ml conical tubes, 352096, 352070	BD Falcon
Whatman Gel Blotting Paper, 10426892	Sigma Aldrich

2.1.8 Oligonucleotides

APE2f (forward):

5'-GAAGGAATGAACGCCATCAAC-3'

Fehler! Verwenden Sie die Registerkarte 'Start', um Überschrift 1;Ü 1 dem Text zuzuweisen, der hier angezeigt werden soll.

APloxPf (forward):	5'-CTGAGTGACATGGAGTTTGAG-3'
APloxPr (reverse):	5'-GGACTTGTGGACTAGTTAGAC-3'
CreF (forward):	5'-GCCTGCATTACCGGTCGATGCAACGA-3'
CreR (reverse):	5'-GTGGCAGATGGCGCGCAACACCATT-3'
betapvPGKf/wt:	5'-GAT TAG ATA AAT GCC TGC TC-3'
betapv 1EmBpi2f/KO:	5'-GTG AAC TTC ACT GGA CTC TT-3'
betapv 2BPE3r:	5'-TCC TTG AAC TTG GGG TCT TCT-3'
TDP forward:	5'-TGT TGC TTG TTT GCC ATC TT-3'
TDP reverse:	5'-TCT GTA ACT TCA AGA TCT GAC ACC-3'

2.1.9 siRNA (Sigma-Aldrich)

α -pv SASI_Hs01__00165014	5'-CGACAAUGGUCGAUCCAAA-3'
α -pv SASI_Hs01__00165015	5'-GAACAAGCAUCUGAAUAAA-3'
Scrambled control: SIC001	

2.1.10 Equipment

Centrifuge Rotina 35R	Hettich-Lab-Technologies
Centrifuge Biofuge primoR	Heraeus
Cryotome	Leica CM350 S
Coulter Counter	Beckman Coulter, Z2
Dissection forceps no.5	Fine Science Tools
Dyna Magnet	Invitrogen
Electrophoresis chamber	biorad
Elisa Reader Infinite F200	Tecan
Embedding carousel	Thermo Shandon

Fehler! Verwenden Sie die Registerkarte 'Start', um Überschrift 1;Ü 1 dem Text zuzuweisen, der hier angezeigt werden soll.

Embedding machine	Sakura Tissue-Tek TEC
Flow system	ibidi
Imaging system PCR	Intas Science Image
Incubator	Binder
Microtome	Reichert-Jung 2030
Microcentrifuge	Eppendorf Centrifuge 5410
Microwafe	LG
Rocker-Shaker (mini)	PMR 30; Grant-Bio
Rotator	Renner Variospeed
Short-blade scissors	Fine Science Tools
Spring scissors	Fine Science Tools
Sonicator UP50H	Hielscher
Sterile hood	Steril VBH compact
Thermoblock	Eppendorf Thermomix comfort
Thermocycler PCR	PTC-100® Peltier Thermal Cycler, MJ Research
Ultra-Turrax	Janke and Kunkel KG
Western blotting system	biorad
Waterbath	Haake SWB25
XCelligence system	Roche

2.1.11 Microscopes

Confocal microscope	Leica SP5, Leica
Stereomicroscope	Zeiss Stemi SV11
Fluorescence microscope	Zeiss Axiophot
Inverted microscope	Zeiss Axiovert 25

Fehler! Verwenden Sie die Registerkarte 'Start', um Überschrift 1;Ü 1 dem Text zuzuweisen, der hier angezeigt werden soll.

2.1.12 Hardware and software

Excel	Microsoft
ImageJ	Java
PCR gel imaging software	Intas
Photoshop	Microsoft
Western Blot imaging software	Wasabi software 1.4, Hamamatsu Photonics
XCelligence software	Roche

2.2 Methods

2.2.1 Animals

All mouse lines were bred in the animal facility of the Walter Brendel Center (Munich, Germany). Mice were kept under a 12 hours light cycle and provided with standard rodent diet and water. Three weeks after birth, litters were separated according to sex and ear clips were taken, which served for genotyping. At the age of eight weeks, mice were used for breeding. All experiments were performed in accordance with the German Animal Protection Law.

2.2.1.1 Breeding schemes

2.2.1.1.1 Constitutive KO Cre line

To constitutively delete α -pv in ECs, *Tie2-Cre* transgenic mice¹⁶¹ were crossed with mice carrying a loxP-flanked α -pv gene (referred to herein as α -pv^{fl/fl}) and with α -pv^{fl/fl} β -pv^{-/-} mice.

2.2.1.1.2 Inducible KO Cre line

For endothelial-specific depletion of α -pv, transgenic males expressing the *Cdh5*(PAC)-CreERT2¹⁶² were mated with α -pv^{fl/fl} females, yielding α -pv^{fl/fl}; *Cdh5*(PAC)-CreERT2 offsprings (referred to herein as α -pv^{i Δ EC}). Inactivation of endothelial α -pv in adult mice for tumor experiments was triggered by intraperitoneal injection of 100 μ l tamoxifen solution (20 mg/ml in peanut oil) once daily at P3, P4, and P5 after tumor cell injection.

For endothelial-specific TDP-43 deletion, mice carrying a loxP-flanked *TDP-43* gene (referred to herein as TDP-43^{fl/fl}) were mated with mice expressing the *Cdh5*(PAC)-CreERT2¹⁶², leading to TDP-43^{fl/fl}; *Cdh5*(PAC)-CreERT2 offsprings (referred to herein as TDP^{i Δ EC}). The deletion in newborn mice was triggered by intraperitoneal injection of 50 μ l tamoxifen solution (1 mg/ml) once daily at P1, P2, and P3 after birth. Retinas, brains, and lungs were collected from pups at indicated time points. Tamoxifen stock solution was generated by dilution of 10

Fehler! Verwenden Sie die Registerkarte 'Start', um Überschrift 1;Ü 1 dem Text zuzuweisen, der hier angezeigt werden soll.

mg/ml tamoxifen in 1:4 ethanol: peanut oil; injection solution for pups was achieved by dilution of stock solution in peanut oil.

2.2.2 Mouse models to study angiogenesis

2.2.2.1 The mouse embryo hindbrain

The vascularization of the embryonic hindbrain is an extensively used model to study angiogenesis and permits angiogenic studies in genetically mutated mice that show embryonic lethality around midgestation. The vascularization of the hindbrain takes place through invasive sprouting from vessels outside the CNS^{163,164}. Mouse brain vascularization is initiated around E9.5, when vascular sprouts from the perineural vascular plexus (PNVP) invade the ventricular zone of the neuroepithelium. At around E10.5, these radial vessels begin to grow and branch in parallel to the neuroepithelial surface to form the subventricular vascular plexus (SVP). At E12.5, the SVP has formed an extensive vascular network, and sprouting moves to deeper layers¹⁶⁵ (Figure 15). The first perfusion can be observed around E10.5 but arteriovenous differentiation occurs in later states. However, vessel remodeling and further angiogenic sprouting continues even postnatally due to brain growth^{164,165}.

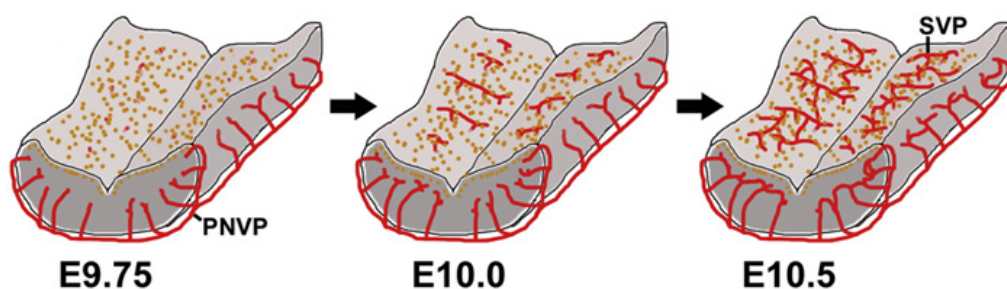


Figure 15. Schematic development of the embryonic mouse hindbrain vascularization. At E9.5 invasive sprouting from the PNVP takes place. At E10.5 the SVP is formed by sprouting parallel to the neuroepithelial surface. PNVP: perineural vascular plexus, SVP: subventricular vascular plexus (modified after¹⁶³).

We characterized the hindbrain vasculatures from α -pv ^{Δ EC} and α -pv ^{Δ EC}; β -pv^{-/-} embryos and the respective control littermates at E11.5. Particularly, we quantified and statistically analyzed a range of morphological parameters including vascular branching points, vessel

Fehler! Verwenden Sie die Registerkarte 'Start', um Überschrift 1;Ü 1 dem Text zuzuweisen, der hier angezeigt werden soll.

diameter, filopodia count, and PE vessel coverage. In addition, the expression and distribution of multiple proteins such as ECM components and membrane transporters were analyzed using immunohistochemistry. Similar analysis was performed to characterize the vascularization of the spinal cord in α -pv^{ΔEC};β-pv^{-/-} embryos.

2.2.2.2 The postnatal mouse retina

The retinal vasculature starts developing from the location of the optical nerve head and grows radially towards the periphery. While forming this planar primary plexus in the ganglion layer of the retina, the sprouts are guided by a template of FN-expressing astrocytes and a VEGF-A gradient which is secreted by astrocytes and neurons¹⁶³. Already during the formation of this plexus, the vessels differentiate into arteries and veins¹⁶⁶. Around postnatal day (P) 8 the superficial vascular plexus reaches the periphery and starts invading into the outer retinal layers at near right angles to form the deep plexus and the intermediate layer^{12,166} (Figure 16).

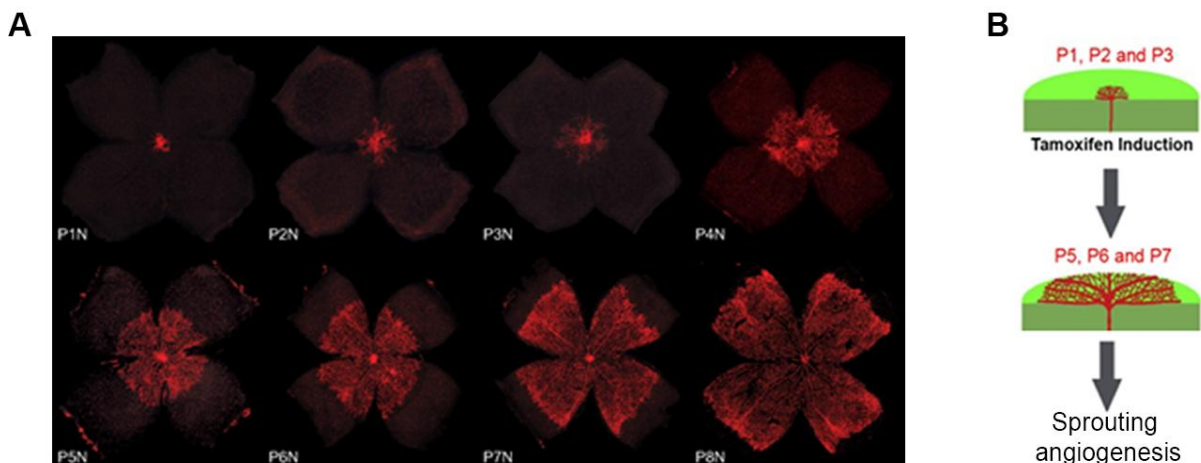


Figure 16. Development of the retinal vasculature. (A) Development of the superficial vascular plexus in the mouse retinas. Retinal whole mounts from P1 to P8 were stained for Isolectin B4 (IB4, red). N (normoxia). During the first week of postnatal development, the superficial plexus extends radially from the optic nerve head into the surrounding tissue, reaching the retinal periphery at ~P8N (B) Tamoxifen induced gene targeting at postnatal day (P) 1, P2, and P3 influences sprouting angiogenesis, which can be visualized at P5 to P7 (modified after^{15,167}).

We used this model to characterize the retinal vasculatures from TDP-43^{iAEC} mice and the respective control littermates at P7 and P8. Particularly, we quantified and statistically analyzed a range of morphological parameters including vessel radial expansion, EC area, vessel sprouting, filopodia per vessel length, and proliferation. In addition, the expression

Fehler! Verwenden Sie die Registerkarte 'Start', um Überschrift 1;Ü 1 dem Text zuzuweisen, der hier angezeigt werden soll.

and distribution of multiple proteins such as tip cell markers, cell-cell adhesion molecules, and vessel lumen markers were analyzed using immunohistochemistry.

2.2.2.3 Tumor angiogenesis in glioblastoma

The glioblastoma experiment was performed in collaboration with Prof. Dr. Rainer Glaß (Neurosurgical Research, LMU Munich) and his team. 8-week old α -pv^{iΔEC} mice and C57BL/6J as control mice were treated with 1 μ l GL261 glioma cell suspension (100.000 cells/ μ l) by intracranial injection¹⁴⁵.

The procedure was done as described previously¹⁶⁸. Briefly, mice were anesthetized with intraperitoneal injections of approximately 100 mg/kg ketamine 10% and 10 mg/kg xylazine 2% in 0.9% NaCl. Then, anesthetized mice were immobilized with a stereotactic head holder. After the skin of the skull was dissected with a scalpel blade, inoculation of GL261 was done 1 mm anterior and 1.5 mm right to the bregma (Figure 17), the skull was carefully drilled with a 23-gauge needle tip and cell suspension was applied 5 mm below the drill hole in the calvarium followed by wound closure by suturing. At P3 to P5 after glioma cell administration, mice were treated with 100 μ l tamoxifen solution (20 mg/ml). At P17 mice were sacrificed, brains were removed and fixed with 4% PFA over night (ON). After treatment with 30% sucrose for 3 days, brains were embedded in TissueTek and stored at -80°C or preceded with cryo sectioning.

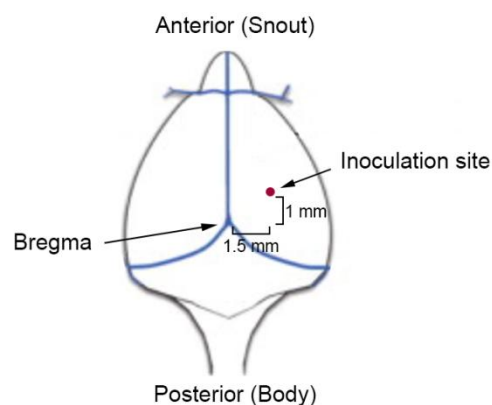


Figure 17. Inoculation site of glioma cells in the mouse brain. Glioma cells were injected 1.5 mm right and 1 mm anterior from the bregma in 5 mm depth (modified after¹⁶⁹).

2.2.3 Histological analysis

2.2.3.1 Preparation of paraffin sections

Embryos were isolated at different time points and YS were carefully removed using a stereomicroscope. Then, embryos were transferred to a 24-well plate and directly fixed with fresh 4% PFA in PBS ON at 4°C. Next day, samples were dehydrated in consecutive ethanol solutions with increasing concentration (2 x 70%, 2 x 96%, 3 x 100%), each for one hour. Then, embryos were transferred to xylol for 180 minutes followed by liquid paraffin for 5 hours. This was achieved by using an automatic embedding carousel. After embedding the embryos in paraffin blocks, they were cut in 10 µm thick sections using a microtome and collected on glass slides coated with Poly-L-Lysin. Slices were dried at 37°C ON and stored at room temperature (RT) until staining.

2.2.3.2 Preparation of cryo sections

The preparation of cryo sections was performed with some changes of the protocol described before¹⁴⁶. Briefly, brains or isolated embryos were transferred to a 24-well plate and directly fixed with fresh 4% PFA in PBS ON at 4°C. The following day, samples were transferred to 30% sucrose in PBS in a 15 ml tube and kept at 4°C for 2-3 days until samples have sunken to the bottom of the tubes. Then, they were embedded in TissueTek and stored at -80°C until cutting. Before proceeding with cutting at a cryotome, samples were transferred to -20°C for 2 hours. Then, embryos were cut into 12 µm thick slices and collected on coverslips and brains were cut into 40 µm thick slices for free floating sections and collected in a 24-well plate with PBS. The coverslips were stored at -20°C and the free floating sections were stored at 4°C until staining.

2.2.3.3 Hematoxylin/Eosin (H&E) staining

H&E staining is a routinely and widely established method to visualize histological structures. Hematoxylin stains basophil structures, as DNA or ribosomes, and is used to visualize the

Fehler! Verwenden Sie die Registerkarte 'Start', um Überschrift 1;Ü 1 dem Text zuzuweisen, der hier angezeigt werden soll.

nucleus in blue, whereas eosin stains acidophil structures in red, such as plasma proteins and mitochondria.

To stain paraffin sections for H&E, sections were deparaffinized by xylol treatment for 2 x 10 minutes, followed by a rehydration row of 100%, 95%, 70% ethanol and PBS each for 10 minutes. Afterwards, slices were transferred to hematoxylin for 5 minutes followed by a wash in running water for 15 minutes. Subsequently, slices were treated with Eosin for 2 minutes followed by a short wash with water. Then, slices were treated with 100% ethanol for 2 minutes and with xylol for 3 minutes. Slices were carefully dried and mounted with Roti-Histokitt mounting medium.

Measurement of tumor size was performed with ImageJ software and calculated with Excel software.

2.2.4 Immunological analysis

2.2.4.1 Whole embryo and tissue immunohistochemistry

Embryos, skin fragments, and YS were dissected in a dish with ice cold PBS and fixed in Dent's fixative ON at 4°C. The following day, samples were rehydrated in 0.1% TritonX 100 in PBS for 2 hours, incubated in blocking buffer for 2 hours and exposed to indicated primary antibodies (diluted in blocking buffer) ON at 4°C. Next day, samples were washed 5-7 hours in 0.1% TritonX 100 in PBS and incubated with appropriate secondary antibodies (diluted in blocking solution) ON at 4°C protected from light. After three washes the following day (each for 1 hour), samples were imaged or mounted on glass slides with Fluoromount before imaging.

Dent's fixative: 80% methanol, 20% DMSO

Blocking buffer: 0.1% TritonX 100, 5% BSA in PBS

2.2.4.2 Hindbrain immunohistochemistry

The dissection and immunofluorescent staining of the hindbrains was performed as previously described¹⁶⁴. Embryos were isolated after sacrificing the mother at indicated time points. Embryos were transferred to a dish of ice cold PBS and hindbrain dissection was performed under a stereomicroscope. After cutting the head and face with a scalpel, the thin roof plate was ruptured with forceps until the hindbrain was visible. After removing the tissue from underneath the hindbrain and cutting off midbrain and spinal cord, the unfurled hindbrain was fixed with 4% PFA in PBS for 2 hours on ice shaking. Then, hindbrains were blocked in blocking buffer for 2 hours at RT and incubated with indicated primary antibodies ON at 4°C. Next day, three washes were performed with washing buffer. Afterwards, hindbrains were incubated in appropriate secondary antibodies for 2 hours at RT protected from light, washed again three times and were flat-mounted on glass slides with Fluoromount. Several parameters were calculated in the hindbrains; branching points per field, vessel diameter, filopodia count, vessel length, and PE coverage. ImageJ software was used for measurements.

Blocking buffer: 0.1% TritonX 100, 1% BSA in PBS

Washing buffer: dilution of blocking buffer in PBS 1:1

2.2.4.3 Whole retina immunohistochemistry

The dissection and immunofluorescent staining of the retinas was performed as previously described¹⁷⁰. The pups were sacrificed at indicated time points, the eyes were collected and immediately fixed with ice cold 4% PFA in PBS for 2 hours on ice shaking. Then, retinas were dissected by removing the cornea, iris, vitreous and hyaloid vessels using a stereomicroscope. Retinas were blocked in blocking buffer for 2 hours at RT and incubated with indicated primary antibodies ON at 4°C. The following day, after three washes with washing buffer, retinas were incubated in secondary antibodies for 2 hours at RT protected from light, washed again three times and flat-mounted on glass slides with Fluoromount. Several parameters were analyzed in retina whole mounts; radial expansion from the optical nerve to the edge of the primary plexus, EC area, sprout number, and filopodia number. For

Fehler! Verwenden Sie die Registerkarte 'Start', um Überschrift 1;Ü 1 dem Text zuzuweisen, der hier angezeigt werden soll.

measurements ImageJ software was used.

Blocking buffer: 0.3% TritonX 100, 1% BSA in PBS

Washing buffer: dilution of blocking buffer in PBS 1:1

2.2.4.4 Immunohistochemistry of cryo and paraffin sections

For visualizing intracellular proteins on paraffin sections, sections were deparaffinized by xylol treatment for 2 x 10 minutes followed by a rehydration row of 100%, 95%, 70% ethanol and PBS, each for 10 minutes. Then, sections were fixed with 2% PFA in PBS for 10 minutes, permeabilized with 0.1% TritonX 100 in PBS for 30 minutes and blocked for 1 hour in blocking buffer at RT. After blocking, the sections were incubated with indicated primary antibodies (diluted in blocking buffer) for 1 hour at RT and after three washes with PBS they were incubated with appropriate secondary antibodies (diluted in blocking buffer) for 1 hour at RT in the dark. After another three washes, slices were dried and covered with glass coverslips using Fluoromount. All steps were performed in a humidified chamber. For the staining procedure a delimiting pen was used. After imaging, vessel diameters were measured with ImageJ software.

Staining of cryo section on glass slides was performed similar to paraffin section staining, beginning from the blocking step for 1 hour. Proliferation was analyzed by counting pH3 positive cells/ EC area and EC area was measured with ImageJ software.

For staining free floating cryo sections, the sections were post fixed with 4% PFA in PBS for 10 minutes at RT, sections were immunostained with indicated primary antibodies in blocking buffer for 2 days at 4°C shaking, and incubated with appropriate secondary antibodies in blocking buffer ON at 4°C protected from light. After three washes with PBS (each for 10 minutes), sections were mounted on glass slides with Fluoromount. In tumor sections, vessel area per field was measured with ImageJ software.

Blocking buffer: 0.1% TritonX 100, 1% BSA in PBS

2.2.4.5 Immunofluorescent staining of cells

All immunostainings of adherent cells were performed on glass coverslips or 8-well slides. Coverslips and slides were coated with 0.1% gelatin or with coating reagents (a crosslinked coating of poly-L-lysine, glutaraldehyde, and gelatin) for 1 hour at 37°C. Cells were seeded in different concentrations and cultured in an incubator for indicated time spans (see 2.2.7). Then, cells were washed once with PBS, fixed with 4% PFA in PBS for 15 minutes, permeabilized with 0.1% TritonX 100 in PBS for 30 minutes and blocked in blocking buffer for 1 hour. After blocking, cells were incubated with indicated primary antibodies (diluted in blocking buffer) ON at 4°C and after three washes with PBS (each for 10 minutes), incubated with appropriate secondary antibodies (diluted in blocking buffer) for 2 hours at RT in the dark. After another three washes (each for 10 minutes), coverslips were mounted on glass slides with Fluoromount. 8-well slides were covered with Fluoromount and a glass coverslip.

Blocking buffer: 0.1% TritonX 100, 1% BSA in PBS

2.2.4.6 Proliferation assay

Proliferating cells in the mouse retina were labeled using Bromodeoxyuridine (BrdU) as described previously¹⁷⁰. BrdU is a thymidine analog that replaces thymidine during S-phase of dividing cells. 3 hours prior to eye collection of the mouse, 300 µg of BrdU was administered intraperitoneally to the pups. After dissection and labeling the retina (see 2.2.4.3) with isolectin-B4 (IB4) to visualize the vasculature and Erg1/2/3 to tag the endothelial nuclei, retinas were post-fixed in 4% PFA for 30 minutes, washed three times with PBS and incubated for 1 hour in formamide-SSC solution at 65°C to denature and expose the BrdU-labeled DNA. Further 30 minutes of incubation in a 2N HCl solution at 37°C completed the exposure of the halogenated nucleotide antigen, which then could be visualized with anti-BrdU antibody after ON incubation at 4°C and appropriate secondary antibody incubation for 2 hours the next day. Quantification was done by manually counting BrdU-positive, Erg1/2/3-positive ECs and BrdU-negative, Erg1/2/3-positive ECs in high-resolution confocal images (at least 14 images per group).

SSC 20x: 4.825 g NaCl, 22.05 g sodium citrate with additional ddH₂O, total volume 250 ml

Fehler! Verwenden Sie die Registerkarte 'Start', um Überschrift 1;Ü 1 dem Text zuzuweisen, der hier angezeigt werden soll.

(pH 7.0)

Formamide-SSC solution: 50% formamide, 5% 20x SSC with additional ddH₂O

2.2.5 Biochemical methods

2.2.5.1 Preparation of protein lysates

2.2.5.1.1 Protein lysates from mouse lungs and brains

Lungs and brains were isolated from mice at different time points. Samples were washed in ice cold PBS and transferred to an appropriate amount of lysis buffer (amount according to sample size) and shredded with an Ultra-Turrax. Afterwards, the samples were sonicated (100% amplitude for 5 cycles), centrifuged for 15 minutes at 4°C, and stored at -20°C until use.

Lysis buffer: 50 mM Tris-HCL (pH 8.0), 150 mM NaCl, 0.1% TritonX 100, 0.5% sodium deoxycholat, 0.1% SDS, 5 mM EDTA, 40 µl/ml Complete, 5 µl/ml NaF, 5 µl/ml Na₃VO₄

2.2.5.1.2 Protein lysates from adherent cells

Adherent cells were washed once with ice cold PBS, treated with an appropriate amount of lysis buffer, and scraped on ice with a cell scraper. The lysates were transferred to microcentrifuge tubes, sonicated at 4°C (100% amplitude for 5 cycles), and centrifuged at 13000 rpm at 4°C. The supernatant was stored at -20°C until use.

Lysis buffer: 50 mM Tris-HCL (pH 8.0), 150 mM NaCl, 0.1% TritonX 100, 0.5% sodium deoxycholat, 0.1% SDS, 5 mM EDTA, 40 µl/ml Complete, 5 µl/ml NaF, 5 µl/ml Na₃VO₄

2.2.5.2 Protein quantification assay

The Bicinchoninic acid assay (BCA) was used to determine protein concentrations in lysates. The assay was done according to the manufacturer's protocol of the BCA Kit. Proteins reduce

Fehler! Verwenden Sie die Registerkarte 'Start', um Überschrift 1;Ü 1 dem Text zuzuweisen, der hier angezeigt werden soll.

Cu^{2+} , which is then detected by bicinchoninic acid that is chelated by Cu^+ ions forming a purple complex. The amount of protein was quantified by measuring the high spectrophotometric absorbance of the complex at 550 nm with an Elisa reader and calculated with Excel software.

2.2.5.3 SDS-polyacrylamide-gel electrophoresis (SDS-PAGE)

SDS-PAGE is a widely used method to separate proteins. Proteins become negatively charged inside the SDS containing gel and therefore can be separated by their electrical charge according to molecular size. Protein lysates were boiled with Laemmli buffer for 5 minutes at 95°C before loading. Then, they were separated in a gel with two different buffered layers; a stacking and a resolving layer. In the stacking layer proteins are concentrated before entering the resolving layer. In the resolving layer the proteins get separated according to molecular size by application of 90 Volt for at least 60 minutes. The gel is fully surrounded by running buffer. 1kDA gene ruler was added as a size marker.

Laemmli buffer (6 x): 1.2 g SDS, 6 mg bromphenol blue, 4.7 ml glycerol, 1.2 ml Tris (0.5 M, pH 8.0), 4.1 ml H_2O , 5% β -mercaptoethanol

Stacking gel: 4.1 ml H_2O , 3.3 ml Acrylamid, 2.5 ml 0.5 M Tris-HCL (pH 6.8), 0.1 ml 10% SDS, 50 μl 10% APS, 10 μl TEMED

Resolving gel: 4.1 ml H_2O , 3.3 ml Acrylamid, 2.5 ml 1.5 M Tris-HCL (pH 8.8), 0.1 ml 10% SDS, 50 μl 10% APS, 5 μl TEMED

Running buffer: 25 mM Tris-base, 190 mM glycine, 0,1% SDS (pH 8.3)

2.2.5.4 Western blotting and immunodetection

After separating the proteins in SDS-PAGE, they were transferred to a nitrocellulose membrane via a semi-dry transfer sandwich. The membrane and blotting papers were equilibrated in transfer buffer and proteins were transferred at 80 mA for 1 hour at RT. After the membrane has been washed shortly in washing buffer and blocked in 5% nonfat milk in

Fehler! Verwenden Sie die Registerkarte 'Start', um Überschrift 1;Ü 1 dem Text zuzuweisen, der hier angezeigt werden soll.

washing buffer for 1 hour at RT, it was incubated with primary antibodies (diluted in washing buffer with 5% BSA) ON at 4°C. Next day, the membrane was washed 3 x 10 minutes with washing buffer and incubated with secondary antibodies (diluted in washing buffer with 5% nonfat-dried milk) for 2 hours at RT. After 3 x 10 minute washes, protein bands were visualized with a chemiluminescence-based detection kit and Wasabi software 1.4. Quantification of western blots was done with ImageJ software.

Transfer buffer: 5.8 g Tris-base, 2.9 g glycine, 0.37 g SDS, 100 ml methanol in 1 l H₂O

Washing buffer (10 x): 300 g Tris-base, 438.5 g glycine, in 5 l H₂O (pH 7.5)

2.2.5.5 Protein pull-down assay

For the analysis of active Rac1, a Rac1 pull-down Kit was used. Cells were washed once with ice cold PBS, lysed with an appropriate amount of lysis buffer, scraped with cell scraper and incubated for 5 minutes on ice shaking. After sonification (100% amplitude for 5 cycles) of the lysates, a BCA assay to determine the amount of protein was performed (see 2.2.5.2). The experiment was done according to the manufacturer's protocol. Briefly, cell lysates were incubated with GST-human PAC-1 and agarose beads for 1 hour on 4°C shaking. After centrifugation and several washing steps of the resin, the bound active Rac1 to the beads was lysed with reducing sample buffer and stored at -20°C until proceeding with western blot analysis (see 2.2.5.4).

2.2.6 Molecular biological methods

2.2.6.1 Extraction of DNA

For isolating mouse DNA, ear clips were transferred to microcentrifuge tubes, lysed ON at 55°C with 250µl of DirectTail lysis buffer containing 1% proteinase K. Next day, samples were centrifuged at 10000 rpm for 10 minutes and further used for genotyping (see 2.2.6.2).

Fehler! Verwenden Sie die Registerkarte 'Start', um Überschrift 1;Ü 1 dem Text zuzuweisen, der hier angezeigt werden soll.

2.2.6.2 Polymerase chain reaction (PCR)

PCR is a widely used method for amplifying DNA fragments. The PCR reaction consists of a DNA template, primers, dNTPs and DNA polymerase.

2.2.6.2.1 PCR reactions

The following PCR reactions were performed during this study. Reagents from the Taq Kit were used.

α pv-flox-PCR/ β pv-flox-PCR

Isolated DNA	1 μ l
H ₂ O	15.8 μ l
10x buffer	2 μ l
dNTPs 1mM	0.4 μ l
10 μ M Primer1	0.2 μ l
10 μ M Primer2	0.2 μ l
10 μ M Primer3	0.2 μ l
Taq	0.2 μ l

Cre-PCR

Isolated DNA	1 μ l
H ₂ O	16.8 μ l
10x buffer	2 μ l
dNTPs 1mM	0.6 μ l
10 μ M Primer1	0.1 μ l
10 μ M Primer2	0.1 μ l
Taq	0.2 μ l

TDP-PCR

Isolated DNA	1 μ l
H ₂ O	4.55 μ l
10x buffer	2.40 μ l
25 mM MgCl ₂	0.96 μ l
dNTPs 10 mM	0.24 μ l
20 μ M Primer 1	0.30 μ l
20 μ M Primer 2	0.30 μ l
Taq	0.05 μ l

10x buffer: 1.00 ml Tris-Cl (pH 8.4), 2.50 ml KCl, 0.15 ml MgCl₂, 6.35 ml ddH₂O

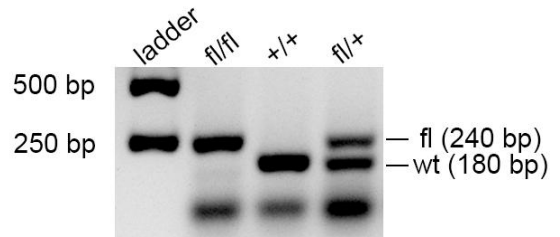
Fehler! Verwenden Sie die Registerkarte 'Start', um Überschrift 1;Ü 1 dem Text zuzuweisen, der hier angezeigt werden soll.

2.2.6.2.2 PCR programs

Programme α v-flox-PCR

Lid Temp. 105°C
Preheating on

1. 95°C 5min
2. 95°C 30s
3. 53°C 30s
4. 72°C 30s go to step 2 cycle 34
5. 72°C 5min
6. 4°C hold

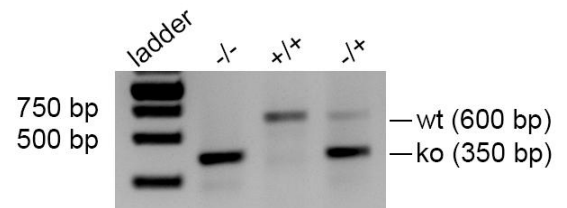


Product size: wt: 180 bp// fl: 240 bp

Programme β pv-flox-PCR

Lid Temp. 105°C
Preheating on

1. 95°C 5min
2. 95°C 30s
3. 53°C 30s
4. 72°C 30s go to step 2 cycle 34
5. 72°C 5min
6. 4°C hold

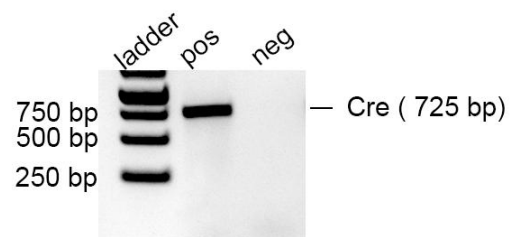


Product size: wt: 600bp//ko: 350bp

Programme Cre-PCR

Lid Temp. 105°C
Preheating on

1. 95°C 5min
2. 95°C 45s
3. 70°C 45s
4. 72°C 1min go to step 2 cycle 34
5. 72°C 5min
6. 4°C hold

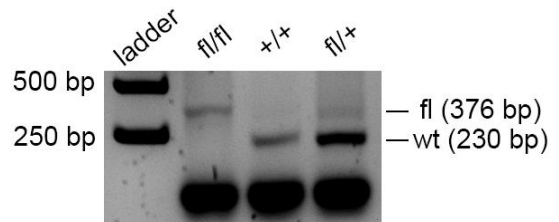


Product size: 725 bp

Fehler! Verwenden Sie die Registerkarte 'Start', um Überschrift 1;Ü 1 dem Text zuzuweisen, der hier angezeigt werden soll.

Programme TDP-PCR

Step #	Temp °C	Time
1.	94°C	2 min
2.	94°C	20sec
3.	65°C	15sec -0.5 C per cycle decrease
4.	68°C	10sec
5.		repeat steps 2-4 for 10 cycles
6.	94°C	15sec
7.	60°C	15sec
8.	72°C	10sec
9.		repeat steps 6-8 for 28 cycles
10.	72°C	2 min
11.	10°C	hold



Product size: wt: 230 bp// fl: 376 bp

2.2.6.3 Agarose gel electrophoresis

Agarose gel electrophoresis is commonly used for separating DNA fragments. Agarose gels were prepared by mixing an appropriate amount of agarose (1-2%) with TAE buffer. Then, the mixture was boiled in a microwave, supplemented with an adequate amount of GelRed (0,5%), and poured into a casting tray for cooling down. The polymerized gel was transferred into an electrophoresis chamber and loaded with the samples (samples were mixed with 10x loading dye). 100-150 Volt were applied to the chamber for approximately 30-50 minutes. A 1kb DNA ladder was used as a size marker. After completing the electrophoresis, the gel was imaged at 366nm UV light with Intas GDS machine and software.

TAE buffer: 242 g Tris, 18.0 g EDTA 2 H₂O, 57.1 ml acetic acid, add H₂O to 1 l (pH 8.3)

2.2.6.4 Lipofectamin transfection

Before the transfection of cells, human umbilical vein endothelial cells (HUVECs) were cultured until 70-80% confluency on a 6-well plate. The transfection was done with two different siRNAs against α -pv by using SASI_Hs01__00165014 and SASI_Hs01_00165015 (100 μ M) and scrambled control. Lipofectamin 2000 transfection reagent and siRNA were diluted 1:250 in reduced serum medium (Opti-MEM). Cells were starved with Opti-MEM medium for

Fehler! Verwenden Sie die Registerkarte 'Start', um Überschrift 1;Ü 1 dem Text zuzuweisen, der hier angezeigt werden soll.

30 minutes before being treated with the transfection mixture. Cells were incubated for 6 hours at 37°C, 5% CO₂ and 95% humidity. After the incubation time, Opti-MEM medium was replaced with culture medium and cells were cultured for 72 hours before further use.

2.2.7 Cell culture

Cell culture was performed under a sterile hood using sterile working methods. Cells were cultivated in an incubator providing 37°C, 5% CO₂ and 95% humidity. Cells were centrifuged at 1200 rpm for 5 minutes for pelleting.

2.2.7.1 Culture of HUVECs

HUVECs were purchased from Promocell and cultured with culture medium.

Cells were stored at -80°C for short term (up to 6 months) or in liquid nitrogen (-196°C) for longer term storage. For freezing the cells, they were trypsinized for 5 minutes at 37°C, trypsin was stopped with culture medium, the suspension was centrifuged and medium was completely aspirated before resuspending the cells in ice cold freezing medium. Cells were transferred to cryogenic vials on ice and kept at -80°C.

For taking cells into culture, vials were defrozen at 37°C in a water bath. Then, cells were immediately added to 6 ml of culture medium, centrifuged, resuspended in culture medium and plated on gelatin coated (0.1%) cell culture plates until confluency if not indicated otherwise. Cells were used for experiments in passage three or four. Western blot analysis (see 2.2.5.4) or immunofluorescence staining (see 2.2.4.5) for the EC marker VEcad was used to characterize ECs.

Culture medium: ECGM and Medium 199 mixed 1:1, 1% Penicillin/Streptomycin, 10% FCS

Freezing medium: 90% FCS, 10% DMSO

2.2.7.2 Migration assay

For the migration assay a modified Boyden chamber for EC migration was used which consists of FluoroBlock inserts for a 24-well plate. The two chambers are separated by a FN coated membrane through which cells can transmigrate using 3 μm pores. When transmigrated to the lower side of the membrane, cells were labeled with calcein for 90 minutes and detected by fluorescence measurement.

Cultured HUVECs were trypsinized for 5 minutes at 37°C to determine the cell number using a Coulter Counter. 200000 cells/ml were plated in the upper chamber with serum free Medium 199, while medium with 10% FCS was filled into the lower chamber. After 22 hours of incubation, the membrane was incubated with 4 $\mu\text{g}/\mu\text{l}$ calcein for 90 minutes and detected with an Elisa Reader at 488 nm and imaged with confocal microscopy. To analyze the number of transmigrated HUVECs, cells per image were counted. 8 images were taken per group in each experiment.

2.2.7.3 Transendothelial cell resistance (TEER)

TEER is a method to monitor monolayer formation using transendothelial impedance measurement of the forming monolayer. HUVECs were trypsinized, counted, and plated in E-plates onto a gold electrode and transendothelial resistance was recorded by electric cell-substrate impedance sensing during monolayer formation. E-plates were equilibrated with 100 μl culture medium for 30 minutes at RT before plating 50000 cells/well in additional 100 μl culture medium. Impedance was recorded for 24 hours in an XCelligence system and analyzed with XCelligence software.

Culture medium: ECGM and Medium 199 mixed 1:1, 1% Penicillin/Streptomycin, 10% FCS

2.2.7.4 Isolation of mouse ECs

Tissue from mouse embryos, brains or lungs were used for EC isolation. ECs were isolated either for cultivation and immunostaining or for western blot analysis.

Fehler! Verwenden Sie die Registerkarte 'Start', um Überschrift 1;Ü 1 dem Text zuzuweisen, der hier angezeigt werden soll.

Embryos or tissue from pups were cut into small pieces after PBS washing and were transferred to 3 ml/animal digestion solution. Samples were incubated at 37°C for 1 hour on a rotator and vortexed every 10 minutes. Next, samples were filtered through a 40 µm cell strainer with 5 ml isolation medium. Samples were centrifuged at 1200 rpm for 5 minutes and resuspended in 5 ml buffer followed by another centrifugation step. Samples were resuspended in 100 µl buffer/animal with additional 100 µl VEcad-coated Dynabeads solution and incubated for 30 minutes at RT protected from light. After incubation, VEcad-positive cells were purified by 5 washes in buffer with Dyna magnets and plated in culture medium on 8-well slides or glass coverslips until confluency was reached. Cells were used in passage one.

Digestion solution: collagenase 2 2.5 mg/ml, collagenase 4 2.5 mg/ml, desoxyribonuclease 1 mg/ml, 10% FCS in PBS

Isolation medium: DMEM + 10% FCS

Buffer: PBS + 1% P/S + 1%FCS

Bead solution: 6 µl/animal sheep anti-rat Dyna beads were washed 5 times in buffer with the Dyna magnet, incubated with 6 µl VEcad antibody/animal for 1-2 hours at RT protected from light, washed 3 times and resuspended in 100 µl buffer/animal

Culture medium: ECGM, 1% Penicillin/Streptomycin, 10% FCS

2.2.8 Statistical analysis

Statistical analysis was performed using the unpaired Student's *t*-Test calculated with Excel software after testing for normal distribution. When more than two groups were analyzed, the two sided Anova test, followed by a post hoc Dunnet test was calculated with Stata11. All data is shown as mean ± SEM (standard error of the mean). At least three independent experiments were performed per experimental group. P-values lower than 0.05 (*), 0.01 (**), 0.001 (***) or 0.0001 (****) were considered significant.

3 Results

3.1 Role of parvins in ECs during angiogenesis

The results of the first part are already published. The results of the second part were recently submitted:

Endothelial alpha-parvin controls integrity of developing vasculature and is required for maintenance of cell-cell junctions. Fraccaroli A*, **Pitter B***, Taha AA, Seebach J, Huveneers S, Kirsch J, Casaroli-Marano RP, Zahler S, Pohl U, Gerhardt H, Schnittler HJ, Montanez E. *Circ Res.* 2015 117(1):29-40. (**equal contribution*)

Parvins are required for apical-basal polarity of endothelial cells during embryonic blood vessel formation. **Bettina Pitter**, Ann-Cathrin Werner, Eloi Montanez, ATVB 2017; *manuscript submitted 29th September 2017.*

3.1.1 Analysis of α -pv functions in ECs

3.1.1.1 Deletion of α -pv in ECs in mice leads to embryonic lethality associated with hemorrhages

To determine the function of α -pv in ECs, mice carrying a *loxP*-flanked α -pv gene (α -pv^{fl/fl}) were crossed with mice expressing the Cre recombinase under the *Tie-2* promoter (*Tie2-Cre*)¹⁶¹. Intercrosses between α -pv^{fl/+};Tie2-Cre males and α -pv^{fl/+} females failed to yield viable newborn α -pv^{fl/fl};Tie2-Cre (referred to herein as α -pv ^{Δ EC}) mice, indicating that *Tie2*-mediated deletion of α -pv gene is embryonically lethal (Figure 18).

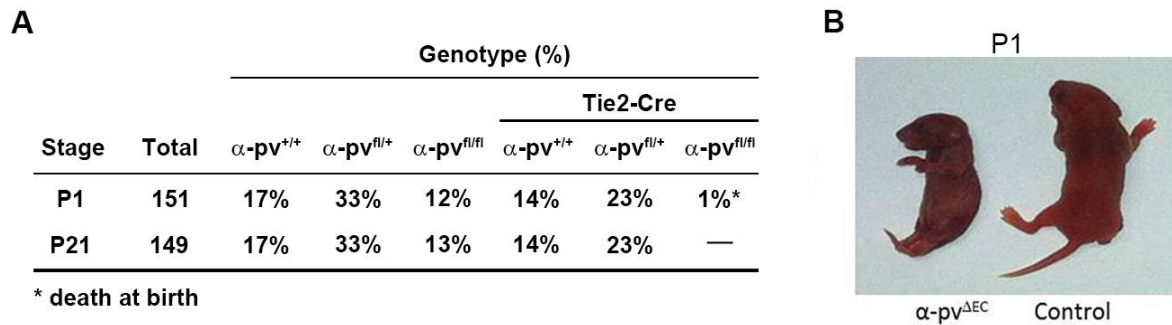


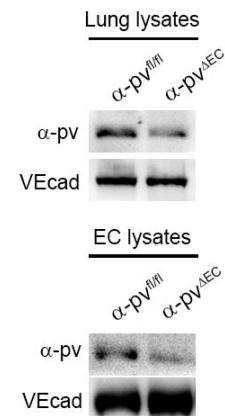
Figure 18. Deletion of endothelial α -pv is embryonically lethal. (A) Genotypes of the progeny from α -pv^{fl/+};Tie2-Cre males and α -pv^{fl/+} females intercrossoes. (B) Representative images of P1 α -pv ^{Δ EC} and control mice. The analysis showed that at P1 all α -pv ^{Δ EC} mice were dead (modified after¹⁰⁸).

To determine when α -pv ^{Δ EC} embryos die, we performed time-mating intercrossoes between α -pv^{fl/+};Tie2-Cre males and α -pv^{fl/fl} females and found that α -pv ^{Δ EC} embryos were present at expected Mendelian ratio up to E15.5 and that lethality of α -pv ^{Δ EC} embryos started at E14.5 (Figure 19, A). By E13.5, α -pv ^{Δ EC} embryos were slightly smaller and showed subcutaneous hemorrhages in the head and trunk areas (Figure 19, B). Western blot analysis of lung and EC lysates from E13.5 control and α -pv ^{Δ EC} embryos showed reduced protein levels of α -pv in α -pv ^{Δ EC} embryos compared to control littermates (Figure 19, C). H&E staining of histological cross-sections of E15.5 embryos confirmed the presence of hemorrhages in α -pv ^{Δ EC} embryos (Figure 19, D).

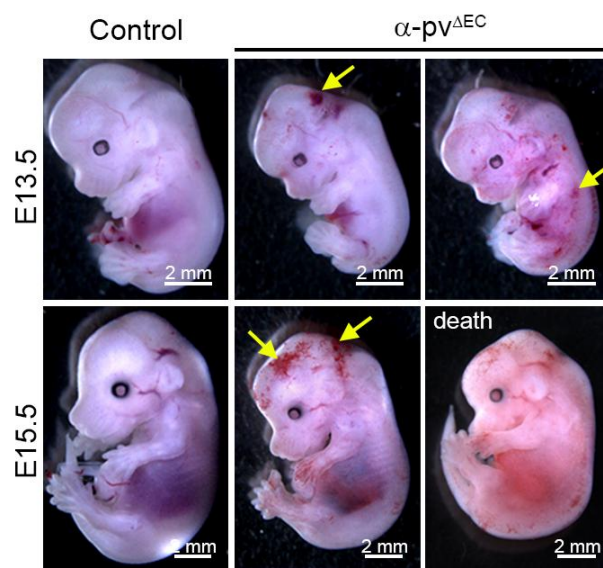
A

Stage	Total	Resorb	Genotype (%)			
			α -pv ^{fl/fl}		Tie2-Cre	
			α -pv ^{fl/+}	α -pv ^{fl/fl}	α -pv ^{fl/+}	α -pv ^{fl/fl} (alive)
E13.5	136	4	17%	22%	36%	25% (100%)
E14.5	52	1	25%	21%	31%	23% (91%)
E15.5	128	7	21%	20%	36%	24% (70%)
E17.5	32	2	25%	20%	43%	12% (40%)
E18.5	33	3	27%	25%	33%	15% (40%)

C



B



D

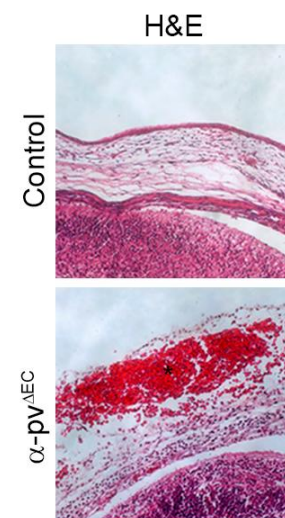


Figure 19. Loss of endothelial α -pv leads to hemorrhages and late embryonic lethality. (A) Genotypes of the embryonic progeny from α -pv^{fl/+};Tie2-Cre males and α -pv^{fl/fl} females intercrossoes. (B) Freshly dissected E13.5 and E15.5 control and α -pv ^{Δ EC} embryos. Arrows indicate bleeding areas. (C) Western blot of lung and EC lysates from α -pv ^{Δ EC} and control embryos showed downregulation of α -pv expression in α -pv ^{Δ EC} lysates compared to control lysates. VEcad was used as a loading control. (D) H&E staining of paraffin sections of E15.5 α -pv ^{Δ EC} and control embryos. Asterisk indicates bleeding area (modified after¹⁰⁸).

3.1.1.2 Altered vascular morphology in α -pv ^{Δ EC} mice

To investigate the vascular abnormalities in α -pv ^{Δ EC} embryos, we performed whole-mount immunostaining for the EC marker CD31, of YS and skin of E15.5 control and α -pv ^{Δ EC} embryos. The analysis showed a disorganized and tortuous vascular network in α -pv ^{Δ EC} embryos compared to the homogenous organization of the vasculature in control embryos (Figure 20, A, B). Furthermore, capillaries of the α -pv ^{Δ EC} embryos displayed reduced diameter and appeared unstable compared to the capillaries of control embryos. Occasionally, we observed micro-aneurysms in α -pv ^{Δ EC} embryos (Figure 20, C).

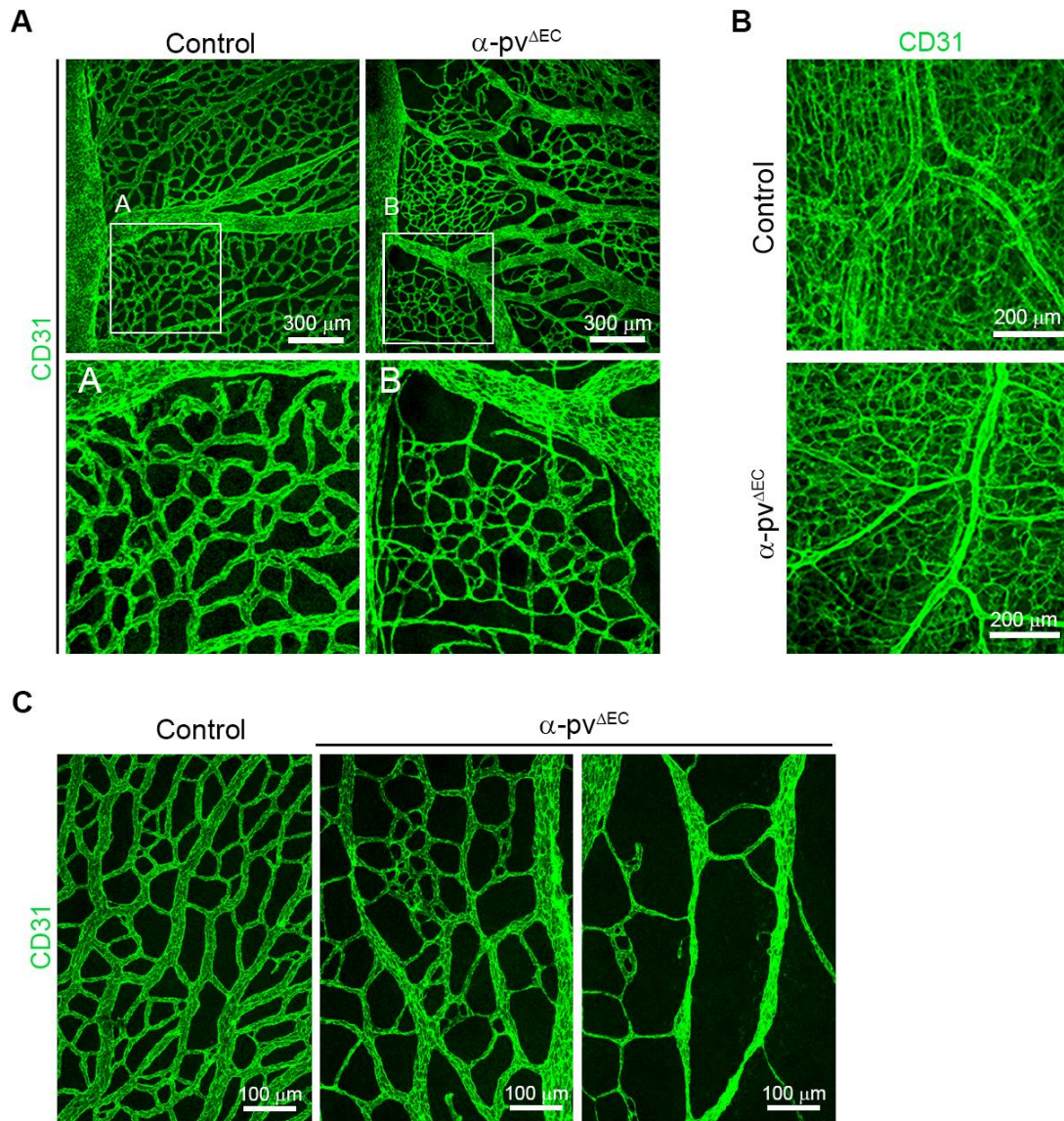


Figure 20. Abnormal vessel morphology in α -pv^{AEC} tissues. (A) Representative images of whole-mounts of YS immunostained for CD31 displayed an irregular and tortuous vascular network and instable vessel morphology in α -pv^{AEC} compared to controls. A and B show higher magnifications. (B) Embryonic skin whole-mounts of α -pv^{AEC} embryos showed reduced vascular density and a less developed vascular network in α -pv^{AEC} tissues compared to control tissues. (C) Capillaries of YS in α -pv^{AEC} embryos displayed reduced diameters compared to control embryos (modified after¹⁰⁸).

3.1.1.3 Normal mural cell coverage of vessels in α -pv^{AEC} embryos

During angiogenesis, mural cells are recruited to newly formed vessels to add vessel stability¹³⁴. Since α -pv is necessary for recruiting mural cells to the vessel wall in embryos¹⁰¹, we analyzed the coverage of vessels by mural cells in control and α -pv^{AEC} embryos. To do this, we performed whole-mount immunostainings of YS and skin from E15.5 α -pv^{AEC} and control embryos with antibodies against α -smooth muscle actin (α SMA) and CD31. The

Fehler! Verwenden Sie die Registerkarte 'Start', um Überschrift 1;Ü 1 dem Text zuzuweisen, der hier angezeigt werden soll.

analysis showed comparable mural cell coverage of vessels in α -pv ^{Δ EC} and control embryos (Figure 21), suggesting that *Tie2*-mediated deletion of α -pv did not alter mural cell recruitment to the vessel wall.

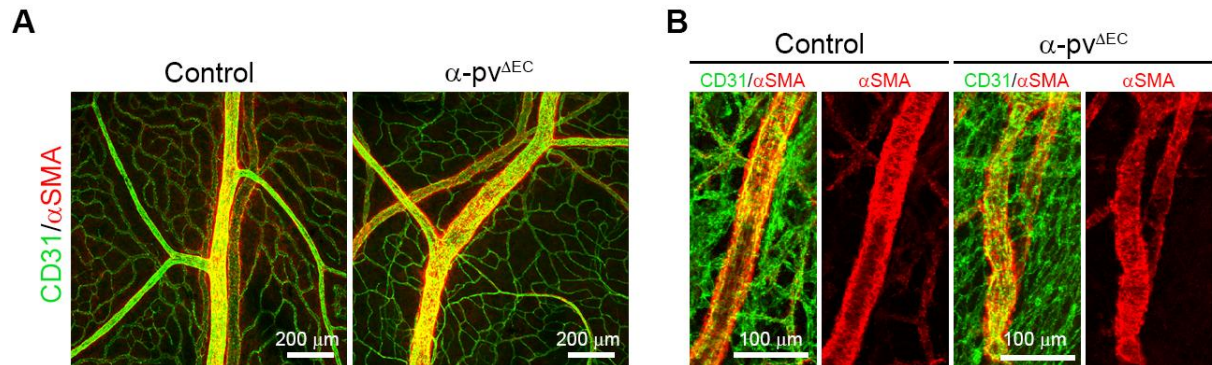


Figure 21. Normal mural cell recruitment to the vessel wall in α -pv ^{Δ EC} embryos. Representative whole-mount immunostainings for CD31 (green) and α -SMA (red) in YS (A) and skin tissue (B). Mural cell coverage of vessels in α -pv ^{Δ EC} and control embryos at E15.5 did not reveal any difference (modified after¹⁰⁸).

3.1.1.4 Loss of endothelial α -pv impairs cell-cell junction integrity

Vascular mispatterning, vessel instability, and hemorrhages can directly result from defects in cell-cell junctions between ECs¹¹⁴. To investigate whether loss of α -pv affects cell-cell junctions, we visualized cell junctions in the YS vasculature from control and α -pv ^{Δ EC} embryos using the junctional markers VEcad and CD31. The analysis showed sharp, linear, and continuous VEcad and CD31 stains at cell boundaries in vessels of control embryos (Figure 22, A, B). In contrast, vessels in α -pv ^{Δ EC} embryos displayed diffuse, discontinuous, and scattered stains (Figure 22, A, B). Additionally, we frequently observed gaps between cells in vessels of α -pv ^{Δ EC} embryos (Figure 22, A). Statistical analysis showed a two-fold increase of gaps between ECs (intercellular space index: number of intercellular spaces/cell number) in vessels of α -pv ^{Δ EC} embryos compared to vessels of control embryos (Figure 22, C). Together, these data indicate that α -pv is required for endothelial junction integrity *in vivo*.

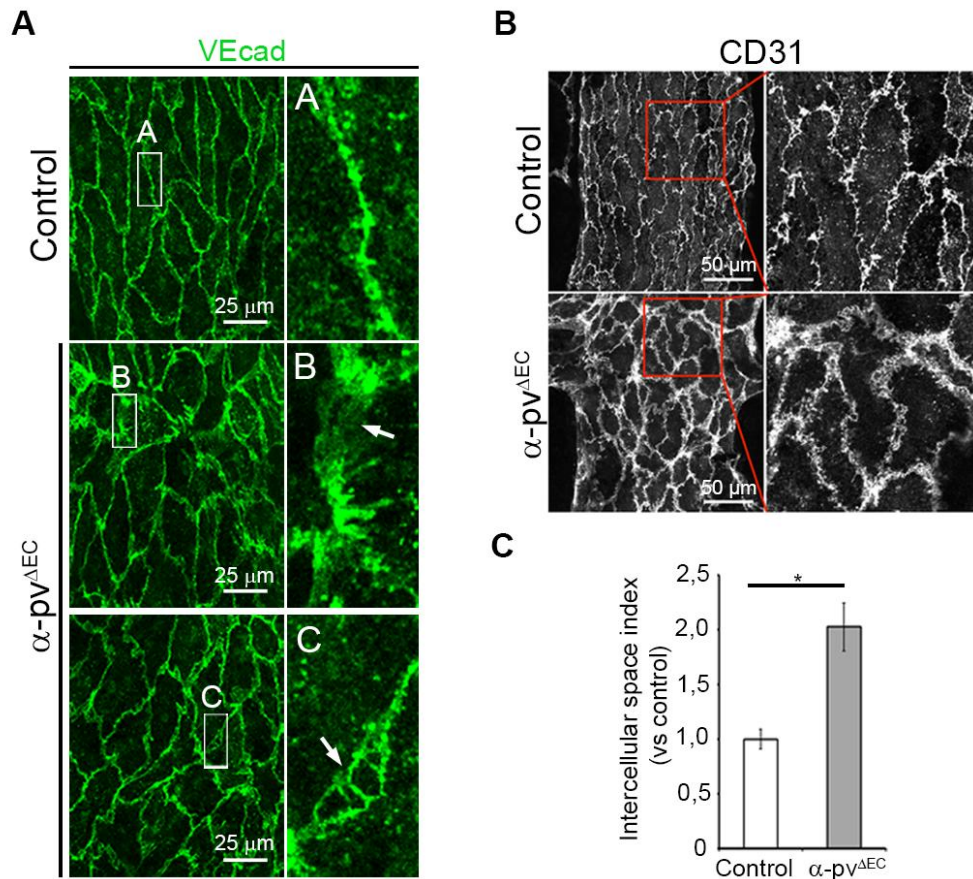


Figure 22. Impaired junction morphology in α -pv^{ΔEC} YS vasculature. (A) VECad (green) immunostaining of YS vasculature. α -pv^{ΔEC} vessels showed discontinuous junctions and gaps between cells (see arrows). A, B, C show higher magnifications. (B) CD31 immunostaining of YS vessels. Junctions of α -pv^{ΔEC} vessels appeared more scattered compared to control junctions. (C) Intercellular space index (calculated by number of intercellular spaces/cell number) of control vs α -pv^{ΔEC} junctions showed a significant increase of gaps in α -pv^{ΔEC} vessels. Values represent mean \pm SEM. *P \leq 0.05, number of embryos (n=3) (modified after¹⁰⁸).

3.1.1.5 α -pv localizes to FXs, FAs and JAIL in ECs *in vitro*

To elucidate the molecular mechanism by which α -pv controls vascular patterning, junctional integrity, and EC behavior, we first analyzed the subcellular localization of α -pv in ECs *in vitro*. To do this, we cultured HUVEC on gelatin for 12 hours and performed immunostaining with antibodies against α -pv, Pax and VECad. Labeled-phalloidin was used to visualize the F-actin. As expected, under sparse culture conditions, α -pv localized at FAs at the tips of stress fibers colocalizing with the F-actin and Pax (Figure 23). A closer analysis revealed that α -pv also localized at the FXs, nascent cell-ECM adhesion contacts, close to the edge of the lamellipodium (Figure 23, B, C).

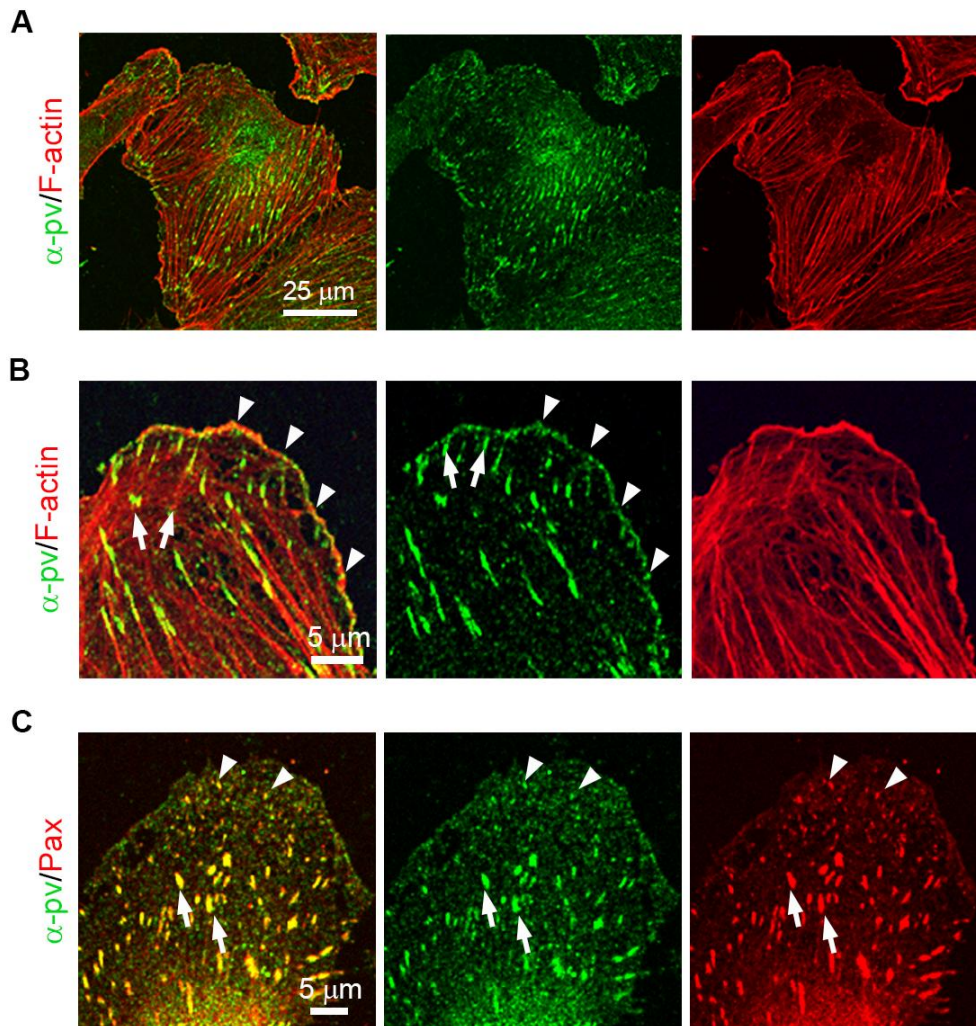


Figure 23. Subcellular localization of α -pv in HUVECs. (A) HUVECs were immunostained for α -pv (green) and F-actin (red) in sparse conditions. (B) α -pv was localized at FXs at the edge of lamellipodia (see arrowheads) and at FAs connected to stress fibers (see arrows). (C) Immunostaining for α -pv (green) and Pax (red) showed colocalization at FXs and FAs (modified after¹⁰⁸).

Interestingly, at sites where two adjacent cells adhere and overlap, α -pv also localized in small, punctate clusters that resemble FXs along the edge of the overlapping membranes in a close proximity to VEcad clusters (Figure 24). Under subconfluent cell culture conditions, α -pv was also distributed along the edge of JAIL at overlapping plasma membranes (Figure 24, B). The analysis also showed the presence of α -pv clusters in a very close proximity to discontinuous AJs, where it occasionally and partially colocalized with VEcad (Figure 24, B C). Triple-labelling for VEcad, F-actin and α -pv showed α -pv dot-like structures at the cell-cell junctions associated with the F-actin and occasionally connected via actin filaments to α -pv positive FA-like structures (Figure 24, D). Finally, we did not observe α -pv at stable, linear AJs (Figure 24, B).

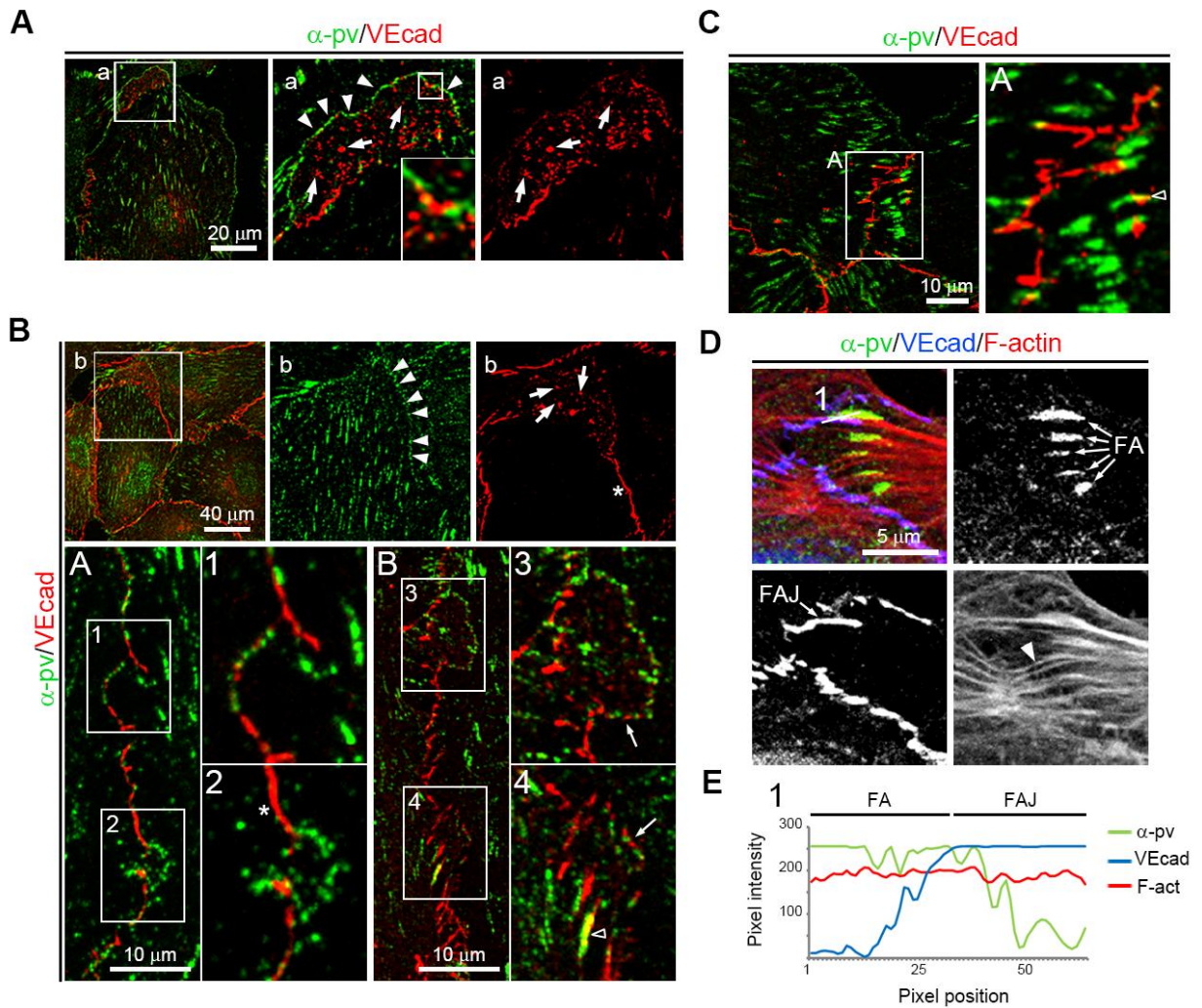


Figure 24. Localization of α -pv in subconfluent conditions. (A) Immunostaining of α -pv (green) and VEcad (red) showed α -pv localization along overlapping membranes. Arrowheads point to α -pv at the edge of membranes. Arrows point to VEcad clusters. (B) α -pv was localized at JAIL close to VEcad clusters (see arrows). (C) Partial colocalization of α -pv with VEcad at discontinuous AJs. See empty arrowheads. (D) Triple-immunostaining of α -pv (green), F-actin (red) and VEcad (blue) revealed α -pv at FAs connected to AJs with F-actin filaments (FAJ). (E) Intensity profiles of α -pv, F-actin and VEcad along the line 1 in the image shown in D. Asterisks show stable AJs without α -pv. a, b, A, B, 1-4 indicate higher magnifications (modified after¹⁰⁸).

3.1.1.6 Depletion of α -pv in HUVECs

Next, we depleted α -pv in HUVECs by siRNA and analyzed cell morphology. We performed all experiments with two different siRNAs against α -pv and as a control we used a scrambled (Scr) siRNA. The downregulation of α -pv protein expression was confirmed by western blot analysis of cell lysates of cultured cells after 72 hours of siRNA administration (Figure 25).

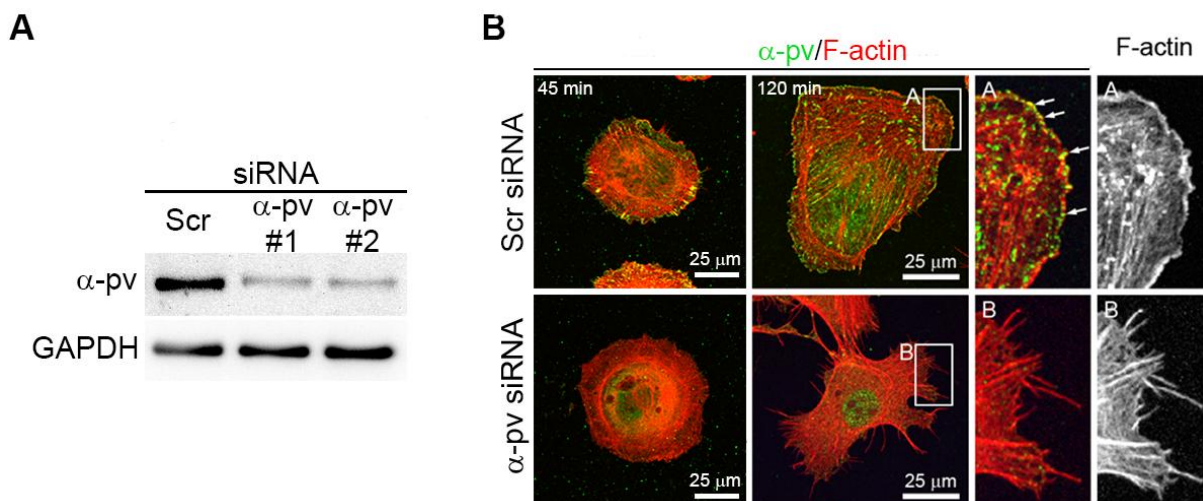


Figure 25. Deletion of α -pv in HUVECs with siRNAs. (A) Western blot analysis of lysates from HUVECs transfected with two different siRNAs against α -pv and Scr. GAPDH was used as loading control. (B) Scr siRNA treated and α -pv depleted HUVECs were plated on gelatin for 45 min and 120 min, and immunostained for α -pv (green) and F-actin (red). A, B, indicate higher magnifications (modified after¹⁰⁸).

3.1.1.7 α -pv depleted ECs show reduced FX formation and impaired lamellipodia

Then, we performed immunostainings for α -pv and F-actin in control and α -pv depleted ECs plated on gelatin. After 2 hours on gelatin, control HUVECs were able to spread, displayed long and thin stress fibers, and showed a single lamellipodia. In contrary, α -pv depleted HUVECs showed short and thick stress fibers and multiple lamellipodia-like protrusions. Moreover, α -pv depleted cells displayed many finger-like protrusions (Figure 25, B).

Cell spreading and lamellipodia formation is dependent on proper integrin-mediated cell-ECM adhesion structure formation¹⁷¹. To analyze integrin-mediated cell-ECM adhesion structure formation in the absence of α -pv, we performed immunostaining for Pax and Vinc, which are FA markers, and F-actin in control and α -pv depleted HUVECs. The analysis showed multiple FXs along the leading edges in the proximity of the FAs in control cells (Figure 26, A, B). In contrary, α -pv depleted cells displayed few Pax positive clusters at the leading edge, and Pax staining was concentrated at the FAs, which seemed larger than control FAs (Figure 26, A, B). At the FXs Pax is phosphorylated on the tyrosine residue (Y) 118¹⁷². Consistent with the reduced levels of FXs in α -pv depleted cells, western blot analysis showed a significant reduction of phosphorylation of Pax at Y 118 in these cells (Figure 26, C). Together, these results suggest that α -pv is required for integrin-mediated cell-ECM adhesion structure formation. These findings could be verified in postnatal endothelial-

Fehler! Verwenden Sie die Registerkarte 'Start', um Überschrift 1;Ü 1 dem Text zuzuweisen, der hier angezeigt werden soll.

specific depletion of α -pv in the retinal vasculature and was visualized by immunostaining for p-Pax¹⁷² (Figure 26, D).

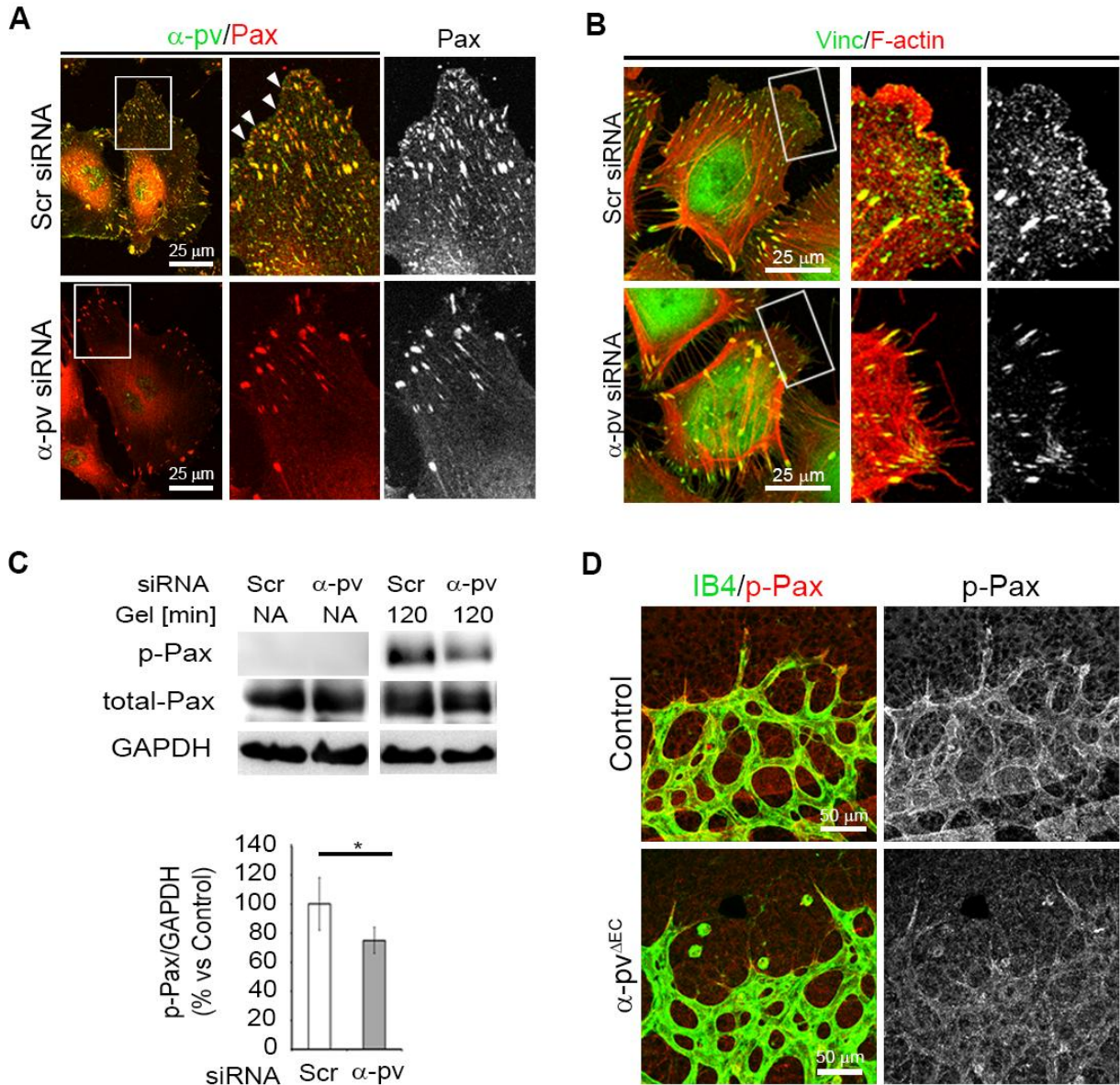


Figure 26. Pax phosphorylation is reduced in the absence of α -pv. (A) Coimmunostaining of α -pv (green) and Pax (red) showed a decreased number of FXs due to α -pv deficiency. Arrowheads point to Pax positive FXs. (B) Immunostaining for Vinc (green) and F-actin (red) showed decrease of FXs at lamellipodia in α -pv depleted HUVECs compared to controls. (C) Western blot for p-Pax of lysates of control and α -pv depleted HUVECs. Quantification revealed a significant decrease of p-Pax due to α -pv deficiency compared to control HUVECs. Values represent mean \pm SEM. * $P \leq 0.05$, (n=3). (D) Immunostaining for IB4 (green) and p-Pax (red) in α -pv^{i Δ EC} retinas. Immunostainings revealed decreased fluorescent intensity of p-Pax in α -pv^{i Δ EC} retinas compared to control retinas (modified after¹⁰⁸).

3.1.1.8 Depletion of α -pv in ECs leads to decreased Rac1 activity and cell migration

Migration and lamellipodia formation are dependent on proper FX formation and activity of the small GTPase Rac1¹⁷³. To analyze whether Rac1 activity is altered in α -pv depleted HUVECs, we plated control and α -pv depleted cells on gelatin for 30 minutes, measured Rac1 activity, and found that Rac1 activity was significantly decreased in α -pv depleted HUVECs compared to control HUVECs (Figure 27, A). Next, we performed a chemotactic migration assay in modified Boyden-chambers, which revealed decreased migration ability towards serum of α -pv depleted HUVECs than control HUVECs (Figure 27, B). Together, these results suggest that α -pv regulates EC migration via controlling Rac1 activity.

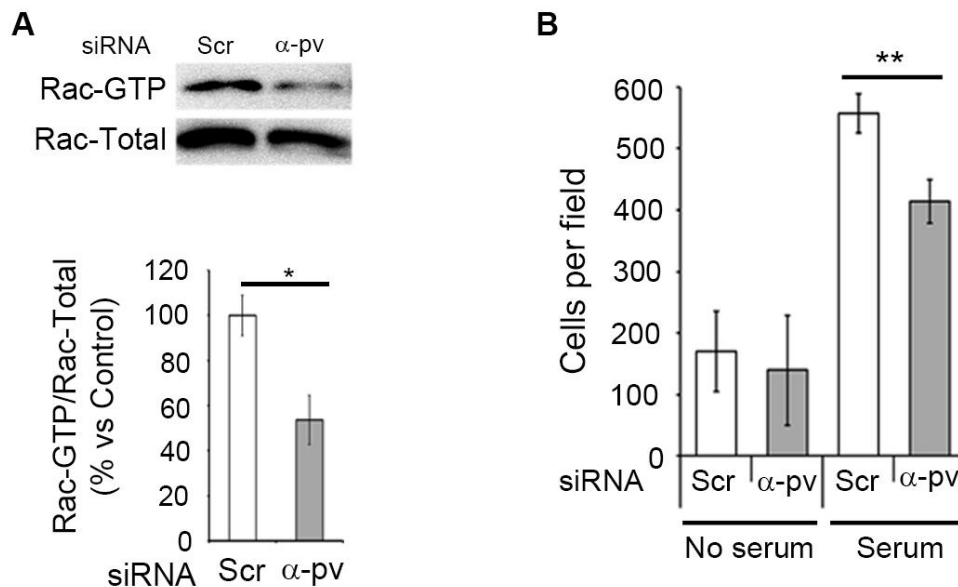


Figure 27. Rac1 activity and cell motility is decreased in α -pv deficiency. (A) Western blot analysis of active Rac1 pull-down in α -pv depleted and control HUVECs compared to total Rac1. α -pv depleted HUVECs showed significantly decreased Rac1 activity compared to control HUVECs. (B) Chemotactic migration assay with α -pv depleted and control HUVECs: Boyden-chamber assay was performed with 10% serum as an attractant to show migration of α -pv depleted and control HUVECs. Analysis revealed a significant decrease of migration ability in absence of α -pv compared to control cells. Values represent mean \pm SEM. * $P \leq 0.05$, ** $P \leq 0.01$, (n=3) (modified after¹⁰⁸).

3.1.1.9 Depletion of α -pv in ECs impairs cell-cell junction formation and monolayer integrity

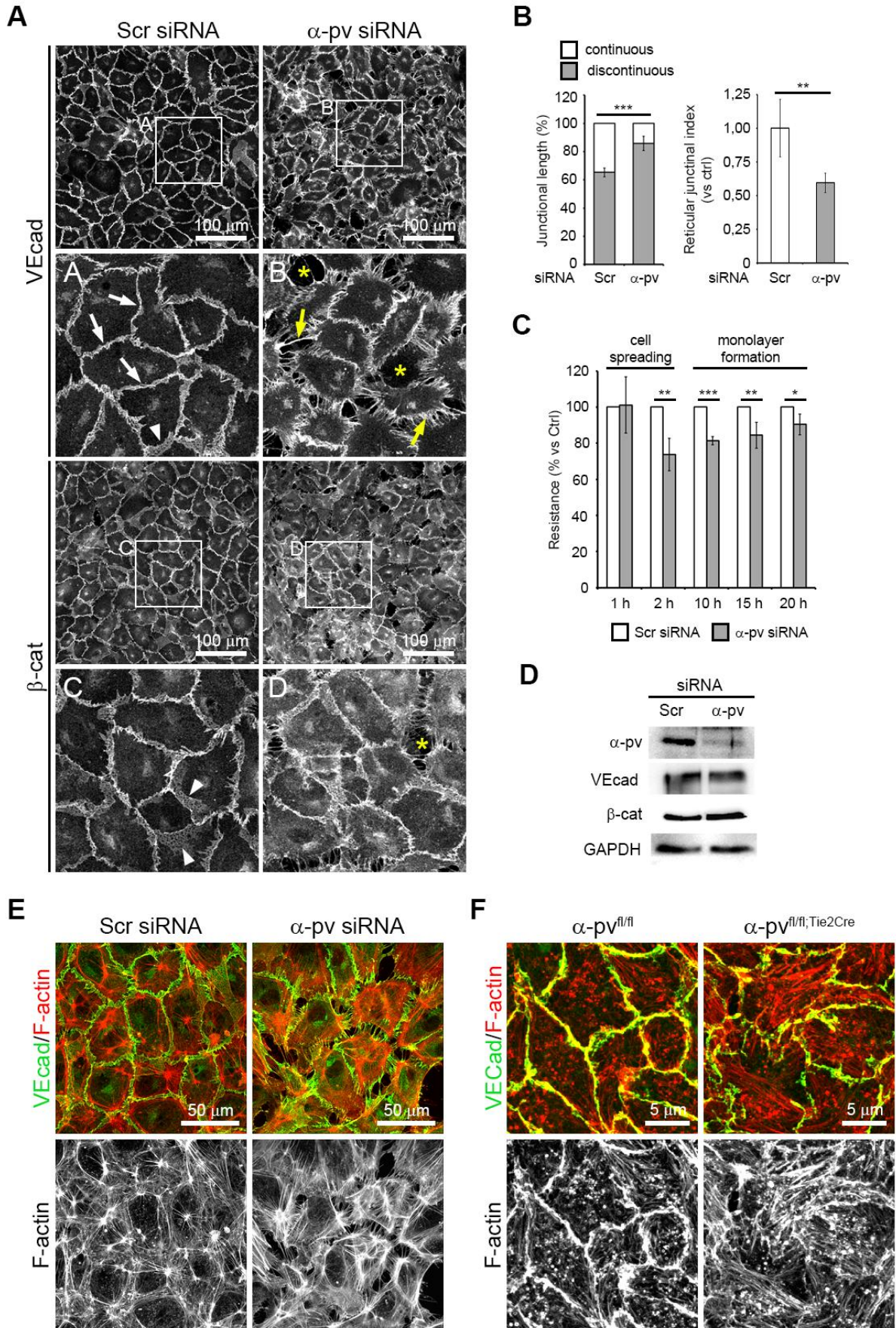
Loss of α -pv *in vivo* leads to impaired cell-cell junction integrity. To determine how α -pv controls cell-cell junctions, we cultured α -pv depleted and control HUVEC on gelatin for 24

Fehler! Verwenden Sie die Registerkarte 'Start', um Überschrift 1;Ü 1 dem Text zuzuweisen, der hier angezeigt werden soll.

hours, performed immunostaining for VEcad and β -cat, and analyzed monolayer formation. While control HUVECs were able to establish a regular, cobblestone-like monolayer, α -pv depleted HUVECs displayed irregular shapes, disrupted monolayer formation, and an increased incidence of intercellular gaps (Figure 28, A). Statistical analysis showed a significant decrease in stable, continuous AJs in α -pv depleted cells compared to control cells (total discontinuous AJs length/total junctional length) (Figure 28, B). Furthermore, the percentage of reticular junctions, shown by the reticular junctional index (calculated with the formula (total reticular junctional area/total cell area)/cell number), was decreased in α -pv depleted HUVECs compared to controls (Figure 28, B). Next, we analyzed monolayer integrity by performing TEER analysis. To do this, control and α -pv depleted HUVECs were seeded on a gold electrode and TEER was recorded by electric cell-substrate impedance sensing. TEER was measured continuously for 24 hours. During the first hour cell spreading is measured, whereas the following hours reflected monolayer formation and junctional integrity¹⁷⁴. The analysis showed that α -pv depletion in HUVECs did not alter cell spreading, but severely impaired monolayer formation. Importantly, the protein levels of VEcad and β -cat were not altered in α -pv depleted HUVECs, indicating that junctional defects in α -pv depleted HUVECs are not caused by reduction of VEcad and β -cat protein levels (Figure 28, C, D). These results indicate that α -pv is required for formation and/or maintenance of stable AJs *in vitro*.

The actin cytoskeleton plays a major role in AJ formation and maintenance¹⁷⁵. Therefore, we analyzed the actin cytoskeleton in EC monolayers by immunostaining for VEcad and F-actin. Cells depleted of α -pv displayed reduced cortical actin associated to the junctions, and increased levels of radial actin bundles compared to control ECs (Figure 28, E). To corroborate these results, ECs from α -pv ^{Δ EC} and control embryos were isolated and plated on gelatin for 48 hours and immunostaining for VEcad and F-actin. This confirmed the previous results (Figure 28, F).

Fehler! Verwenden Sie die Registerkarte 'Start', um Überschrift 1;Ü 1 dem Text zuzuweisen, der hier angezeigt werden soll.



Fehler! Verwenden Sie die Registerkarte 'Start', um Überschrift 1;Ü 1 dem Text zuzuweisen, der hier angezeigt werden soll.

Figure 28. α -pv depleted HUVECs show altered junction formation. (A) VEcad and β -cat immunostaining of α -pv depleted and control HUVECs plated on gelatin for 24 hours. Yellow arrows show radial VEcad bundles. Asterisks highlight intercellular gaps. A, B show higher magnifications. (B) Quantification of percentages of continuous and discontinuous AJs (total discontinuous AJs length/total junctional length), and the reticular junctional index in control and α -pv depleted HUVECs. Reticular junctional index was calculated using the formula (total reticular junctional area/total cell area)/cell number. Values represent mean \pm SEM. ** $P \leq 0.01$, *** $P \leq 0.001$, (n=3). (C) TEER was decreased in α -pv depleted HUVECs compared to controls. Values represent mean \pm SEM. * $P \leq 0.05$, ** $P \leq 0.01$, *** $P \leq 0.001$, (n=3). (D) Western blot analysis of protein levels of VEcad and β -cat in control and α -pv depleted HUVECs revealed similar protein levels. (E) Control and α -pv depleted HUVECs, and (F) isolated ECs from control and α -pv ^{Δ EC} embryos were plated on gelatin for 48 hours and immunostained for VEcad (green) and F-actin (red). Cells showed perturbed actin network and impaired cell-cell junction formation (modified after¹⁰⁸).

These results suggest that α -pv regulates cell-cell junction integrity via actin cytoskeleton rearrangement.

3.1.1.10 α -pv localizes at JAIL and is crucial for JAIL formation

Recently it has been reported that JAIL, actin-mediated lamellipodia structures that occur at cell-cell junctions, control the integrity of EC monolayers via regulating VEcad dynamics at the junctions¹²⁶. Since α -pv is localized at the edge of JAIL, we analyzed JAIL formation and dynamics in the absence of α -pv (Figure 29).

To do this, we collaborated with Prof. Hans-Joachim Schnittler (Institute of Anatomy and Vascular Biology, Muenster). Together, we depleted α -pv in HUVECs expressing Lifeact-GFP, and analyzed JAIL dynamics using spinning disc fluorescent life cell imaging¹⁷⁶. Control HUVECs frequently formed JAIL in subconfluent conditions that were stable up to five minutes until retraction. JAIL displayed round and broad lamella. In contrast, α -pv depleted HUVECs displayed unstable and irregular JAIL, and extended filopodia-like structures followed by edge withdrawal. The number of intercellular gaps was increased in α -pv depleted HUVECs, whereas control HUVECs prevented intercellular gap formation (Figure 29, A, B). Quantification of JAIL frequency, that was measured by counting the number of leading edges throughout a movie (16 movies per group), showed a significant reduction in α -pv deficient HUVECs compared to control HUVECs (Figure 29, C). These data indicate that α -pv is important for normal JAIL formation and maintenance.

Fehler! Verwenden Sie die Registerkarte 'Start', um Überschrift 1;Ü 1 dem Text zuzuweisen, der hier angezeigt werden soll.

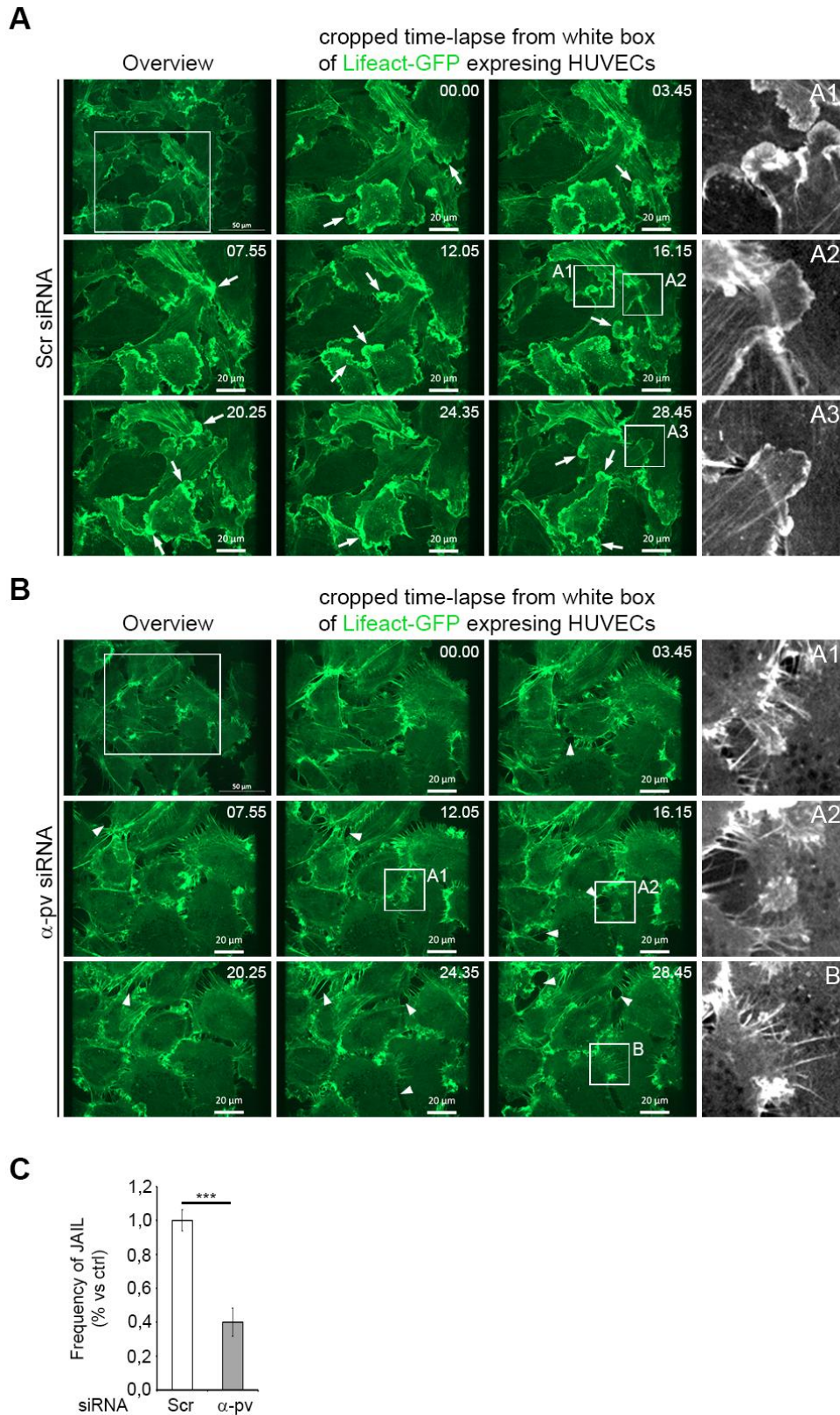


Figure 29. Lifect-GFP transfected HUVECs are analyzed for JAIL formation. (A, B) Stills from Lifect-GFP transfected control and α -pv deficient HUVECs in spinning disc live-cell imaging. Depleted cells displayed a reduced frequency and maintenance of JAIL formation. Arrows point at JAIL. Arrowheads highlight intercellular gaps. (C) Quantification of JAIL frequency. Frequency of JAIL in α -pv deficient HUVECs was significantly reduced compared to control HUVECs. Values represent mean \pm SEM. *** $P \leq 0.001$, (n=3), A-B indicate higher magnifications (modified after¹⁰⁸).

3.1.2 Analysis of α -pv and β -pv functions in ECs

3.1.2.1 Mice with ECs lacking α -pv and β -pv are embryonically lethal and display abnormal vessel morphology

The $\beta 1^{\Delta EC}$ mice die embryonically at E10.5^{57,58}. Moreover, our data showed that α -pv $^{\Delta EC}$ mice die between E15.5 and birth (see 3.1.1)¹⁰⁸. Since ECs express α -pv and β -pv, this difference in lethality between $\beta 1^{\Delta EC}$ and α -pv $^{\Delta EC}$ mice could be due to a partial compensation of α -pv by β -pv. To test this hypothesis, we generated mice lacking α -pv and β -pv in ECs. To do this, we took the advantage that β -pv $^{-/-}$ mice are viable, fertile and do not show any embryonic phenotype. α -pv $^{fl/fl}$ mice were mated with β -pv $^{-/-}$ mice to generate α -pv $^{fl/fl};\beta$ -pv $^{-/-}$ mice. Next, we intercrossed α -pv $^{fl/fl};\beta$ -pv $^{-/-}$ females with α -pv $^{fl/+};\beta$ -pv $^{-/-};Tie2$ -Cre males to delete α -pv in ECs. These intercrosses failed to generate viable α -pv $^{fl/fl};\beta$ -pv $^{-/-};Tie2$ -Cre (referred to herein as α -pv $^{\Delta EC};\beta$ -pv $^{-/-}$) offsprings, indicating embryonic lethality of α -pv $^{\Delta EC};\beta$ -pv $^{-/-}$ mice. Timed mating intercrosses revealed that the lethality of α -pv $^{\Delta EC};\beta$ -pv $^{-/-}$ embryos started at E11.5 and no alive α -pv $^{\Delta EC};\beta$ -pv $^{-/-}$ embryos were found at E13.5 (Figure 30, A). α -pv $^{\Delta EC};\beta$ -pv $^{-/-}$ embryos displayed subcutaneous hemorrhages in the head and trunk areas (Figure 30, B).

Fehler! Verwenden Sie die Registerkarte 'Start', um Überschrift 1;Ü 1 dem Text zuzuweisen, der hier angezeigt werden soll.

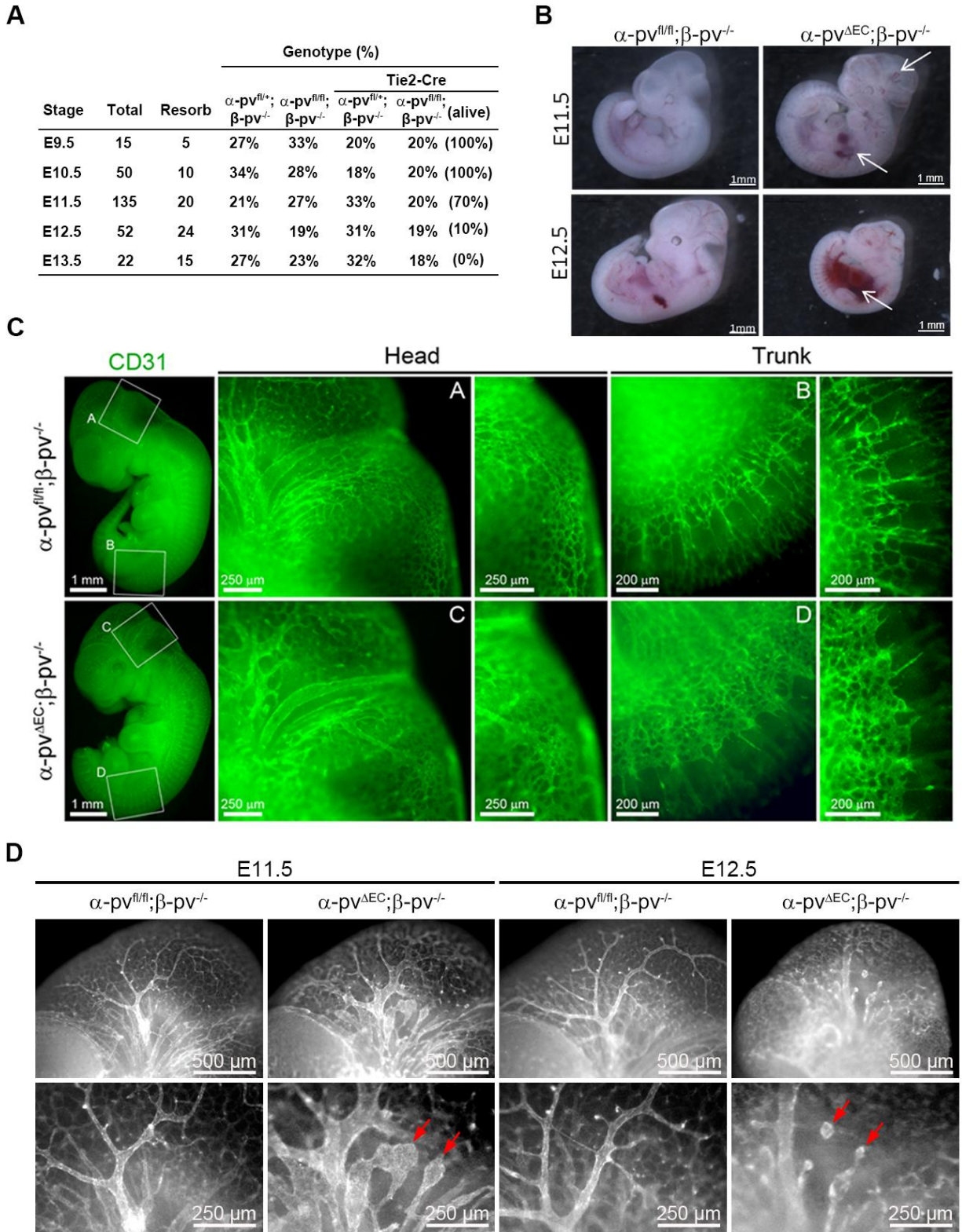


Figure 30. Embryonic lethality and impaired vasculature of α -pv^{ΔEC}; β -pv^{-/-} embryos. (A) Genotypes of the progeny from α -pv^{fl/fl}; β -pv^{-/-} and α -pv^{fl/+}; β -pv^{-/-}; Tie2-Cre intercrosses. (B) Freshly isolated α -pv^{ΔEC}; β -pv^{-/-} and α -pv^{fl/fl}; β -pv^{-/-} embryos. α -pv^{ΔEC}; β -pv^{-/-} embryos showed bleedings in the head and trunk areas (arrows point to bleedings). (C, D) CD31 whole-mount immunostainings of E11.5 and E12.5 α -pv^{ΔEC}; β -pv^{-/-} and α -pv^{fl/fl}; β -pv^{-/-} embryos. α -pv^{ΔEC}; β -pv^{-/-} embryos displayed altered vessel formation in the head (A,C) and trunk areas (B,D) compared to α -pv^{fl/fl}; β -pv^{-/-} embryos. α -pv^{ΔEC}; β -pv^{-/-} embryos had blunt vessel ends and aneurysms compared to α -pv^{fl/fl}; β -pv^{-/-} embryos. Arrows point to aneurysms in the head (see higher magnifications).

Fehler! Verwenden Sie die Registerkarte 'Start', um Überschrift 1;Ü 1 dem Text zuzuweisen, der hier angezeigt werden soll.

To visualize the vascular defects of α -pv ^{Δ EC}; β -pv^{-/-} mice in more detail, we performed whole mount immunostaining for CD31 in E11.5 α -pv ^{Δ EC}; β -pv^{-/-} and α -pv^{fl/fl}; β -pv^{-/-} embryos. The analysis showed enlargement of vessels in the head area and reduced intersomitic vessels in α -pv ^{Δ EC}; β -pv^{-/-} embryos compared to α -pv^{fl/fl}; β -pv^{-/-} embryos (Figure 30, C). Higher magnification of the head vasculature of α -pv ^{Δ EC}; β -pv^{-/-} and α -pv^{fl/fl}; β -pv^{-/-} embryos at E11.5 and E12.5 also revealed, that vessel segments in the head of α -pv ^{Δ EC}; β -pv^{-/-} embryos appeared more dilated, had blunt vessel ends, and displayed huge bleb-like structures. (Figure 30, D).

3.1.2.2 α -pv and β -pv are crucial for hindbrain vascularization

To analyze the vascular defects in more detail, we used the embryonic mouse hindbrain model (see 2.2.2.1). Hindbrains of α -pv^{fl/fl}; β -pv^{+/+} (Control), α -pv^{fl/fl}; β -pv^{-/-} (Control), α -pv ^{Δ EC}; β -pv^{+/+}, and α -pv ^{Δ EC}; β -pv^{-/-} embryos at E11.5 were immunostained for IB4 and the ventricular sides, displaying the SVP of the hindbrains, were analyzed. The analysis identified a homogenous vessel pattern and formation of the SVP in α -pv^{fl/fl}; β -pv^{+/+} hindbrains. As expected, no vascular defects were observed in α -pv^{fl/fl}; β -pv^{-/-} hindbrains and branching points, vessel diameter, and filopodia per vessel length were similar to α -pv^{fl/fl}; β -pv^{+/+} embryos (Figure 31, A, C). Hindbrains from α -pv ^{Δ EC}; β -pv^{+/+} embryos showed a reduction in number of branching points and normal vessel diameter. Interestingly, hindbrains from α -pv ^{Δ EC}; β -pv^{-/-} embryos revealed a reduction in branching points and strong increased vessel diameter compared to all other genotypes (Figure 31, A, B). α -pv ^{Δ EC}; β -pv^{-/-} vessels presented an increased formation of filopodia, brush-like tip cells, and tufted sprouts (Figure 31, B, C).

Fehler! Verwenden Sie die Registerkarte 'Start', um Überschrift 1;Ü 1 dem Text zuzuweisen, der hier angezeigt werden soll.

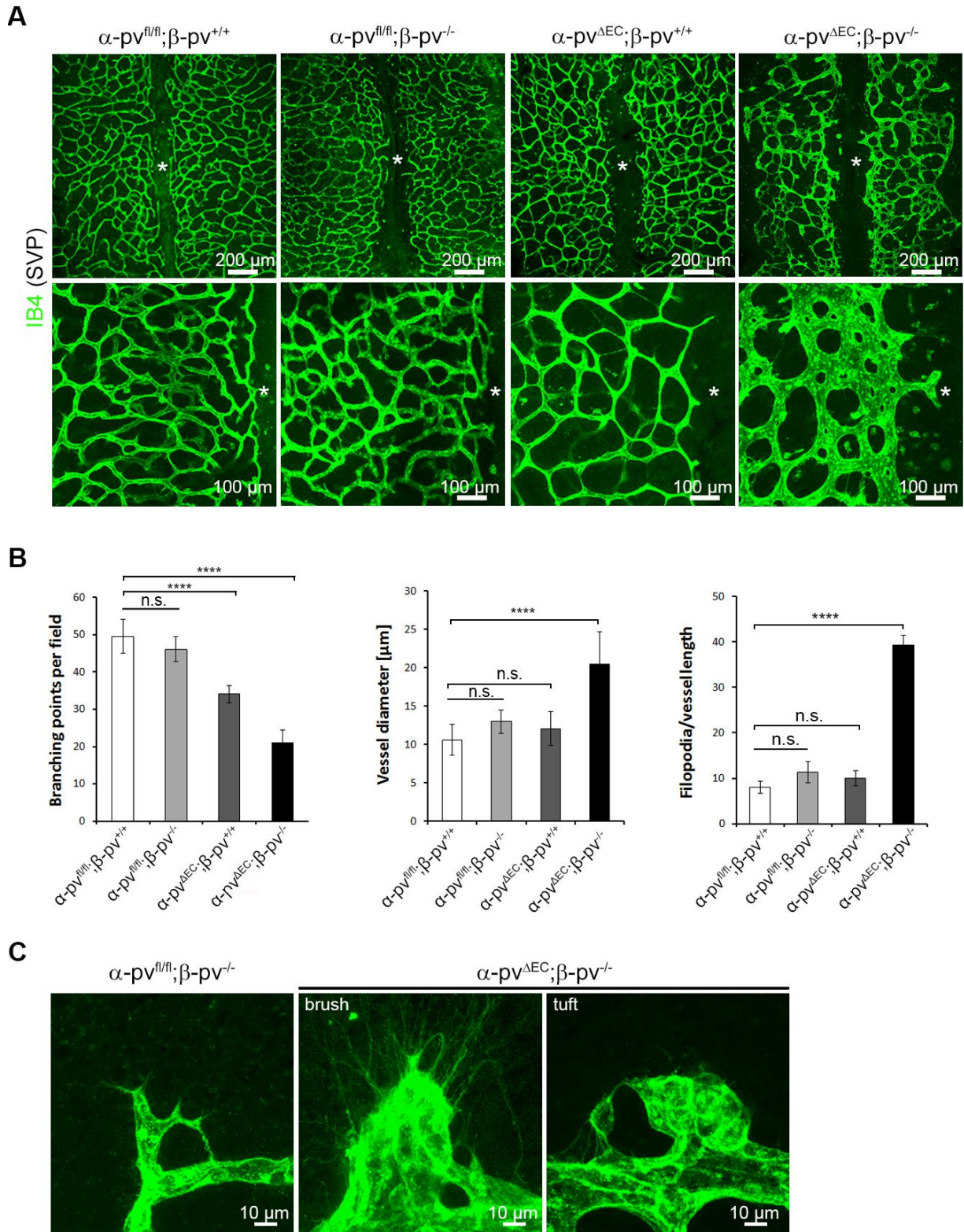


Figure 31. The embryonic hindbrain of $\alpha\text{-pv}^{fl/fl};\beta\text{-pv}^{+/+}$, $\alpha\text{-pv}^{fl/fl};\beta\text{-pv}^{-/-}$, $\alpha\text{-pv}^{\Delta EC};\beta\text{-pv}^{+/+}$, and $\alpha\text{-pv}^{\Delta EC};\beta\text{-pv}^{-/-}$. (A) Severe malformation of the hindbrain vascularization is seen in $\alpha\text{-pv}^{\Delta EC};\beta\text{-pv}^{-/-}$ embryos at E11.5 immunostained for IB4 compared to hindbrain vascularization of $\alpha\text{-pv}^{fl/fl};\beta\text{-pv}^{+/+}$, $\alpha\text{-pv}^{fl/fl};\beta\text{-pv}^{-/-}$ and $\alpha\text{-pv}^{\Delta EC};\beta\text{-pv}^{+/+}$. Asterisk mark central area of the hindbrains. (B) Quantification of number of branching points per field, vessel diameter, and filopodia per vessel length. Branching points were decreased in $\alpha\text{-pv}^{\Delta EC};\beta\text{-pv}^{-/-}$ hindbrains compared to controls, whereas vessel diameter and filopodia were significantly increased. Values represent mean \pm SEM. **** $P \leq 0.0001$, number of hindbrains (n=4). (C) Tip cell formation was altered in $\alpha\text{-pv}^{\Delta EC};\beta\text{-pv}^{-/-}$ hindbrains and displayed brushed and tufted structures compared to controls.

Fehler! Verwenden Sie die Registerkarte 'Start', um Überschrift 1;Ü 1 dem Text zuzuweisen, der hier angezeigt werden soll.

Further analysis showed micro aneurisms of the vasculature in α -pv ^{Δ EC}; β -pv^{-/-} hindbrains (Figure 32, A, B). These data indicate that the vascularization of α -pv ^{Δ EC}; β -pv^{-/-} hindbrains at E11.5 is strongly impaired due to the absence of endothelial α -pv and β -pv.

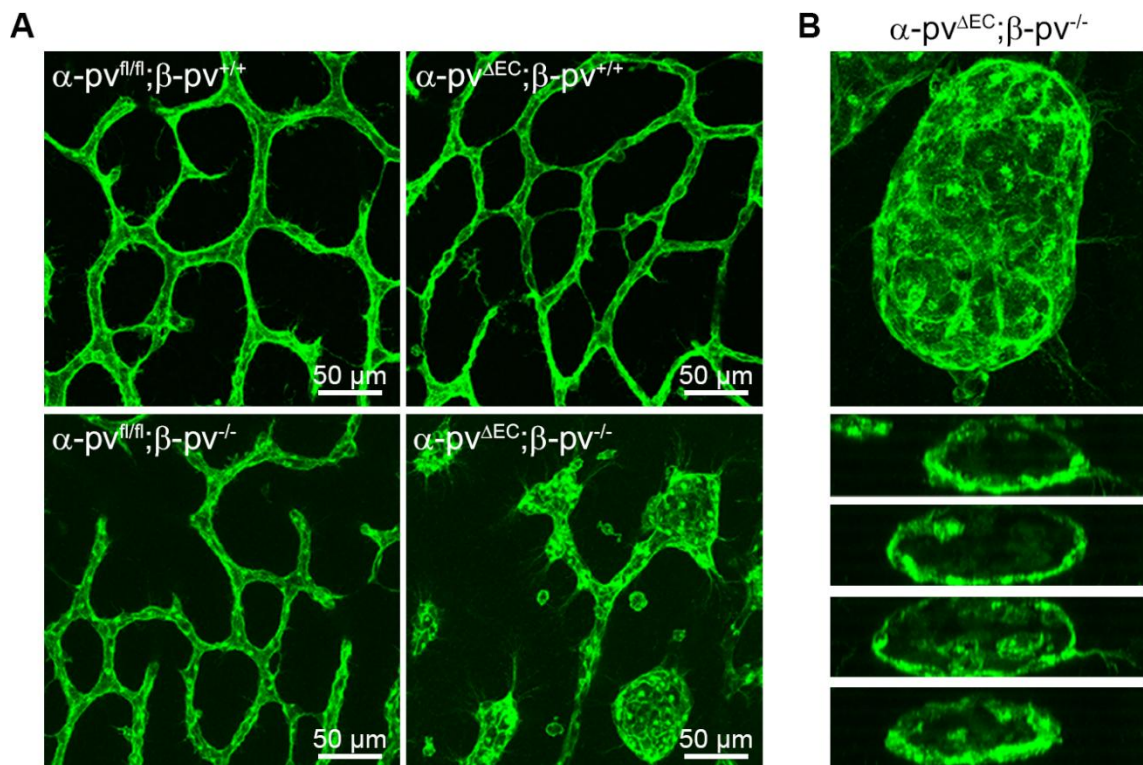


Figure 32. Micro aneurisms in α -pv ^{Δ EC}; β -pv^{-/-} embryos at E11.5. Immunostaining for IB4 showed (A) highly impaired vascularization and huge, isolated bleb-like structures in α -pv ^{Δ EC}; β -pv^{-/-} hindbrains compared to other phenotypes. (B) Isolated but lumenized bleb-like structures were present in α -pv ^{Δ EC}; β -pv^{-/-} hindbrains.

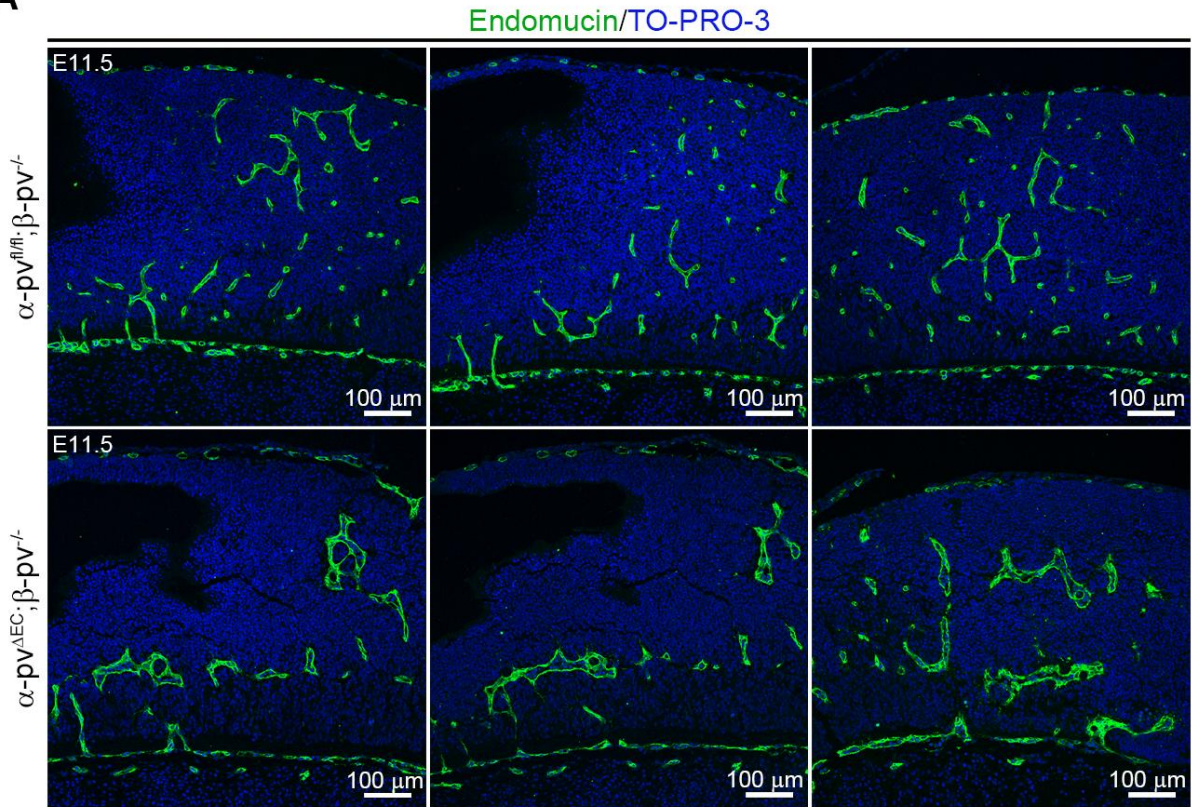
3.1.2.3 α -pv ^{Δ EC}; β -pv^{-/-} embryos showed reduced spinal cord vascularization

Next, we investigated the vascularization of the spinal cord of α -pv ^{Δ EC}; β -pv^{-/-} and α -pv^{fl/fl}; β -pv^{-/-} embryos. To do this, we performed immunostaining in paraffin sections of E11.5 embryos for the endothelial marker Endomucin. We observed a decreased number of vessels in the spinal cord in α -pv ^{Δ EC}; β -pv^{-/-} sections compared to α -pv^{fl/fl}; β -pv^{-/-} sections. The vessels of α -pv ^{Δ EC}; β -pv^{-/-} embryos displayed glomeruloid structures and the invasion depth of the sprouts was diminished in α -pv ^{Δ EC}; β -pv^{-/-} sections, whereas α -pv^{fl/fl}; β -pv^{-/-} sections revealed a dense and structured pattern of vessels in the spinal cord (Figure 33, A). The quantification of vessel number per field and vessel diameter showed a decrease of vessels in α -pv ^{Δ EC}; β -pv^{-/-} sections and increased diameter compared to α -pv^{fl/fl}; β -pv^{-/-} (Figure 33, A,

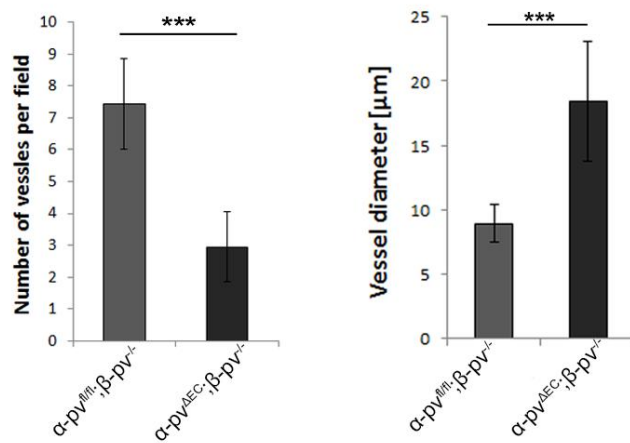
Fehler! Verwenden Sie die Registerkarte 'Start', um Überschrift 1;Ü 1 dem Text zuzuweisen, der hier angezeigt werden soll.

B). To investigate whether these defects are caused by increased EC proliferation, we immunostained for the proliferation marker p-histone 3 (pH3), and found no difference between α -pv ^{Δ EC}; β -pv^{-/-} embryos and α -pv^{fl/fl}; β -pv^{-/-} embryos (Figure 33, C). This vascular phenotype is similar to the vascular abnormalities observed in the brain.

A



B



C

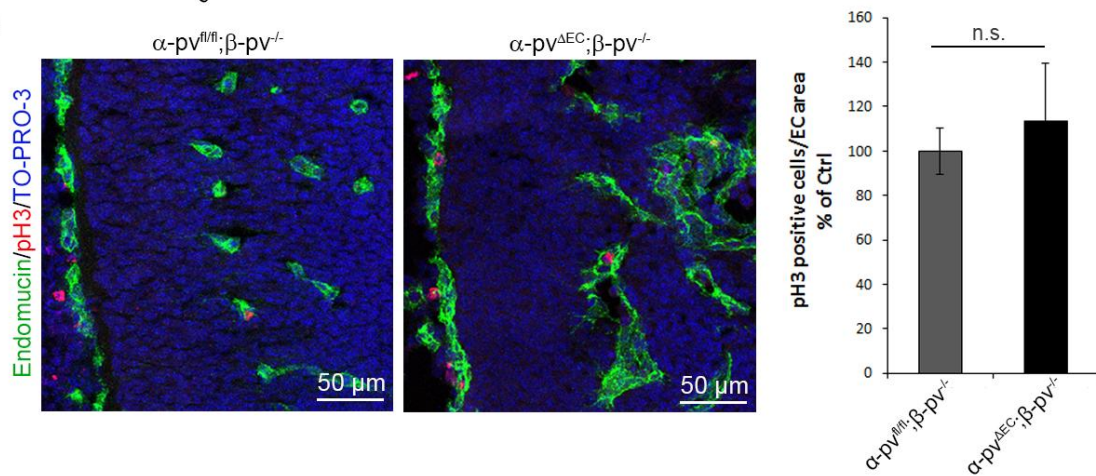


Figure 33. Reduced spinal cord vascularization in $\alpha\text{-pv}^{\Delta\text{EC}};\beta\text{-pv}^{-/-}$ embryos at E11.5. (A) Immunostaining for Endomucin (green) and TO-PRO3 (blue) revealed a decreased number of sprouts and penetration depth in the spinal cord of $\alpha\text{-pv}^{\Delta\text{EC}};\beta\text{-pv}^{-/-}$ embryos but not in control embryos. (B) Quantification of vessel number per field

Fehler! Verwenden Sie die Registerkarte 'Start', um Überschrift 1;Ü 1 dem Text zuzuweisen, der hier angezeigt werden soll.

and vessel diameter revealed a significant reduction of vessel number in $\alpha\text{-pv}^{\Delta\text{EC}};\beta\text{-pv}^{-/-}$ tissue and increased diameter compared to $\alpha\text{-pv}^{\text{fl/fl}};\beta\text{-pv}^{-/-}$ sections. (C) Immunostaining for Endomucin (green), pH3 (red), and TO-PRO3 (blue) in $\alpha\text{-pv}^{\Delta\text{EC}};\beta\text{-pv}^{-/-}$ and control sections did not show any proliferation difference in ECs. Values represent mean \pm SEM. *** $P \leq 0.001$, number of embryos ($n=3$).

3.1.2.4 Impaired vessel maturation in $\alpha\text{-pv}^{\Delta\text{EC}};\beta\text{-pv}^{-/-}$ embryos

$\alpha\text{-pv}^{\Delta\text{EC}};\beta\text{-pv}^{-/-}$ hindbrains revealed bleeding areas compared to $\alpha\text{-pv}^{\text{fl/fl}};\beta\text{-pv}^{-/-}$ hindbrains (Figure 34, A). These results suggest that the vessel integrity in $\alpha\text{-pv}^{\Delta\text{EC}};\beta\text{-pv}^{-/-}$ embryos is perturbed and vessel morphology is altered due to the lack of endothelial $\alpha\text{-pv}$ and $\beta\text{-pv}$. Paraffin sections confirmed the bleedings in the hindbrain and blood cells could be visualized by their auto fluorescence (Figure 34, B).

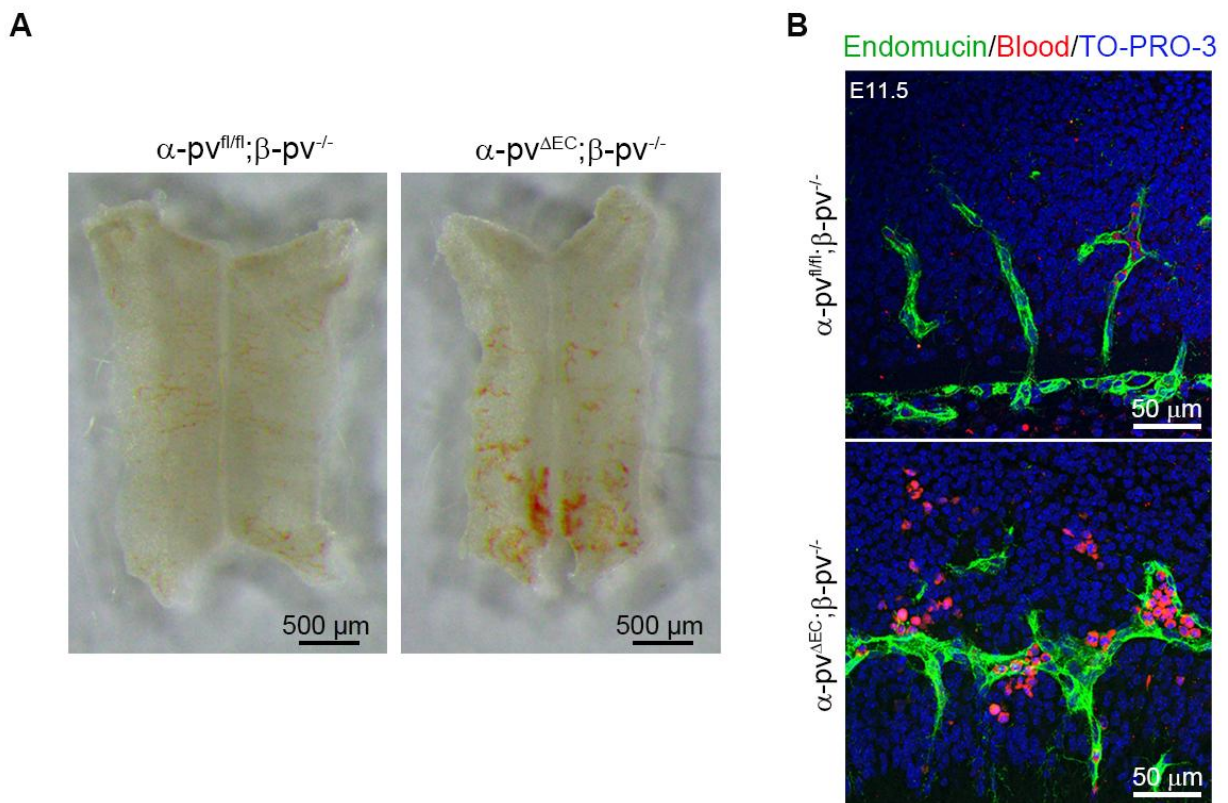


Figure 34. Bleedings in $\alpha\text{-pv}^{\Delta\text{EC}};\beta\text{-pv}^{-/-}$ embryos. (A) Freshly isolated $\alpha\text{-pv}^{\Delta\text{EC}};\beta\text{-pv}^{-/-}$ hindbrains displayed bleedings compared to $\alpha\text{-pv}^{\text{fl/fl}};\beta\text{-pv}^{-/-}$ hindbrains. (B) Immunostaining for Endomucin (green) and TO-PRO-3 (blue) showed blood cells (red) outside the vessels in $\alpha\text{-pv}^{\Delta\text{EC}};\beta\text{-pv}^{-/-}$ sections compared to $\alpha\text{-pv}^{\text{fl/fl}};\beta\text{-pv}^{-/-}$ sections.

The barrier function of vessels depends on the interaction of ECs, ECM, and the embedded PE¹⁵¹. Immunostaining for the PE marker NG2 and IB4 in $\alpha\text{-pv}^{\Delta\text{EC}};\beta\text{-pv}^{-/-}$ and $\alpha\text{-pv}^{\text{fl/fl}};\beta\text{-pv}^{-/-}$ hindbrains showed that PE were spread and completely covered the vessels in $\alpha\text{-pv}^{\text{fl/fl}};\beta\text{-pv}^{-/-}$

Fehler! Verwenden Sie die Registerkarte 'Start', um Überschrift 1;Ü 1 dem Text zuzuweisen, der hier angezeigt werden soll.

hindbrains. In contrast, the vessels of $\alpha\text{-pv}^{\Delta\text{EC}};\beta\text{-pv}^{-/-}$ hindbrains displayed PE, which were less spread and appeared round (Figure 35, A). The measurement of vessel coverage showed significantly reduced PE coverage (Figure 35, B). These data indicate that the loss of endothelial $\alpha\text{-pv}$ and $\beta\text{-pv}$ results in impaired vessel maturation.

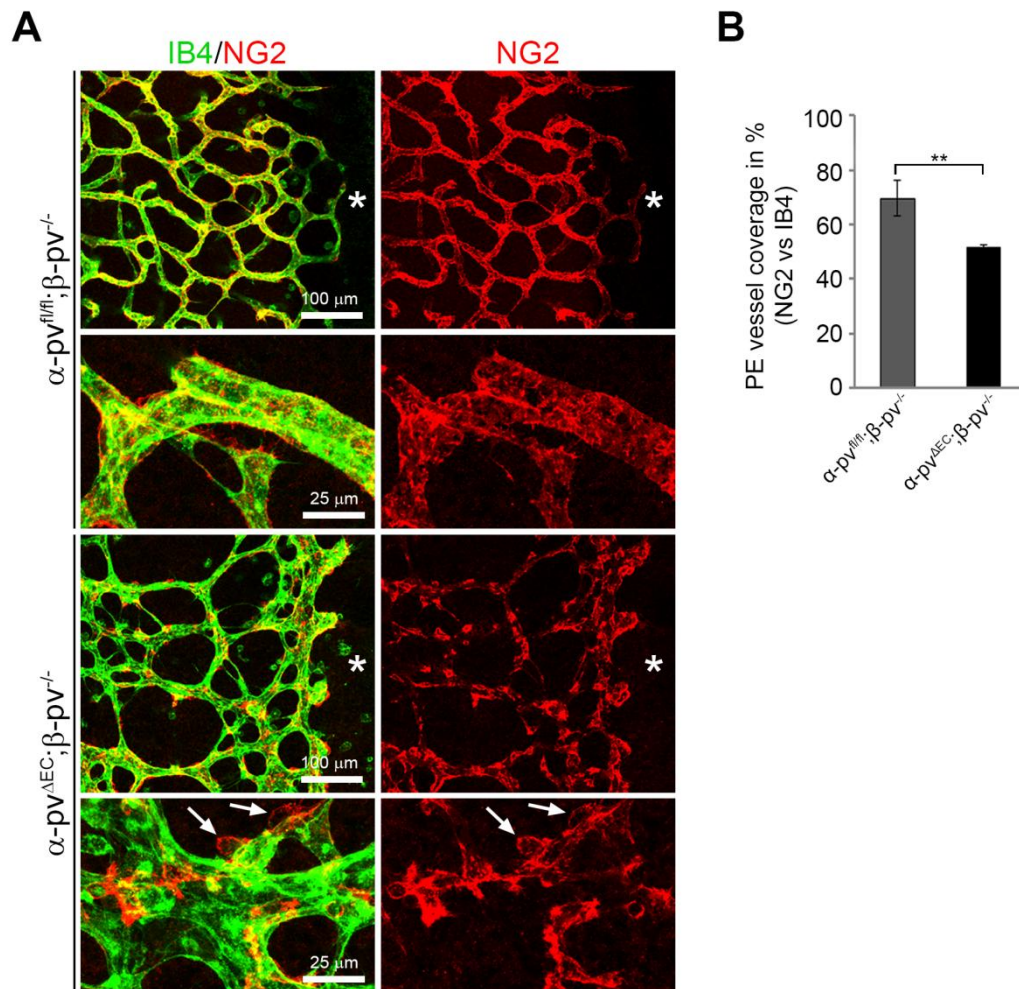


Figure 35. Altered PE attachment to the vessel walls in $\alpha\text{-pv}^{\Delta\text{EC}};\beta\text{-pv}^{-/-}$ hindbrains. (A) Immunostaining for IB4 (green) and NG2 (red) revealed altered PE spreading to vessels of $\alpha\text{-pv}^{\Delta\text{EC}};\beta\text{-pv}^{-/-}$ embryos compared to $\alpha\text{-pv}^{\text{fl/fl}};\beta\text{-pv}^{-/-}$ vessels. Asterisk mark central area of the hindbrains. Arrows point at PE that failed to spread. (B) Quantification of PE vessel coverage. Quantification revealed significant decrease of PE covered vessel area in $\alpha\text{-pv}^{\Delta\text{EC}};\beta\text{-pv}^{-/-}$ hindbrains compared to $\alpha\text{-pv}^{\text{fl/fl}};\beta\text{-pv}^{-/-}$ hindbrains. Values represent mean \pm SEM. ** $P \leq 0.05$, number of hindbrains (n=3).

To investigate, whether loss of endothelial parvins leads to BBB impairment, we stained hindbrains from $\alpha\text{-pv}^{\Delta\text{EC}};\beta\text{-pv}^{-/-}$ and $\alpha\text{-pv}^{\text{fl/fl}};\beta\text{-pv}^{-/-}$ embryos for Glut-1, a marker for BBB functions in the hindbrain vasculature. The analysis showed that $\alpha\text{-pv}^{\text{fl/fl}};\beta\text{-pv}^{-/-}$ vessels homogenously expressed Glut-1 at E11.5, whereas $\alpha\text{-pv}^{\Delta\text{EC}};\beta\text{-pv}^{-/-}$ vessels revealed a decrease of Glut-1 expression in some vessels and increased presence of Glut-1 outside the vessels, suggesting a loss of BBB integrity in $\alpha\text{-pv}^{\Delta\text{EC}};\beta\text{-pv}^{-/-}$ vasculature (Figure 36).

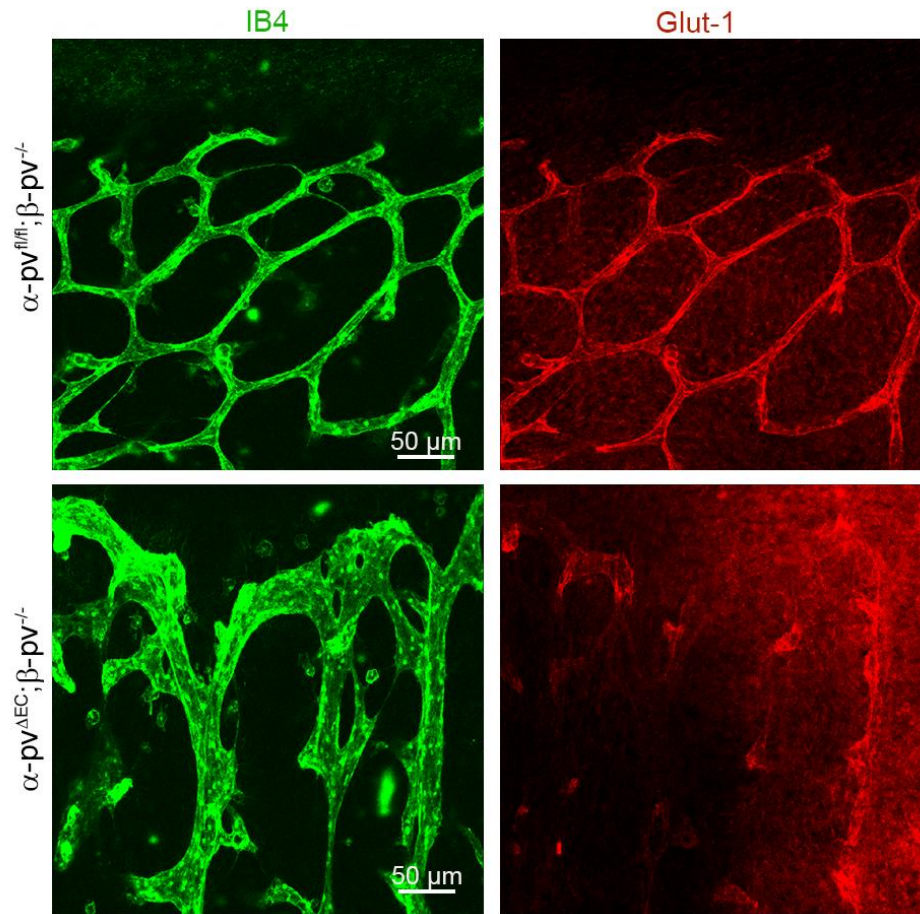


Figure 36. Altered Glut-1 expression in the vasculature of $\alpha\text{-pv}^{\Delta EC}; \beta\text{-pv}^{-/-}$ compared to $\alpha\text{-pv}^{fl/fl}; \beta\text{-pv}^{-/-}$ hindbrains. Immunostaining for IB4 (green) and Glut-1 (red) in $\alpha\text{-pv}^{\Delta EC}; \beta\text{-pv}^{-/-}$ showed reduced presence of Glut-1 in the vessels and increased presence outside compared to $\alpha\text{-pv}^{fl/fl}; \beta\text{-pv}^{-/-}$ vessels.

Since integrin-mediated signaling regulates ECM component deposition, we further analyzed whether the depletion of endothelial $\alpha\text{-pv}$ and $\beta\text{-pv}$ caused impairment of BM and ECM formation. Therefore, we immunostained $\alpha\text{-pv}^{\Delta EC}; \beta\text{-pv}^{-/-}$ and $\alpha\text{-pv}^{fl/fl}; \beta\text{-pv}^{-/-}$ hindbrains for Col-IV and FN. The analysis revealed similar expression of Col-IV and FN on the vessels of $\alpha\text{-pv}^{\Delta EC}; \beta\text{-pv}^{-/-}$ and $\alpha\text{-pv}^{fl/fl}; \beta\text{-pv}^{-/-}$ hindbrains, suggesting no obvious difference in ECM formation (Figure 37, A, B).

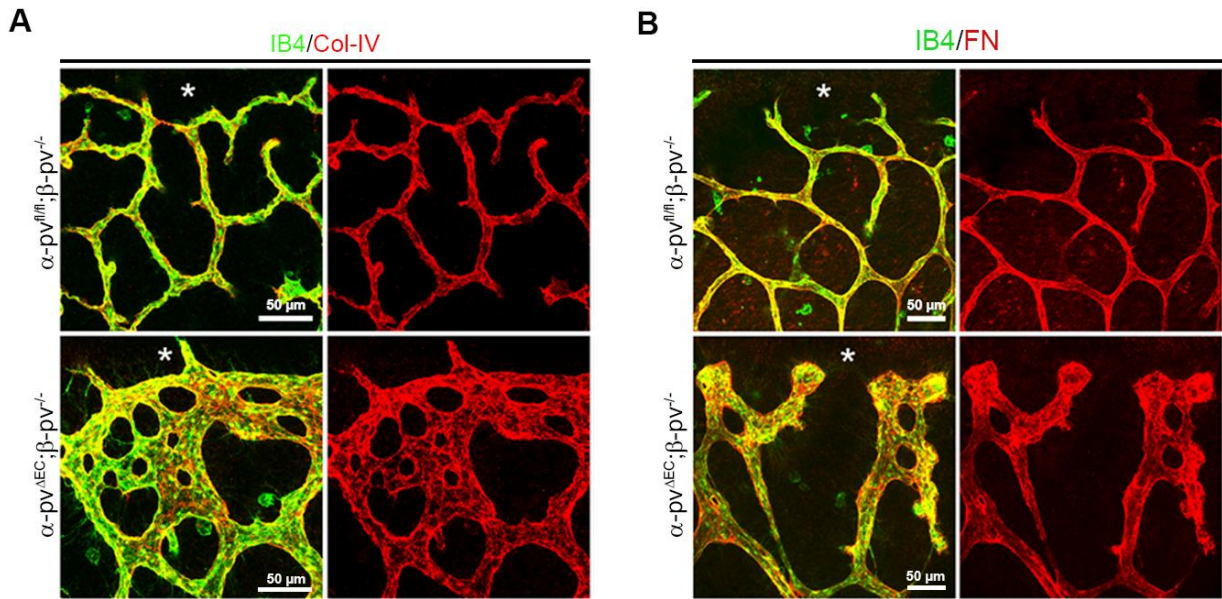


Figure 37. Similar BM/ECM components at vessels in $\alpha\text{-pv}^{\Delta EC};\beta\text{-pv}^{-/-}$ and $\alpha\text{-pv}^{fl/fl};\beta\text{-pv}^{-/-}$ hindbrains. (A) immunostaining of IB4 (green)/Col-IV (red) and (B) IB4 (green)/FN (red) in hindbrains of $\alpha\text{-pv}^{\Delta EC};\beta\text{-pv}^{-/-}$ and $\alpha\text{-pv}^{fl/fl};\beta\text{-pv}^{-/-}$ revealed similar coverage with BM/ECM components.

To investigate whether apical/basal polarity of ECs is defective due to the depletion of $\alpha\text{-pv}$ and $\beta\text{-pv}$, we immunostained $\alpha\text{-pv}^{\Delta EC};\beta\text{-pv}^{-/-}$ and $\alpha\text{-pv}^{fl/fl};\beta\text{-pv}^{-/-}$ cryo sections for Endomucin and the apical/basal polarity marker podocalyxin (PODXL) (Figure 38, A), and Endomucin and Col-IV (Figure 38, B). We observed basal Col-IV expression and apical PODXL expression on vessels of cryo sections of control embryos. $\alpha\text{-pv}^{\Delta EC};\beta\text{-pv}^{-/-}$ cryo section, however, showed luminal Col-IV expression, Col-IV clustering and abnormally distributed PODXL compared to control vessels, suggesting impaired BM integrity and abnormal apical/basal EC polarity (Figure 38).

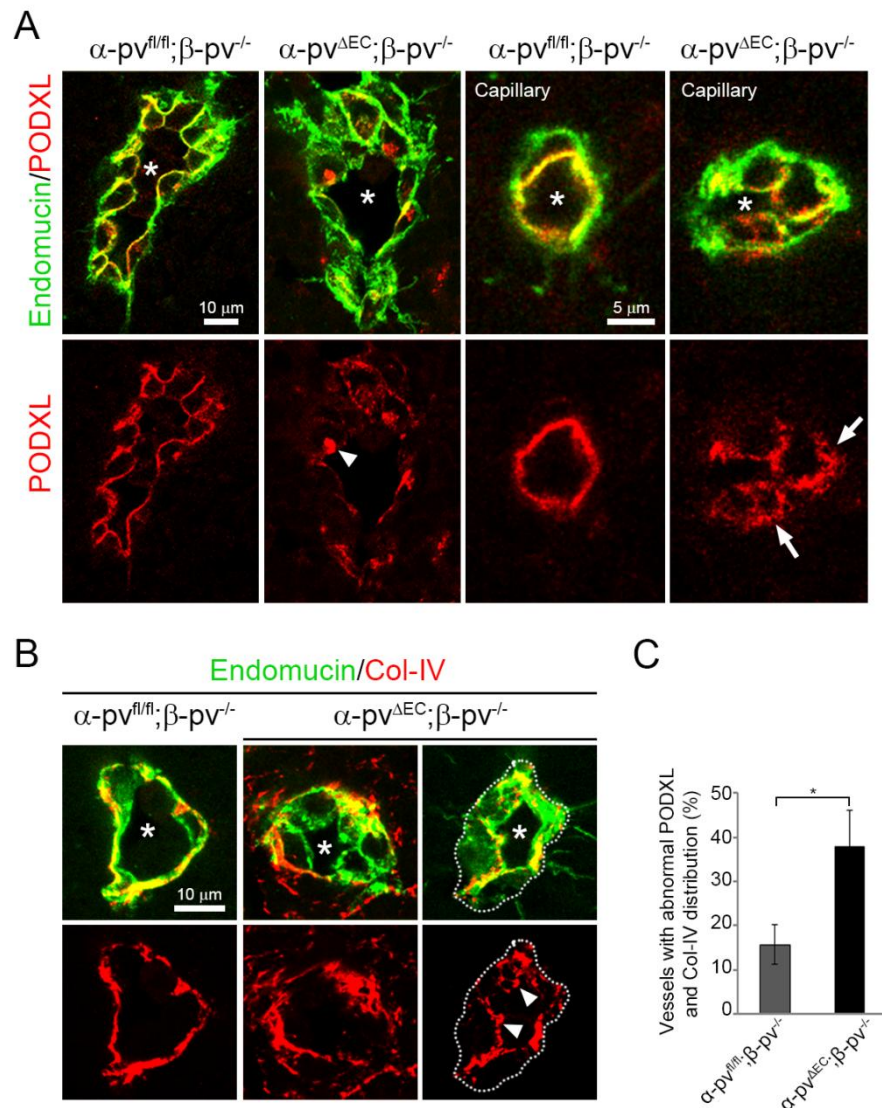


Figure 38: Impaired EC polarity and BM integrity in α -pv^{ΔEC};β-pv^{-/-} vessels. (A) Cryo section stained for Endomucin (green) and PODXL (red). Arrowhead points at PODXL cluster. Arrows point at abnormally polarized PODXL. (B) Cryo sections stained for Endomucin (green) and Col-IV (red). Asterisk marks luminal side. Dotted line marks basal side. Arrowheads point at luminal Col-IV. (C) Quantitative analysis of abnormal PODXL and Col-IV distribution. Values represent mean ± SEM. *P≤0.01, number of embryos (n=3).

3.1.2.5 Altered cell morphology of ECs in α -pv^{ΔEC};β-pv^{-/-} embryos

Integrins are involved in modulating EC morphology³⁶. We therefore analyzed EC shape in the absence of parvins. To do this, we immunostained paraffin sections of α -pv^{ΔEC};β-pv^{-/-} and α -pv^{fl/fl};β-pv^{-/-} for Endomucin. The results showed rounder and less elongated cell shapes of ECs in α -pv^{ΔEC};β-pv^{-/-} sections compared to α -pv^{fl/fl};β-pv^{-/-} sections. This was quantified by the elongation index of ECs (cell length/width) (Figure 39, A, B). To analyze EC morphology also *in vitro*, we isolated ECs from E11.5 α -pv^{ΔEC};β-pv^{-/-} and α -pv^{fl/fl};β-pv^{-/-} embryos and plated

Fehler! Verwenden Sie die Registerkarte 'Start', um Überschrift 1;Ü 1 dem Text zuzuweisen, der hier angezeigt werden soll.

them on triple coating (a crosslinked coating of poly-L-lysine, glutaraldehyde, and gelatin) for 24 hours and immunostained for CD31. ECs from α -pv^{fl/fl}; β -pv^{-/-} embryos formed gap-free tube-like structures with tip cells like formations with filopodia and elongated cell shapes. ECs from α -pv ^{Δ EC}; β -pv^{-/-} embryos instead, were unable to form tube-like structures without gaps in culture while showing a rounder cell shapes. This was also quantified by the elongation index (cell length/width) (Figure 39, C, D).

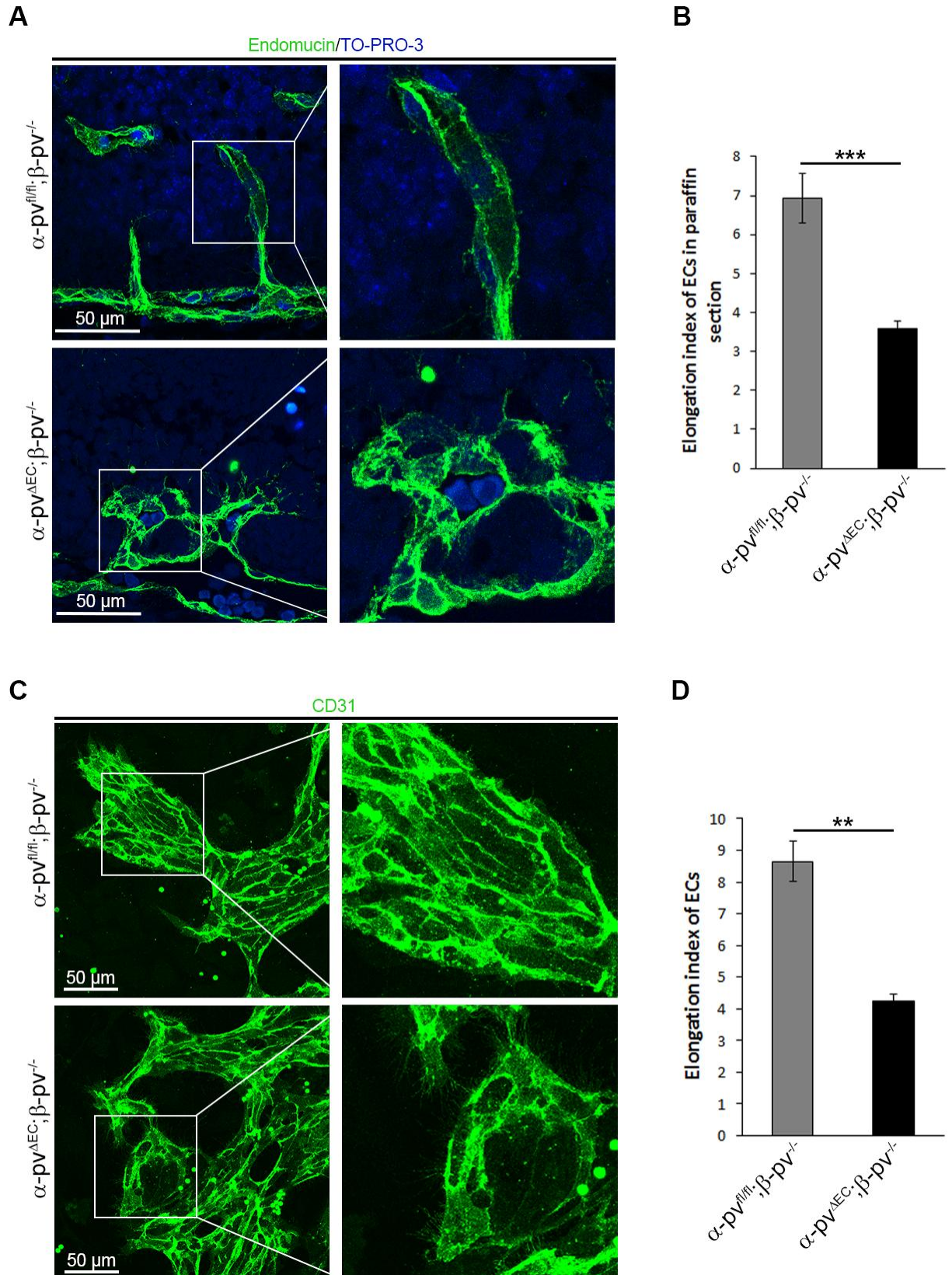


Figure 39. Cell shapes in paraffin section and isolated ECs from E11.5 embryos. (A) Immunostaining for Endomucin and TO-PRO-3 of paraffin sections of $\alpha\text{-pv}^{\Delta EC}; \beta\text{-pv}^{-/-}$ and $\alpha\text{-pv}^{fl/fl}; \beta\text{-pv}^{-/-}$ embryos. (B) Quantification of elongation index of ECs (calculated by length/width) in paraffin sections showed significant difference between $\alpha\text{-pv}^{\Delta EC}; \beta\text{-pv}^{-/-}$ and $\alpha\text{-pv}^{fl/fl}; \beta\text{-pv}^{-/-}$ sections. (C) Immunostaining for CD31 of isolated $\alpha\text{-pv}^{\Delta EC}; \beta\text{-pv}^{-/-}$ and $\alpha\text{-pv}^{fl/fl}; \beta\text{-pv}^{-/-}$ ECs were plated on triple coating (a crosslinked coating of poly-L-lysine, glutaraldehyde, and gelatin) for 24 hours. $\alpha\text{-pv}^{\Delta EC}; \beta\text{-pv}^{-/-}$ ECs failed to form gap-free vessel like structures compared to $\alpha\text{-pv}^{fl/fl}; \beta\text{-pv}^{-/-}$

Fehler! Verwenden Sie die Registerkarte 'Start', um Überschrift 1;Ü 1 dem Text zuzuweisen, der hier angezeigt werden soll.

cells. (D) Quantification of elongation index of ECs (calculated by length/width) showed significant difference of ECs from α -pv ^{Δ EC}; β -pv^{-/-} embryos compared to ECs from α -pv^{fl/fl}; β -pv^{-/-} embryos. Values represent mean \pm SEM. **P \leq 0.01, ***P \leq 0.001, number of experiments (n=3).

3.1.3 Reduced tumor angiogenesis in absence of α -pv

Integrin signaling is crucial in tumor angiogenesis¹³³. Our studies showed that α -pv is important in physiological angiogenesis. To study whether parvins are also important in pathological angiogenesis, we performed the tumor neovascularization mouse glioblastoma model (see 2.2.2.3). To do this, we collaborated with Prof. Dr. rer. nat. Rainer Glaß (Neurosurgical Research, LMU Munich). Adult C57BL/6J (control) mice, and α -pv^{fl/fl} mice expressing the inducible endothelial-specific Cadh5(PAC)-CreERT2¹⁶² were inoculated intracerebrally with 1 μ l of glioma cells (GL261, 100000 cells/ μ l) at day 0. Tamoxifen administration (100 μ l, 20 μ g/ μ l) at day 3-5 once daily, induced endothelial-specific α -pv deletion (herein referred to as α -pv ^{Δ EC} mice). At day 17, mice were sacrificed and tumors were analyzed (Figure 40, A).

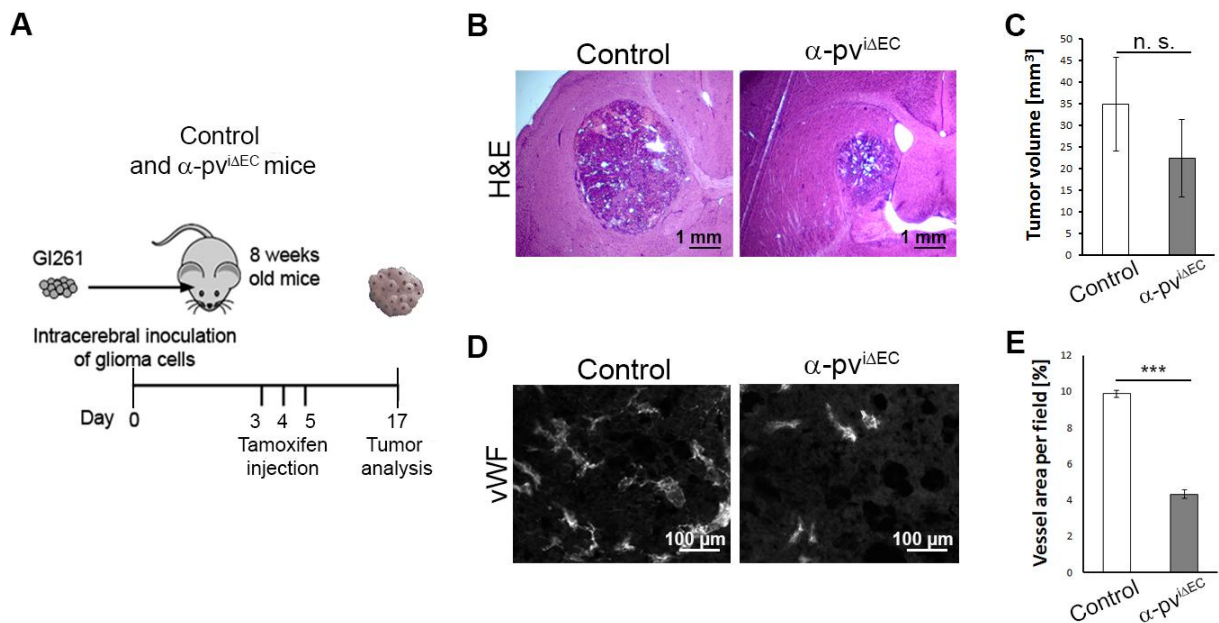


Figure 40. α -pv depletion in ECs reduces tumor growth and vascularization in α -pv ^{Δ EC} mice. (A) Schematic overview of the glioma experiment. Injection of GL261 cells at day 0; tamoxifen administration at day 3-5; tumor analysis at day 17. (B) H&E staining of brain section of α -pv ^{Δ EC} mice indicate reduced tumor size. (C) Quantification of tumor size showed slight reduction (not significant) in α -pv ^{Δ EC} mice compared to control mice. (D) Staining of brain sections with vWF. (E) Quantification of vessel area per field showed reduced vessel density in α -pv ^{Δ EC} compared to control mice. Values represent mean \pm SEM. ***P \leq 0.001, number of controls (n=8), number of α -pv ^{Δ EC} (n=7).

Fehler! Verwenden Sie die Registerkarte 'Start', um Überschrift 1;Ü 1 dem Text zuzuweisen, der hier angezeigt werden soll.

Brain sections of control and α -pv^{iΔEC} mice were stained with H&E and the tumor size was analyzed. α -pv^{iΔEC} mice showed a reduction in tumor size compared to control mice, although the reduction was not significant (Figure 40, B, C). Sections of control and α -pv^{iΔEC} brains were stained with the vessel marker von-Willebrand-Factor (vWF), revealing a significant loss of vessel density in α -pv^{iΔEC} tumors compared to control tumors (Figure 40, D, E). These results indicate that endothelial α -pv is important for tumor angiogenesis.

3.2 Role of TDP-43 in ECs during angiogenesis

The constitutive loss of TDP-43 in zebrafish leads to vascular miss-patterning¹³¹. The role of endothelial TDP-43 is, however, not known so far. To determine the role of endothelial TDP-43 during angiogenesis, we used an endothelial-specific inducible mouse model and analyzed postnatal retinal vascularization over time. We intercrossed TDP-43^{fl/fl} mice¹⁷⁶ with mice expressing the Cadh5(PAC)-CreERT2¹⁶² and induced deletion of the *TDP-43* gene in newborns with three consecutive tamoxifen injections starting at P1 and retinas were analyzed at P7.5. Western blot analysis from lung lysates of P7.5 TDP-43^{fl/fl};Cadh5(PAC)-CreERT2 (referred to herein as TDP-43^{iΔEC}) and TDP-43^{fl/fl} (Control) mice showed reduced protein levels in TDP-43^{iΔEC} mice. VEcad and GAPDH served as loading controls (Figure 41, A). Whole mount immunostainings of TDP-43^{iΔEC} and control retinas for IB4 showed a significant reduction in radial outgrowth of the retinal vasculature in TDP-43^{iΔEC} retinas compared to control retinas (Figure 41, B, C). Furthermore, TDP-43^{iΔEC} mice displayed an increase of vessel density in the front of the retinal vasculature compared to control retinas. These highly dense areas appeared more prominently in the peri-venous vessel plexus (Figure 41, B, C).

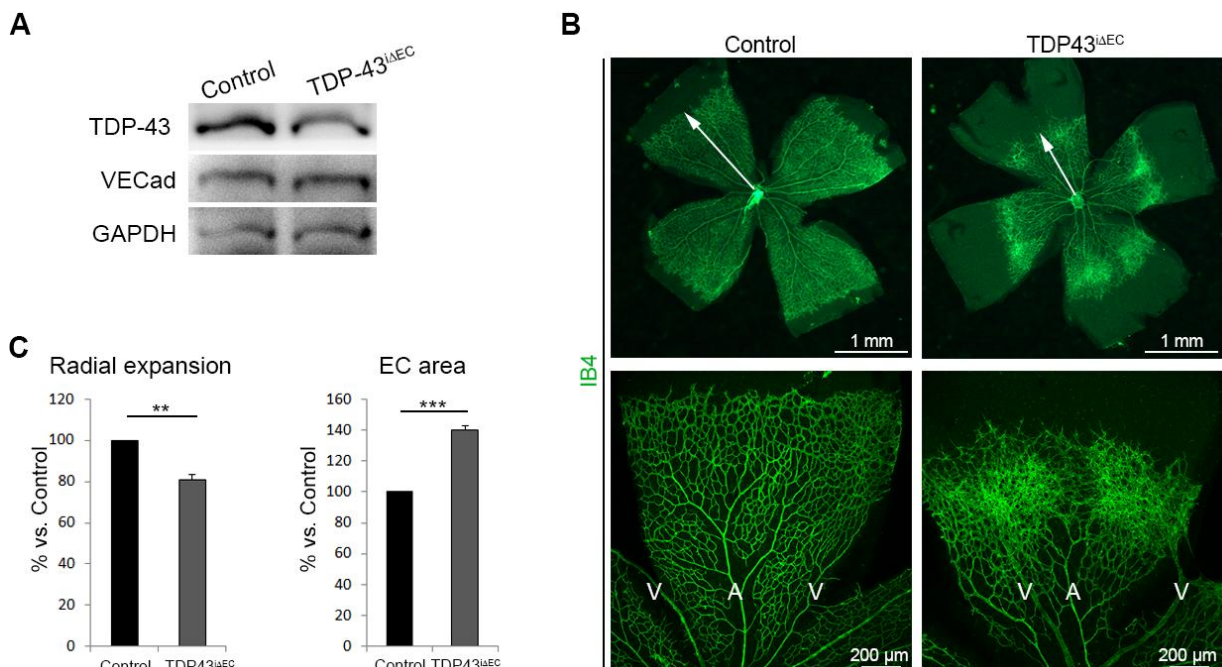


Figure 41. Endothelial-specific deletion of TDP-43 leads to vascular defects in retinal vasculature. (A) Western blot analysis of lung lysates from P7.5 control and TDP-43^{iΔEC} mice. VEcad and GAPDH were used as loading controls. (B) IB4 immunostaining of P7.5 control and TDP-43^{iΔEC} retinas. Arrows indicate radial outgrowth. (C) Quantification of radial length and vessel density. Reduced radial length and increased vessel density was observed in absence of endothelial TDP-43. Values represent mean ± SEM. **P≤0.01, ***P≤0.001, number of retinas (n=4).

Fehler! Verwenden Sie die Registerkarte 'Start', um Überschrift 1;Ü 1 dem Text zuzuweisen, der hier angezeigt werden soll.

Higher magnifications of the retinal front revealed that sprouts of TDP-43^{iΔEC} retinas appeared chaotic and some sprouts extended far beyond the angiogenic front without connecting to other vessel segments (Figure 42, A). Moreover, TDP-43^{iΔEC} retinas showed a significant increase of filopodia number compared to control retinas (Figure 42, A, B). These results suggest a role of TDP-43 on tip cell formation.

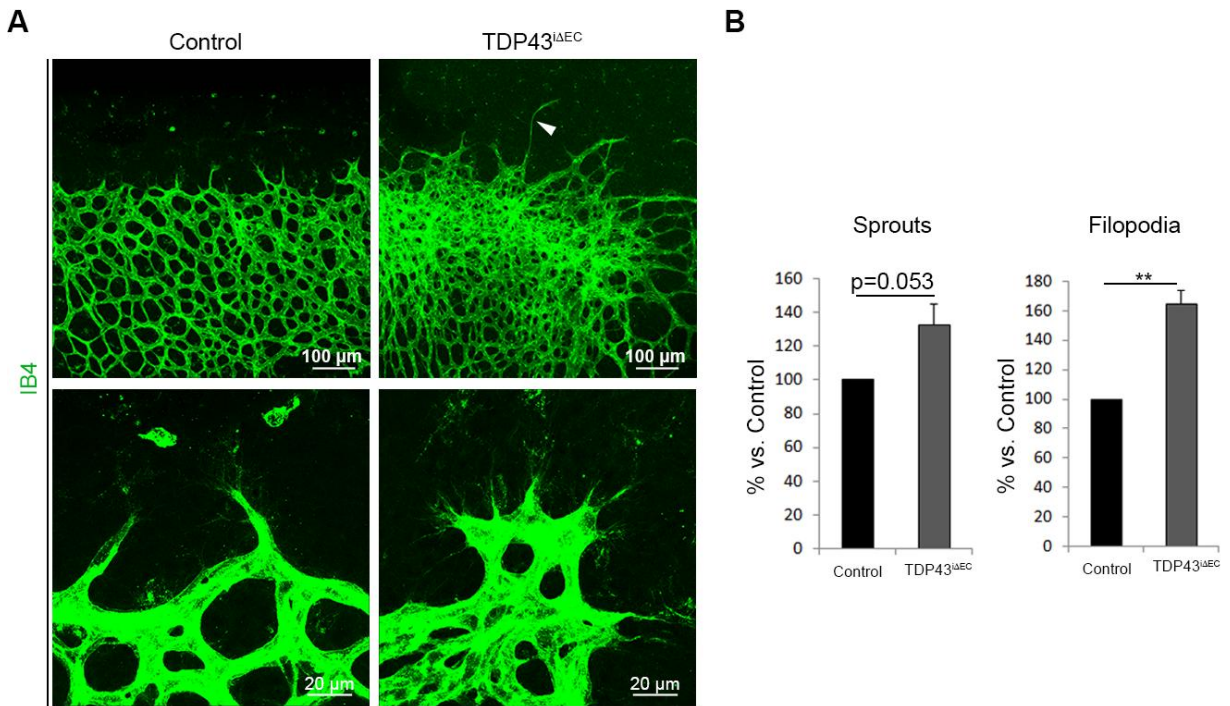


Figure 42. Loss of endothelial TDP-43 results in hyper-sprouting and increased number of filopodia. (A) P7.5 TDP-43^{iΔEC} and control retinas were immunostained for IB4. TDP-43^{iΔEC} retinas showed several vessel layers compared to controls. Arrowhead points at long sprout. (B) Quantification of sprout and filopodia numbers. TDP-43^{iΔEC} retinas revealed increased sprout and filopodia numbers compared to control retinas. Values represent mean \pm SEM. ** $P \leq 0.01$, number of retinas (n=3).

Therefore, we performed whole mount immunostaining for the tip cell marker Esm1, and observed an ectopic expression of Esm1 in TDP-43^{iΔEC} compared to controls (Figure 43). Furthermore, immunostaining for VEcad showed altered VEcad distribution in TDP-43^{iΔEC} vessels (Figure 43). Control vessels presented a sharp and continuous VEcad stain, whereas TDP-43 depleted vessels revealed prominent VEcad aggregates.

Fehler! Verwenden Sie die Registerkarte 'Start', um Überschrift 1;Ü 1 dem Text zuzuweisen, der hier angezeigt werden soll.

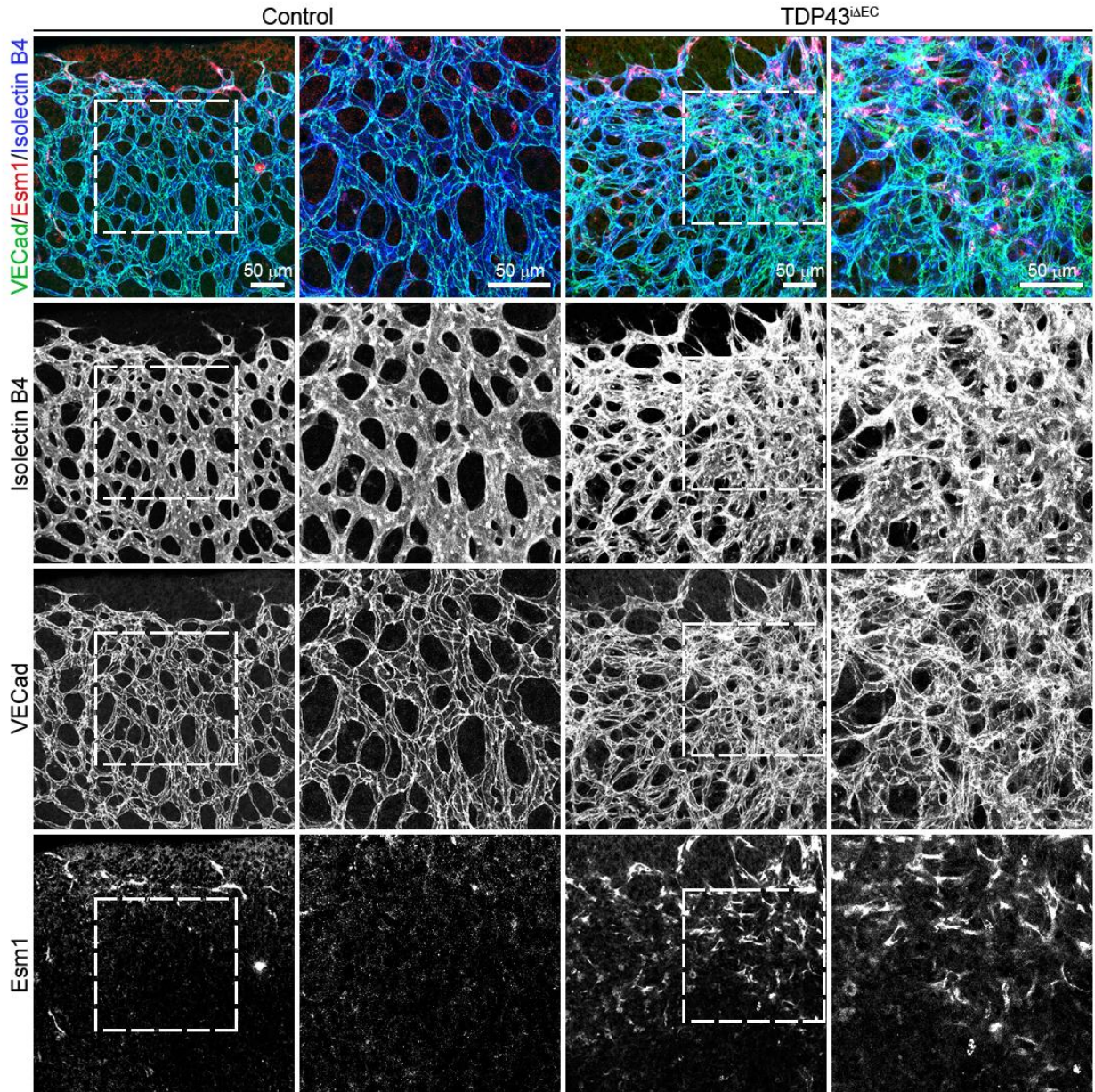


Figure 43. Ectopic expression of tip cell marker and VECad in TDP-43^{iΔEC} retinas. P7.5 control and TDP-43^{iΔEC} retinas labeled for VECad (green), Esm1 (red), and IB4 (blue). TDP-43^{iΔEC} retinas revealed ectopic tip cell expression in perivenous areas and abnormal VECad staining compared to controls retinas. Dotted square mark higher magnifications.

To analyze whether vessel hyper density is caused by increased EC proliferation in the absence of TDP-43, we performed BrdU labeling together with the EC nucleus marker Erg 1/2/3 to visualize and quantify proliferating ECs (Figure 44). The quantitative analysis revealed no significant difference between TDP-43^{iΔEC} and control retinas.

Fehler! Verwenden Sie die Registerkarte 'Start', um Überschrift 1;Ü 1 dem Text zuzuweisen, der hier angezeigt werden soll.

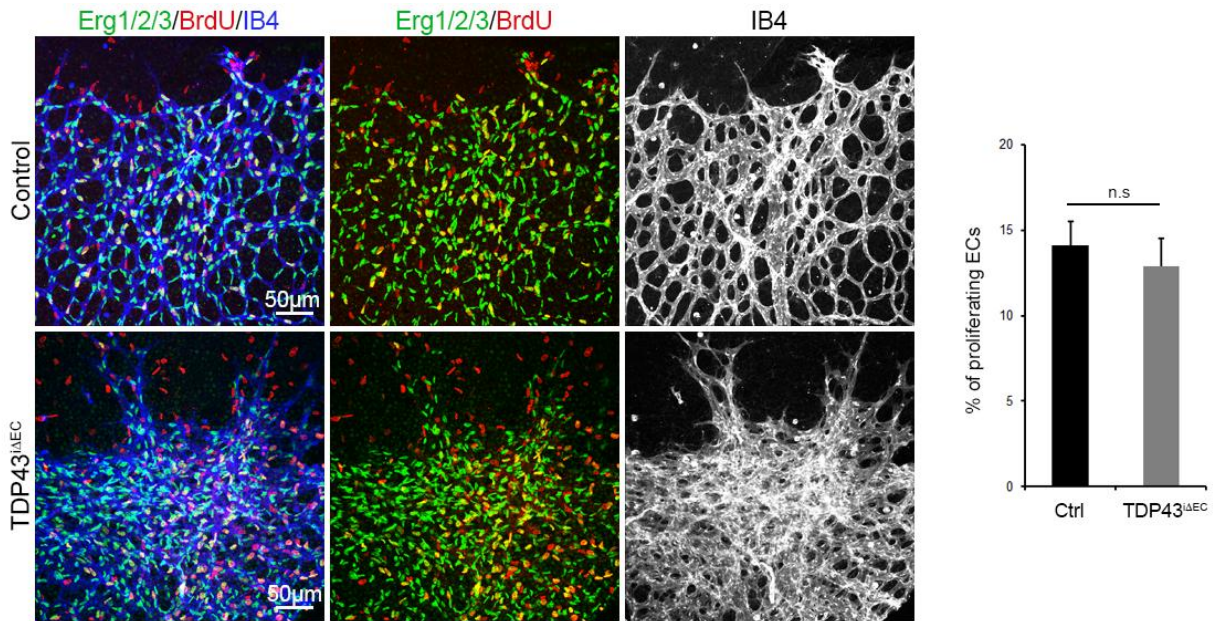


Figure 44. TDP-43^{iΔEC} retinas do not show increased EC proliferation. Immunostaining of Erg1/2/3 (green), BrdU (red) and IB4 (blue) to visualize proliferating ECs in P7.5 TDP-43^{iΔEC} and control retinas. Quantification did not reveal a significant difference. Values represent mean ± SEM, number of retinas (n=3).

Loss of TDP-43 in zebrafish leads to impaired vessel perfusion¹³¹. To analyze this, we immunostained TDP-43^{iΔEC} retinas and control retinas for IB4 and ICAM-2, an apical/basal vessel marker. This revealed discontinuous and fragmented ICAM-2 stain in many vessel segments in TDP-43^{iΔEC} compared to vessels in control retinas, indicating a defect in apical/basal EC polarity in the absence of TDP-43 (Figure 45).

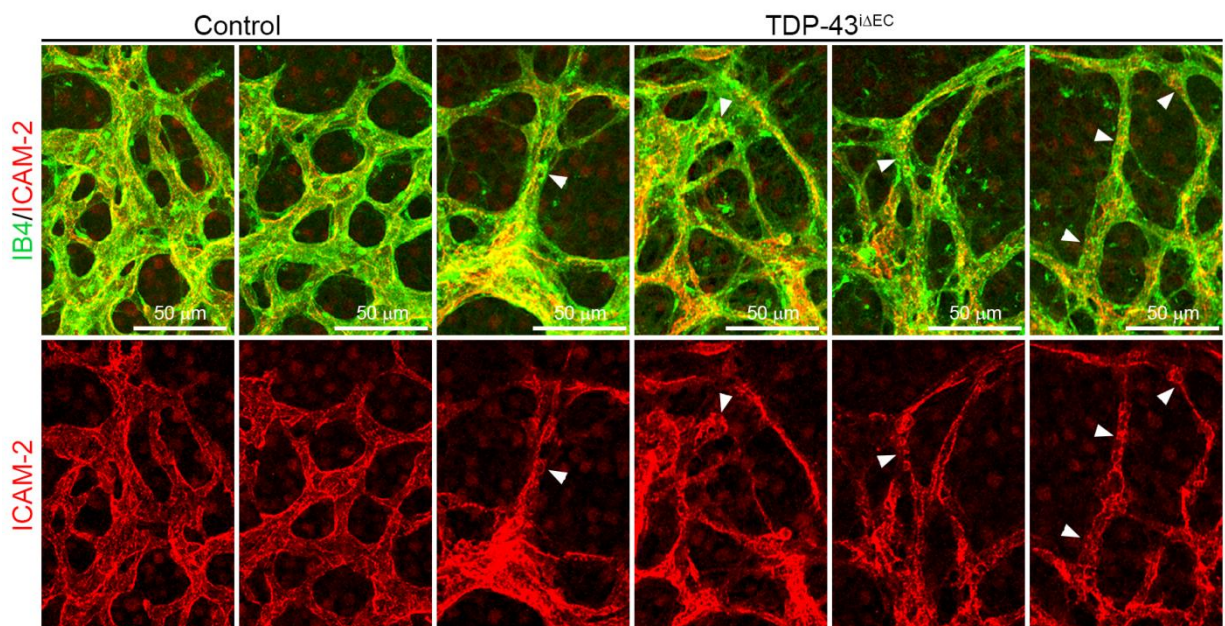


Figure 45. Altered apical/basal orientation in TDP-43^{iΔEC} retinal vasculature. P7.5 control and TDP-43^{iΔEC} retinas labeled for IB4 (green) and the vessel lumen marker ICAM-2 (red). Many vessel segments in TDP-43^{iΔEC} retinas showed discontinuous or absent ICAM-2 signal (see arrowheads).

Fehler! Verwenden Sie die Registerkarte 'Start', um Überschrift 1;Ü 1 dem Text zuzuweisen, der hier angezeigt werden soll.

These results indicate that endothelial TDP-43 controls vessel morphology, proper vessel formation and sprouting angiogenesis in mice. Furthermore, the angiogenic phenotype in the zebrafish could be confirmed in the EC-specific depletion of TDP-43 in the mouse retina.

4 Discussion

4.1 α -pv regulates vessel integrity and is crucial for cell-cell junction integrity

The depletion of endothelial α -pv in mice leads to reduced vessel stability, impaired cell-cell junction morphology in blood vessels, and hemorrhages, resulting in embryonic lethality between E15.5 and birth. *In vitro*, α -pv depletion in ECs leads to impaired monolayer formation due to instable cell-cell junctions. Furthermore, ECs lacking α -pv display reduced migration associated with perturbed actin cytoskeleton organization, reduced Rac1 activity and decreased formation of integrin-based cell-ECM adhesion structures. We conclude that α -pv facilitates proper actin cytoskeleton organization that is needed for cell migration and cell-cell junction integrity during vessels formation.

The formation and integrity of blood vessels require integrin-mediated EC-ECM interactions^{37,177}. Integrin signaling is needed for cell shape, polarity, cell migration, and junction integrity, thereby regulating lumen formation, sprouting, anastomosis, and vessel stability^{39,53}. Due to this, the depletion of endothelial β 1 integrin in mice causes embryonic lethality at E10.5^{57,178}. Although integrin signaling is crucial for vascular development, the molecular mechanisms of integrin-mediated cellular processes during vascular development *in vivo* are not fully understood. Integrins bind to the actin cytoskeleton through actin binding molecules, such as parvins³⁵. ECs express two different parvin isoforms, α -pv and β -pv. Our results show that lack of endothelial α -pv results in embryonic lethality beginning at E15.5 up to birth. Therefore, we conclude that α -pv is essential for integrin signaling during embryonic development.

α -pv and β -pv can form two different IPP complexes in one cell, together with ILK and PINCH, which then is crucial in integrin signaling³⁵. Depletion of one component leads to the

Fehler! Verwenden Sie die Registerkarte 'Start', um Überschrift 1;Ü 1 dem Text zuzuweisen, der hier angezeigt werden soll.

decomposition of the complex and to degradation of the other components. ILK depletion in ECs results in embryonic lethality starting at E10.5, revealing that the IPP complex is essential for integrin signaling^{57,103}. This is in agreement with our results that α -pv ^{Δ EC} mice die at E15.5 and α -pv ^{Δ EC}; β -pv^{-/-} embryos die similar to ILK ^{Δ EC} embryos.

The integrity of vessels depends on VEcad-mediated cell-cell junctions^{109,114}. It has been shown that β 1 integrin regulates cell-cell junction integrity by regulating VEcad internalization. This mechanism involves β 1 integrin mediated phospho-myosin light chain (p-MLC) levels and the Rap1/MRCK and Rho/Rho-kinase pathways⁵⁹. Furthermore, it has been reported that laminin α 5 binding to β 1 integrin is important for FA formation and VEcad dependent cell-cell junction integrity¹⁷⁹. Loss of α -pv in ECs leads to impaired VEcad-mediated cell-cell junctions, discontinuous junctions, and gaps between cells. Interestingly, in α -pv depleted ECs we do not observe VEcad internalization defects. These results propose that loss of VEcad-based cell-cell junction integrity in α -pv depleted ECs underlies a different process than in β 1 integrin depleted ECs.

The structural integrity of cell-cell junctions is regulated by local rearrangement of the actin cytoskeleton at cell-cell contacts^{180,181}. Stable AJs are associated with the cortical actin^{182,183}. Recently it has been shown that actin driven lamellipodia at the cell-cell junctions regulate dynamic rearrangement of VEcad, thereby controlling junction stability¹²⁶. These structures are called JAIL. We show that α -pv localizes at the leading edge of JAIL and is important for proper JAIL formation and thereby VEcad dynamics. These results suggest that α -pv deficiency affects cell-cell junction integrity and vessel stability via integrin-mediated signaling to the actin cytoskeleton. In accordance with this conclusion, the depletion of α -pv leads to impaired cortical actin cytoskeleton rearrangement associated with unstable AJs *in vitro*.

The Arp2/3 complex drives lamellipodia protrusion and regulates JAIL formation. Rac1 is important for the Arp2/3 complex and therefore monolayer integrity and vessel stability^{124,184}. Whether Rac1 is needed for JAIL formation is not known so far. We observe that loss of α -pv leads to reduced Rac1 activity, suggesting that α -pv could regulate JAIL formation via Rac1. Moreover, Vinc is an important mediator in integrin-based adhesion, and VEcad-mediated cell-cell junctions. Vinc binds to the Arp2/3 complex and thereby

Fehler! Verwenden Sie die Registerkarte 'Start', um Überschrift 1;Ü 1 dem Text zuzuweisen, der hier angezeigt werden soll.

couple the actin polymerization machinery to the membrane and enable lamellipodia protrusion^{185,186}. The depletion of endothelial α -pv results in loss of Vinc localization to the leading edge¹⁰⁸, which can lead to a defective recruitment and complex formation of Arp2/3 and Vinc at the lamellipodia.

Vessel formation depends on integrin-mediated vessel sprouting and elongation, in which β 1 integrin signaling is crucial^{59,187}. Integrin-mediated FX formation and FA maturation, and actin rearrangement are important for cell motility and therefore for normal vessel formation and elongation^{182,188}. FX are located at lamellipodia, mediating protrusion of the membrane and therefore cell migration. ECs deficient for α -pv display impaired migration abilities in endothelial-specific depletion of α -pv in the retina¹⁰⁸, and also *in vitro* due to reduced FXs and FA structures. Our results also show heterogeneity in vessel diameters in vessels from α -pv ^{Δ EC} embryos, suggesting that α -pv is involved in collective EC migration, and is therefore important for vessel elongation during angiogenesis. We conclude that α -pv contributes to vessel elongation and sprouting by modulating the actin cytoskeleton at the ECM adhesion and cell-cell junctions.

PINCH and ILK are also important for the regulation of cell-cell junctions in epithelial cells^{107,189}. AJs in epithelial cells are part of a stable barrier and are not as dynamic as AJs in ECs¹²². Since α -pv is important for keeping structural junction integrity in ECs, the members of the IPP complex could also have a role in endothelial cell-cell junctions. α -pv may also have further functions separately from the IPP complex. This, however, has not been investigated. Whether ILK and PINCH are important for junction integrity in ECs is not known yet.

α -pv ^{Δ EC} and β 1 ^{Δ EC} both result in vascular defects, leading to embryonic lethality. β 1 ^{Δ EC} show increased sprouting, proliferation, and vessel hyperdensity result in embryonic lethality at E10.5. α -pv ^{Δ EC} instead show reduced proliferation, and increased apoptosis, leading to vessel hypodensity and embryonic lethality starting at E15.5. Since integrin signaling depends on the IPP complex, endothelial depletion of ILK results in complex degeneration and in embryonic lethality between E10.5 and E12.5, comparable to β 1 ^{Δ EC} lethality^{35,103} (Figure 46, A). The difference in lethality might be explained by a compensational effect of α -pv by β -pv. However, this has not been shown yet. Our results show that the depletion of both, α -pv and

Fehler! Verwenden Sie die Registerkarte 'Start', um Überschrift 1;Ü 1 dem Text zuzuweisen, der hier angezeigt werden soll.

β -pv in ECs, result in embryonic lethality at E11.5 to E12.5, similar to $\beta 1^{\Delta EC}$ (Figure 46, A). Therefore, we can conclude that the different lethality of $\beta 1^{\Delta EC}$ and $ILK^{\Delta EC}$, and α -pv $^{\Delta EC}$ can be explained by the ability of β -pv to compensate for endothelial α -pv during early embryogenesis. The ratio between α -pv and β -pv in ECs was not investigated. α -pv and β -pv mutually regulate the expression of each other. β -pv is negatively regulated by α -pv^{101,190}.

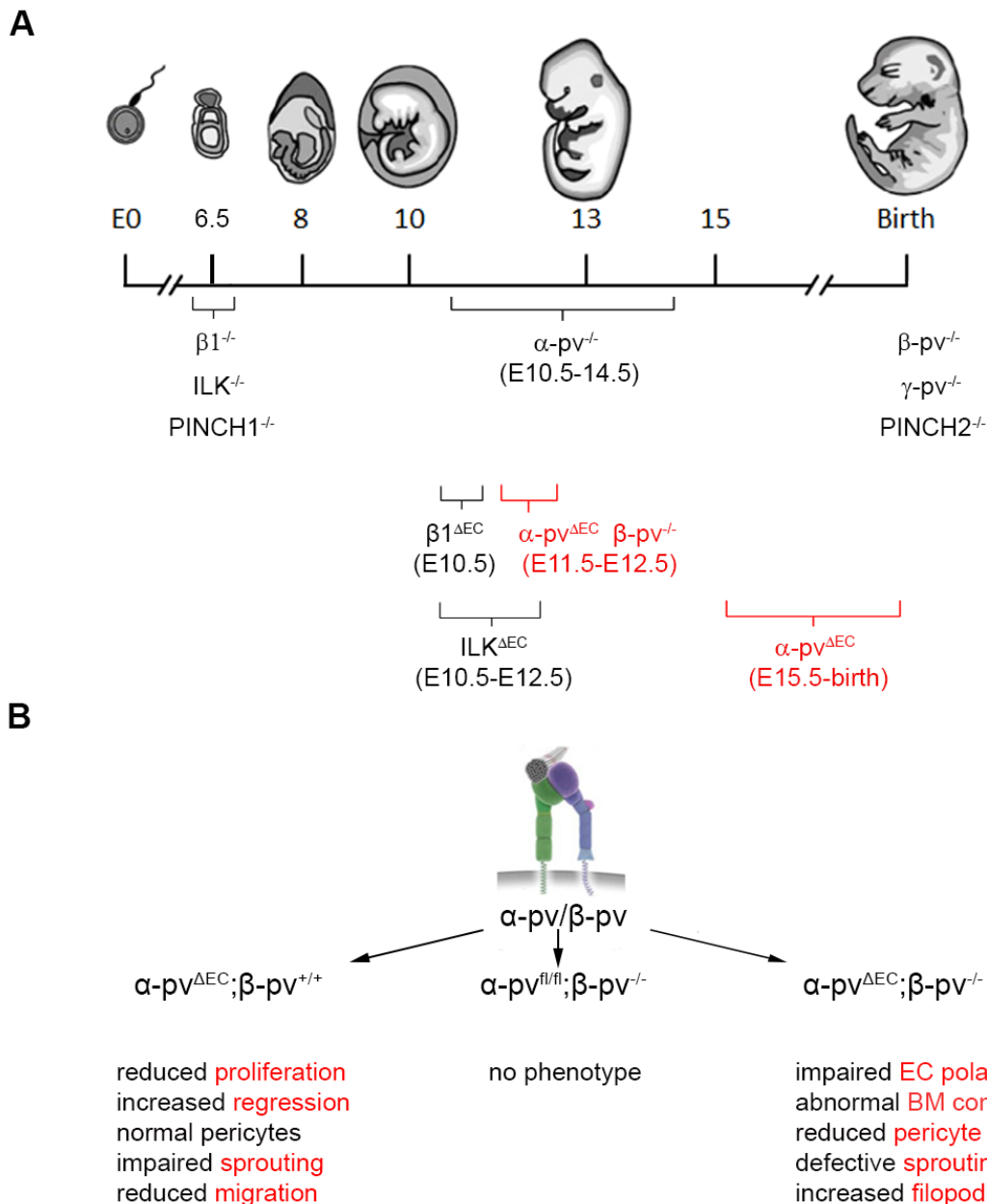


Figure 46. Comparison of the different outcomes of parvin depletions. (A) Impact of gene deletions of the integrin signaling cascade on embryonic lethality in mice. $\beta 1^{\Delta EC}$, $ILK^{\Delta EC}$, and α -pv $^{\Delta EC}; \beta$ -pv $^{-/-}$, but not α -pv $^{\Delta EC}$ results in embryonic lethality up to E12.5. β -pv can compensate for endothelial α -pv in early embryogenesis. (B) Summary of α -pv $^{\Delta EC}; \beta$ -pv $^{+/+}$, α -pv $^{fl/fl}; \beta$ -pv $^{-/-}$, α -pv $^{\Delta EC}; \beta$ -pv $^{-/-}$, phenotypes. Different parvin depletions result in distinct phenotypes.

4.2 Impaired integrin-mediated parvin signaling results in severe vascular malformations

Loss of parvins in ECs leads to severe embryonic vascular malformations in the brain and the spinal cord. Vessels display reduced sprouting into the brain and the spinal cord, increased filopodia numbers, enlarged vessel diameters, and glomeruloid structures in the CNS vasculature. The vessel walls show incomplete PE coverage, and abnormal Glut-1 expression, both important for normal BBB formation. ECs lacking α -pv and β -pv appear round and less elongated but they reveal no proliferation defects. These results show that the endothelial depletion of both parvins cause severe defects in the vascularization of the CNS.

The phenotypes of α -pv ^{Δ EC} and α -pv ^{Δ EC}; β -pv^{-/-} embryos show differences (Figure 46, A, B). The depletion of β -pv does not lead to any obvious embryonic phenotype, whereas depletion of endothelial α -pv impairs proliferation, regression, cell migration, and sprouting. Additional depletion of β -pv in α -pv ^{Δ EC} embryos does not significantly affect proliferation, but PE recruitment, sprouting angiogenesis, and filopodia formation (Figure 46, B). This suggests that α -pv and β -pv depletion impair integrin signaling more severely than α -pv depletion. Therefore, it offers the possibility to study the integrin signaling pathways in more detail, because α -pv ^{Δ EC} does not completely inhibit the integrin signaling pathway as β 1 ^{Δ EC} does. The vascular phenotype of α -pv ^{Δ EC}; β -pv^{-/-} is still less severe than in β 1 ^{Δ EC}, which completely lacks CNS vascularization at E11.5. An overview of total or endothelial-specific deletions of β 1 integrin or other components of the IPP complex, and their effects on embryonic lethality is shown in Figure 46.

Instability and leakiness of vessels can be caused by an impairment of the BBB. This barrier function is dependent on ECM and PE attached to the vessel wall^{151,191,192}. The formation and integrity of newly formed blood vessels also highly depends on the recruitment and coverage of the vessel walls by mural cells^{109,134,193}. Depletion of total α -pv causes impaired mural cell recruitment to the vessel wall¹⁰¹. However, vessels from α -pv ^{Δ EC} embryos do not display abnormal mural cell recruitment and coverage of the vessel wall. But we do observe hemorrhages and cell-cell junction abnormalities, suggesting vessel rupture in α -pv ^{Δ EC} embryos. In α -pv ^{Δ EC}; β -pv^{-/-} embryos we see impaired PE spreading and attachment to the vessels, which can cause instability and hemorrhages. Abnormal apical/basal polarity of ECs

Fehler! Verwenden Sie die Registerkarte 'Start', um Überschrift 1;Ü 1 dem Text zuzuweisen, der hier angezeigt werden soll.

and structural abnormalities of BM components could be causative for defective PE spreading and attachment. *Glut-1* is a target gene of the hypoxia-inducible factor (HIF), which are both expressed reciprocal to angiogenesis and tissue oxygenation¹⁹⁴. The expression of *Glut-1* is also altered in α -pv ^{Δ EC}; β -pv^{-/-} embryos, which presents defective barrier function and abnormal brain development, suggesting a breakdown of the NVU^{149,194,195}. This is also in agreement with the abnormal PE attachment that we observe in α -pv ^{Δ EC}; β -pv^{-/-} embryos. The increased number of filopodia in α -pv ^{Δ EC}; β -pv^{-/-} hindbrains points to an insufficient oxygen supply of the brain, which leads to increased HIF expression and induces VEGF. This can lead to angiogenic sprouting and abnormal PE attachment^{196,197}. VEGF and its receptors, neuropilins (NRPs) and others, are also known to play a major role in the regulation of CNS vascularization¹⁶³. Moreover, the glomeruloid structures observed in α -pv ^{Δ EC}; β -pv^{-/-} embryos could be due to abnormal tip cell formation. Even though we do not see any difference in EC proliferation, reduced migration could cause accumulation of ECs and result in glomeruloid formations. Thus, we conclude that the depletion of both, endothelial α -pv and β -pv, results in defective vasculature and impaired barrier function in the CNS.

The phenotype of the vasculature in α -pv ^{Δ EC}; β -pv^{-/-} embryos resembles the β -cat ^{Δ EC} phenotype in the CNS vasculature. β -cat ^{Δ EC} embryos die at E12.5 and show glomeruloid vascular malformations in their CNS vasculature. Furthermore, hemorrhages are observed in these embryos associated with an impaired expression of the BBB marker *Glut-1*¹⁹⁸. It has been reported that ILK inhibition downregulates β -cat expression in cells¹⁹⁹. Therefore, Wnt/ β -cat signaling is crucial for CNS angiogenesis and barrier formation^{198,200,201}. Moreover, it has been reported that the Wnt ligands *Wnt7a* and *Wnt7b* are involved in the process of invasive sprouting of vessels into the CNS¹⁴⁹. Additionally, Wnt signaling from the neuroepithelium stabilizes the BBB and regulates the glucose transporter *Glut-1* expression in ECs via β -cat^{202,203}. However, whether α -pv and β -pv are involved in Wnt/ β -cat pathway in ECs is not known and needs to be studied.

Cerebral cavernous malformation (CCM) is a human disease that is caused by mutations in the CCM genes and results in dilated capillaries that form caverns connected with thin channels allowing only sluggish blood flow²⁰⁴⁻²⁰⁷. These malformations show multilayers of hyperactive ECs and are aligned by a BM without surrounding PE and astrocytes, which

Fehler! Verwenden Sie die Registerkarte 'Start', um Überschrift 1;Ü 1 dem Text zuzuweisen, der hier angezeigt werden soll.

causes a leaky BBB and prone these lesions to bleedings^{208,209}. The molecular pathogenesis of CCMs is increasingly being investigated in many mouse studies. This phenotype shows similarities to the observed malformations of the vasculature in α -pv ^{Δ EC}; β -pv^{-/-} embryos. So far, it is known, that CCM proteins are involved in cell-cell adhesion and cell-ECM adhesion. Binding of CCM1 to β -cat regulates AJ stability and barrier formation via actin cytoskeleton remodeling¹¹². Moreover, the interaction of CCM1/2 with β 1 integrin controls cell adhesion and migration^{204,209-211}. It would be very interesting to investigate whether parvins are involved in CCM regulation and to test human samples on parvin levels.

NRP1 and β 8 integrin in the neuroepithelium promote TGF β signaling in ECs and thereby control sprouting angiogenesis in the CNS²¹². Its perturbation leads to similar glomeruloid structures in the vasculature of the brain than in α -pv ^{Δ EC}; β -pv^{-/-} embryos, suggesting an involvement of this signaling pathway. But whether these pathways, and to which extent, are involved and altered in the absence of endothelial α -pv and β -pv, has to be analyzed in further experiments.

Angiogenesis also contributes to the progression of many diseases, such as tumor growth. We therefore investigated the role of α -pv in pathological angiogenesis. Gliomas are highly malignant brain tumors that, with regard to their growth, depend on angiogenic sprouting for nutrient supply¹⁴¹. Our experiments reveal that the absence of α -pv significantly reduces vessels in the tumor and also slightly decreases tumor size. These results show that α -pv is also important in pathological angiogenesis. Investigating tumor angiogenesis in α -pv ^{Δ EC}; β -pv^{-/-} mice would give more information about the role of parvins in pathological angiogenesis. This, however, has to be further investigated. Moreover, the glioma model in our mice suits for integrin signaling studies, since integrin signaling is important in tumor growth and the depletion of parvins only partially perturbs integrin signaling in angiogenesis.

4.3 TDP-43 depletion in ECs causes vascular defects

Induced depletion of TDP-43 in ECs in mice leads to retinal vasculature mispatterning. The vasculature shows reduced radial vascular expansion, increased vessel sprouting and ectopic expression of tip cell markers, leading to increased vessel density at the angiogenic front. These defects were not caused by increased EC proliferation. Furthermore, loss of endothelial TDP-43 resulted in impaired cell-cell junction morphology and defective endothelial apical/basal polarity. These results show that endothelial TDP-43 is crucial for the formation of a mature vascular network.

The vascularization of the CNS is crucial for normal neuronal development and function. In fact, the neuronal and the vascular system show many similarities in development and function, such as anatomic structure and importance for information transfer¹⁴⁹. This close interaction at different levels is termed the neurovascular link. Defects in the vessel structure or abnormal vessel growth in the CNS can cause neurological disorders²⁰⁸. Therefore, it seems logic to investigate vascular function in neuronal diseases. Dysfunctions of non-neuronal cells, such as members of the NVU, can also contribute to neurodegeneration. Whether they are cause or effect is, however, not clear. It has further been shown that VEGF has a therapeutic potential in motor neuron degeneration²¹³. ALS patients show EC damage and NVU breakdown. Moreover, in these patients TDP-43 inclusions have been observed. Studies in zebrafish show that the complete depletion of TDP-43 results in vascular mispatterning and perfusion defects, additional to neuron degeneration. So far, the role of TDP-43 in vascular formation is not known and remains to be studied. Until now, there are no studies on the function of TDP-43 in ECs.

We show that endothelial-specific TDP-43 depletion causes vascular defects, revealing an essential and cell autonomous role of endothelial TDP-43 in the angiogenic process. The hyperdense retinal front is not due to increased EC proliferation, but may be caused by migration defects. Increased and ectopic tip cell expression hints to a defective tip/stalk cell specification, which could also be causing the sprouting abnormalities in zebrafish lacking TDP-43. The VEcad aggregates, observed in the retinal vasculature of TDP-43^{ΔEC} retinas, suggest junctional abnormalities between ECs. This could cause a defect in the integrity of the NVU.

Fehler! Verwenden Sie die Registerkarte 'Start', um Überschrift 1;Ü 1 dem Text zuzuweisen, der hier angezeigt werden soll.

Vascular defects observed in ALS patients might be directly or indirectly associated with impaired endothelial TDP-43. ALS occurs in adult patients, in which no developmental angiogenesis takes place, however, animal studies done so far only give conclusions from developmental stages. Therefore, the function of endothelial TDP-43 in adult should be investigated. The importance of TDP-43 in BBB integrity and whether vascular defects cause neurodegeneration has to be shown in further studies. It is also not clear if vascular malformations occur prior to or past neurodegeneration. TDP-43 is found in inclusion in ALS patients, and it is still under discussion, whether TDP-43 contributes to the disease in a loss-of-function, or gain-of-function manner. Gene mutation studies in mice could be a tool to gain more insight into possible disease mechanisms.

5 References

1. Gaengel, K., Genove, G., Armulik, A. & Betsholtz, C. Endothelial-mural cell signaling in vascular development and angiogenesis. *Arteriosclerosis, thrombosis, and vascular biology* **29**, 630-638 (2009).
2. Swift, M.R. & Weinstein, B.M. Arterial-venous specification during development. *Circulation research* **104**, 576-588 (2009).
3. Eelen, G., de Zeeuw, P., Simons, M. & Carmeliet, P. Endothelial cell metabolism in normal and diseased vasculature. *Circulation research* **116**, 1231-1244 (2015).
4. Folkman, J. Angiogenesis: an organizing principle for drug discovery? *Nature reviews Drug discovery* **6**, 273-286 (2007).
5. Carmeliet, P. Angiogenesis in health and disease. *Nature Medicine* **9** (2003).
6. Potente, M., Gerhardt, H. & Carmeliet, P. Basic and therapeutic aspects of angiogenesis. *Cell* **146**, 873-887 (2011).
7. Crawford, Y. & Ferrara, N. Tumor and stromal pathways mediating refractoriness/resistance to anti-angiogenic therapies. *Trends in pharmacological sciences* **30**, 624-630 (2009).
8. Crawford, Y. & Ferrara, N. VEGF inhibition: insights from preclinical and clinical studies. *Cell and tissue research* **335**, 261-269 (2009).
9. Phng, L.K. & Gerhardt, H. Angiogenesis: a team effort coordinated by notch. *Developmental cell* **16**, 196-208 (2009).
10. Augustin, H.G., Koh, G.Y., Thurston, G. & Alitalo, K. Control of vascular morphogenesis and homeostasis through the angiopoietin-Tie system. *Nature Reviews Molecular Cell Biology* **10**, 165-177 (2009).
11. Seano, G., Daubon, T., Genot, E. & Primo, L. Podosomes as novel players in endothelial biology. *European journal of cell biology* **93**, 405-412 (2014).
12. Gerhardt, H., *et al.* VEGF guides angiogenic sprouting utilizing endothelial tip cell

- filopodia. *The Journal of cell biology* **161**, 1163-1177 (2003).
13. Geudens, I. & Gerhardt, H. Coordinating cell behaviour during blood vessel formation. *Development* **138**, 4569-4583 (2011).
 14. Rocha, S.F., *et al.* Esm1 modulates endothelial tip cell behavior and vascular permeability by enhancing VEGF bioavailability. *Circulation research* **115**, 581-590 (2014).
 15. Benedito, R., *et al.* The notch ligands Dll4 and Jagged1 have opposing effects on angiogenesis. *Cell* **137**, 1124-1135 (2009).
 16. Blanco, R. & Gerhardt, H. VEGF and Notch in tip and stalk cell selection. *Cold Spring Harbor perspectives in medicine* **3**, a006569 (2013).
 17. Tammela, T., *et al.* Blocking VEGFR-3 suppresses angiogenic sprouting and vascular network formation. *Nature* **454**, 656-660 (2008).
 18. Jakobsson, L., *et al.* Endothelial cells dynamically compete for the tip cell position during angiogenic sprouting. *Nature cell biology* **12**, 943-953 (2010).
 19. Weinmaster, G. Notch signaling: direct or what? *Current opinion in genetics & development* **8**, 436-442 (1998).
 20. Mumm, J.S. & Kopan, R. Notch signaling: from the outside in. *Dev Biol* **228**, 151-165 (2000).
 21. Williams, C.K., Li, J.-L., Murga, M., Harris, A.L. & Tosato, G. Up-regulation of the Notch ligand Delta-like 4 inhibits VEGF-induced endothelial cell function. *Blood* **107**, 931-939 (2006).
 22. Harrington, L.S., *et al.* Regulation of multiple angiogenic pathways by Dll4 and Notch in human umbilical vein endothelial cells. *Microvascular research* **75**, 144-154 (2008).
 23. Liu, Z.-J., *et al.* Regulation of Notch1 and Dll4 by vascular endothelial growth factor in arterial endothelial cells: implications for modulating arteriogenesis and angiogenesis. *Molecular and cellular biology* **23**, 14-25 (2003).
 24. Hayashi, H. & Kume, T. Foxc transcription factors directly regulate Dll4 and Hey2 expression by interacting with the VEGF-Notch signaling pathways in endothelial cells. *PLoS one* **3**, e2401 (2008).
 25. Shalaby, F., *et al.* Failure of blood-island formation and vasculogenesis in Flk-1-deficient mice. *Nature* **376**, 62-66 (1995).
 26. Fong, G.-H., Rossant, J., Gertsenstein, M. & Breitman, M.L. Role of the Flt-1 receptor tyrosine kinase in regulating the assembly of vascular endothelium. *Nature* **376**, 66-70 (1995).
 27. Carmeliet, P., *et al.* Abnormal blood vessel development and lethality in embryos lacking a single VEGF allele. *Nature* **380**, 435-439 (1996).

Fehler! Verwenden Sie die Registerkarte 'Start', um Überschrift 1;Ü 1 dem Text zuzuweisen, der hier angezeigt werden soll.

28. Dumont, D.J., *et al.* Cardiovascular failure in mouse embryos deficient in VEGF receptor-3. *Science* **282**, 946-949 (1998).
29. Fantin, A., *et al.* Tissue macrophages act as cellular chaperones for vascular anastomosis downstream of VEGF-mediated endothelial tip cell induction. *Blood* **116**, 829-840 (2010).
30. Eble, J.A. & Niland, S. The extracellular matrix of blood vessels. *Current pharmaceutical design* **15**, 1385-1400 (2009).
31. Jain, R.K. Molecular regulation of vessel maturation. *Nature medicine* **9**, 685-693 (2003).
32. Mettouchi, A. The role of extracellular matrix in vascular branching morphogenesis. *Cell adhesion & migration* **6**, 528-534 (2012).
33. Saharinen, P. & Ivaska, J. Blocking integrin inactivation as an anti-angiogenic therapy. *The EMBO journal* **34**, 1293-1295 (2015).
34. Mahabeleshwar, G.H., Feng, W., Phillips, D.R. & Byzova, T.V. Integrin signaling is critical for pathological angiogenesis. *The Journal of experimental medicine* **203**, 2495-2507 (2006).
35. Legate, K.R., Montanez, E., Kudlacek, O. & Fassler, R. ILK, PINCH and parvin: the tIPP of integrin signalling. *Nature reviews. Molecular cell biology* **7**, 20-31 (2006).
36. Takada, Y., Ye, X. & Simon, S. The integrins. *Genome biology* **8**, 215 (2007).
37. Hynes, R. Cell-matrix adhesion in vascular development. *Journal of Thrombosis and Haemostasis* **5**, 32-40 (2007).
38. Hynes, R.O. Integrins: bidirectional, allosteric signaling machines. *Cell* **110**, 673-687 (2002).
39. Barczyk, M., Carracedo, S. & Gullberg, D. Integrins. *Cell and tissue research* **339**, 269-280 (2010).
40. Humphries, J.D., Byron, A. & Humphries, M.J. Integrin ligands at a glance. *Journal of cell science* **119**, 3901-3903 (2006).
41. Hu, P. & Luo, B.H. Integrin bi-directional signaling across the plasma membrane. *Journal of cellular physiology* **228**, 306-312 (2013).
42. Pankov, R., *et al.* Integrin dynamics and matrix assembly tensin-dependent translocation of $\alpha 5\beta 1$ integrins promotes early fibronectin fibrillogenesis. *The Journal of cell biology* **148**, 1075-1090 (2000).
43. Wolfenson, H., Lavelin, I. & Geiger, B. Dynamic regulation of the structure and functions of integrin adhesions. *Developmental cell* **24**, 447-458 (2013).
44. De Smet, F., Segura, I., De Bock, K., Hohensinner, P.J. & Carmeliet, P. Mechanisms of

Fehler! Verwenden Sie die Registerkarte 'Start', um Überschrift 1;Ü 1 dem Text zuzuweisen, der hier angezeigt werden soll.

- vessel branching: filopodia on endothelial tip cells lead the way. *Arteriosclerosis, thrombosis, and vascular biology* **29**, 639-649 (2009).
45. Gardel, M.L., Schneider, I.C., Aratyn-Schaus, Y. & Waterman, C.M. Mechanical integration of actin and adhesion dynamics in cell migration. *Annual review of cell and developmental biology* **26**, 315-333 (2010).
 46. Blanchoin, L., Boujemaa-Paterski, R., Sykes, C. & Plastino, J. Actin dynamics, architecture, and mechanics in cell motility. *Physiological reviews* **94**, 235-263 (2014).
 47. "Used by permission from MBInfo: www.mechanobio.info; Mechanobiology Institute, National University of Singapore"
 48. Sit, S.-T. & Manser, E. Rho GTPases and their role in organizing the actin cytoskeleton. *Journal of cell science* **124**, 679-683 (2011).
 49. Fryer, B.H. & Field, J. Rho, Rac, Pak and angiogenesis: old roles and newly identified responsibilities in endothelial cells. *Cancer letters* **229**, 13-23 (2005).
 50. Lundquist, E.A. Small GTPases. *WormBook : the online review of C. elegans biology*, 1-18 (2006).
 51. Scales, T.M. & Parsons, M. Spatial and temporal regulation of integrin signalling during cell migration. *Current opinion in cell biology* **23**, 562-568 (2011).
 52. Bader, B.L., Rayburn, H., Crowley, D. & Hynes, R.O. Extensive vasculogenesis, angiogenesis, and organogenesis precede lethality in mice lacking all α v integrins. *Cell* **95**, 507-519 (1998).
 53. Hynes, R.O., Bader, B.L. & Hodivala-Dilke, K. Integrins in vascular development. *Brazilian journal of medical and biological research* **32**, 501-510 (1999).
 54. Bouvard, D., *et al.* Functional consequences of integrin gene mutations in mice. *Circulation research* **89**, 211-223 (2001).
 55. Fässler, R. & Meyer, M. Consequences of lack of beta 1 integrin gene expression in mice. *Genes & development* **9**, 1896-1908 (1995).
 56. Stephens, L.E., *et al.* Deletion of beta 1 integrins in mice results in inner cell mass failure and peri-implantation lethality. *Genes & development* **9**, 1883-1895 (1995).
 57. Carlson, T.R., Hu, H., Braren, R., Kim, Y.H. & Wang, R.A. Cell-autonomous requirement for beta1 integrin in endothelial cell adhesion, migration and survival during angiogenesis in mice. *Development* **135**, 2193-2202 (2008).
 58. Lei, L., *et al.* Endothelial expression of beta1 integrin is required for embryonic vascular patterning and postnatal vascular remodeling. *Molecular and cellular biology* **28**, 794-802 (2008).
 59. Yamamoto, H., *et al.* Integrin beta1 controls VE-cadherin localization and blood vessel stability. *Nature communications* **6**, 6429 (2015).

Fehler! Verwenden Sie die Registerkarte 'Start', um Überschrift 1;Ü 1 dem Text zuzuweisen, der hier angezeigt werden soll.

60. Estrach, S., *et al.* Laminin-binding integrins induce Dll4 expression and Notch signaling in endothelial cells. *Circulation research* **109**, 172-182 (2011).
61. Zovein, A.C., *et al.* Beta1 integrin establishes endothelial cell polarity and arteriolar lumen formation via a Par3-dependent mechanism. *Developmental cell* **18**, 39-51 (2010).
62. van Wetering, S., *et al.* VCAM-1-mediated Rac signaling controls endothelial cell-cell contacts and leukocyte transmigration. *American Journal of Physiology-Cell Physiology* **285**, C343-C352 (2003).
63. Vockel, M. & Vestweber, D. How T cells trigger the dissociation of the endothelial receptor phosphatase VE-PTP from VE-cadherin. *Blood* **122**, 2512-2522 (2013).
64. Francis, S.E., *et al.* Central roles of $\alpha 5\beta 1$ integrin and fibronectin in vascular development in mouse embryos and embryoid bodies. *Arteriosclerosis, thrombosis, and vascular biology* **22**, 927-933 (2002).
65. van der Flier, A., *et al.* Endothelial $\alpha 5$ and $\alpha v\beta 3$ integrins cooperate in remodeling of the vasculature during development. *Development* **137**, 2439-2449 (2010).
66. Reynolds, L.E., *et al.* Enhanced pathological angiogenesis in mice lacking $\beta 3$ integrin or $\beta 3$ and $\beta 5$ integrins. *Nature medicine* **8**, 27-34 (2002).
67. Soldi, R., *et al.* Role of $\alpha v\beta 3$ integrin in the activation of vascular endothelial growth factor receptor-2. *The EMBO journal* **18**, 882-892 (1999).
68. Wickstrom, S.A., Lange, A., Montanez, E. & Fassler, R. The ILK/PINCH/parvin complex: the kinase is dead, long live the pseudokinase! *The EMBO journal* **29**, 281-291 (2010).
69. Zhang, Y., *et al.* Assembly of the PINCH-ILK-CH-ILKBP complex precedes and is essential for localization of each component to cell-matrix adhesion sites. *Journal of cell science* **115**, 4777-4786 (2002).
70. Li, F., Zhang, Y. & Wu, C. Integrin-linked kinase is localized to cell-matrix focal adhesions but not cell-cell adhesion sites and the focal adhesion localization of integrin-linked kinase is regulated by the PINCH-binding ANK repeats. *Journal of cell science* **112**, 4589-4599 (1999).
71. Yamaji, S., *et al.* A novel integrin-linked Kinase-Binding protein, affixin, is involved in the early stage of Cell-Substrate interaction. *The Journal of cell biology* **153**, 1251-1264 (2001).
72. Hannigan, G., *et al.* Regulation of cell adhesion and anchorage-dependent growth by a new. *Nature* **379**, 91-96 (1996).
73. Fukuda, T., Chen, K., Shi, X. & Wu, C. PINCH-1 is an obligate partner of integrin-linked kinase (ILK) functioning in cell shape modulation, motility, and survival. *The Journal of biological chemistry* **278**, 51324-51333 (2003).

Fehler! Verwenden Sie die Registerkarte 'Start', um Überschrift 1;Ü 1 dem Text zuzuweisen, der hier angezeigt werden soll.

74. Pasquet, J.-M., Noury, M. & Nurden, A.T. Evidence that the Platelet Integrin IIb3 Is Regulated by the Integrin-Linked Kinase, ILK, in a PI3-Kinase Dependent Pathway. *Thrombosis and haemostasis* **88**, 115-122 (2002).
75. Chiswell, B.P., Zhang, R., Murphy, J.W., Boggon, T.J. & Calderwood, D.A. The structural basis of integrin-linked kinase-PINCH interactions. *Proceedings of the National Academy of Sciences of the United States of America* **105**, 20677-20682 (2008).
76. Zhang, Y., Chen, K., Guo, L. & Wu, C. Characterization of PINCH-2, a new focal adhesion protein that regulates the PINCH-1-ILK interaction, cell spreading, and migration. *The Journal of biological chemistry* **277**, 38328-38338 (2002).
77. Hobert, O., Moerman, D.G., Clark, K.A., Beckerle, M.C. & Ruvkun, G. A conserved LIM protein that affects muscular adherens junction integrity and mechanosensory function in *Caenorhabditis elegans*. *The Journal of cell biology* **144**, 45-57 (1999).
78. Li, S., *et al.* PINCH1 regulates cell-matrix and cell-cell adhesions, cell polarity and cell survival during the peri-implantation stage. *Journal of cell science* **118**, 2913-2921 (2005).
79. Sepulveda, J.L. & Wu, C. The parvins. *Cellular and molecular life sciences : CMLS* **63**, 25-35 (2006).
80. Grashoff, C., Thievessen, I., Lorenz, K., Ussar, S. & Fassler, R. Integrin-linked kinase: integrin's mysterious partner. *Current opinion in cell biology* **16**, 565-571 (2004).
81. Wu, C. The PINCH-ILK-parvin complexes: assembly, functions and regulation. *Biochimica et biophysica acta* **1692**, 55-62 (2004).
82. Turner, C.E. Paxillin and focal adhesion signalling. *Nature cell biology* **2**, E231-E236 (2000).
83. Nikolopoulos, S.N. & Turner, C.E. Molecular dissection of actopaxin-integrin-linked kinase-Paxillin interactions and their role in subcellular localization. *The Journal of biological chemistry* **277**, 1568-1575 (2002).
84. Tsumura, Y., Toshima, J., Leeksa, O.C., Ohashi, K. & Mizuno, K. Sprouty-4 negatively regulates cell spreading by inhibiting the kinase activity of testicular protein kinase. *Biochemical Journal* **387**, 627-637 (2005).
85. LaLonde, D.P., Brown, M.C., Bouverat, B.P. & Turner, C.E. Actopaxin interacts with TESK1 to regulate cell spreading on fibronectin. *The Journal of biological chemistry* **280**, 21680-21688 (2005).
86. Yamaji, S., *et al.* Affixin interacts with alpha-actinin and mediates integrin signaling for reorganization of F-actin induced by initial cell-substrate interaction. *The Journal of cell biology* **165**, 539-551 (2004).
87. Rosenberger, G. Interaction of alphaPIX (ARHGEF6) with beta-parvin (PARVB)

Fehler! Verwenden Sie die Registerkarte 'Start', um Überschrift 1;Ü 1 dem Text zuzuweisen, der hier angezeigt werden soll.

- suggests an involvement of alphaPIX in integrin-mediated signaling. *Human Molecular Genetics* **12**, 155-167 (2003).
88. Mishima, W., *et al.* The first CH domain of affixin activates Cdc42 and Rac1 through α PIX, a Cdc42/Rac1-specific guanine nucleotide exchanging factor. *Genes to Cells* **9**, 193-204 (2004).
 89. Curtis, M., Nikolopoulos, S.N. & Turner, C.E. Actopaxin is phosphorylated during mitosis and is a substrate for cyclin B1/cdc2 kinase. *Biochemical Journal* **363**, 233-242 (2002).
 90. Clarke, D.M., Brown, M.C., LaLonde, D.P. & Turner, C.E. Phosphorylation of actopaxin regulates cell spreading and migration. *The Journal of cell biology* **166**, 901-912 (2004).
 91. Yang, Y., *et al.* Formation and phosphorylation of the PINCH-1-integrin linked kinase-alpha-parvin complex are important for regulation of renal glomerular podocyte adhesion, architecture, and survival. *Journal of the American Society of Nephrology : JASN* **16**, 1966-1976 (2005).
 92. Mackinnon, A.C., Qadota, H., Norman, K.R., Moerman, D.G. & Williams, B.D. C. elegans PAT-4/ILK functions as an adaptor protein within integrin adhesion complexes. *Current Biology* **12**, 787-797 (2002).
 93. Zervas, C.G., Gregory, S.L. & Brown, N.H. Drosophila integrin-linked kinase is required at sites of integrin adhesion to link the cytoskeleton to the plasma membrane. *The Journal of cell biology* **152**, 1007-1018 (2001).
 94. Clark, K.A., McGrail, M. & Beckerle, M.C. Analysis of PINCH function in Drosophila demonstrates its requirement in integrin-dependent cellular processes. *Development* **130**, 2611-2621 (2003).
 95. Kadrmas, J.L., *et al.* The integrin effector PINCH regulates JNK activity and epithelial migration in concert with Ras suppressor 1. *The Journal of cell biology* **167**, 1019-1024 (2004).
 96. Lin, X., Qadota, H., Moerman, D.G. & Williams, B.D. C. elegans PAT-6/actopaxin plays a critical role in the assembly of integrin adhesion complexes in vivo. *Current Biology* **13**, 922-932 (2003).
 97. Liang, X., *et al.* PINCH1 plays an essential role in early murine embryonic development but is dispensable in ventricular cardiomyocytes. *Molecular and cellular biology* **25**, 3056-3062 (2005).
 98. Braun, A., *et al.* PINCH2 is a new five LIM domain protein, homologous to PINCH and localized to focal adhesions ☆. *Experimental cell research* **284**, 237-248 (2003).
 99. Stanchi, F., *et al.* Consequences of loss of PINCH2 expression in mice. *Journal of cell science* **118**, 5899-5910 (2005).

Fehler! Verwenden Sie die Registerkarte 'Start', um Überschrift 1;Ü 1 dem Text zuzuweisen, der hier angezeigt werden soll.

100. Sakai, T., *et al.* Integrin-linked kinase (ILK) is required for polarizing the epiblast, cell adhesion, and controlling actin accumulation. *Genes & development* **17**, 926-940 (2003).
101. Montanez, E., Wickstrom, S.A., Altstatter, J., Chu, H. & Fassler, R. Alpha-parvin controls vascular mural cell recruitment to vessel wall by regulating RhoA/ROCK signalling. *The EMBO journal* **28**, 3132-3144 (2009).
102. Chu, H., *et al.* gamma-Parvin is dispensable for hematopoiesis, leukocyte trafficking, and T-cell-dependent antibody response. *Molecular and cellular biology* **26**, 1817-1825 (2006).
103. Friedrich, E.B., *et al.* Integrin-linked kinase regulates endothelial cell survival and vascular development. *Molecular and cellular biology* **24**, 8134-8144 (2004).
104. Bendig, G., *et al.* Integrin-linked kinase, a novel component of the cardiac mechanical stretch sensor, controls contractility in the zebrafish heart. *Genes & development* **20**, 2361-2372 (2006).
105. Wang, H.-V., *et al.* Integrin-linked kinase stabilizes myotendinous junctions and protects muscle from stress-induced damage. *The Journal of cell biology* **180**, 1037-1049 (2008).
106. Vespa, A., Darmon, A.J., Turner, C.E., D'Souza, S.J. & Dagnino, L. Ca²⁺-dependent localization of integrin-linked kinase to cell junctions in differentiating keratinocytes. *Journal of Biological Chemistry* **278**, 11528-11535 (2003).
107. Vespa, A., D'Souza, S.J. & Dagnino, L. A novel role for integrin-linked kinase in epithelial sheet morphogenesis. *Molecular biology of the cell* **16**, 4084-4095 (2005).
108. Fraccaroli, A., *et al.* Endothelial alpha-parvin controls integrity of developing vasculature and is required for maintenance of cell-cell junctions. *Circulation research* **117**, 29-40 (2015).
109. Giannotta, M., Trani, M. & Dejana, E. VE-cadherin and endothelial adherens junctions: active guardians of vascular integrity. *Developmental cell* **26**, 441-454 (2013).
110. Trani, M. & Dejana, E. New insights in the control of vascular permeability: vascular endothelial-cadherin and other players. *Current opinion in hematology* **22**, 267-272 (2015).
111. Wallez, Y. & Huber, P. Endothelial adherens and tight junctions in vascular homeostasis, inflammation and angiogenesis. *Biochimica et biophysica acta* **1778**, 794-809 (2008).
112. Faurobert, E., *et al.* CCM1–ICAP-1 complex controls β 1 integrin–dependent endothelial contractility and fibronectin remodeling. *The Journal of cell biology* **202**, 545-561 (2013).

Fehler! Verwenden Sie die Registerkarte 'Start', um Überschrift 1;Ü 1 dem Text zuzuweisen, der hier angezeigt werden soll.

113. Bazzoni, G. & Dejana, E. Endothelial cell-to-cell junctions: molecular organization and role in vascular homeostasis. *Physiological reviews* **84**, 869-901 (2004).
114. Dejana, E., Tournier-Lasserre, E. & Weinstein, B.M. The Control of Vascular Integrity by Endothelial Cell Junctions: Molecular Basis and Pathological Implications. *Developmental cell* **16**, 209-221 (2009).
115. Gonzalez-Mariscal, L., Tapia, R. & Chamorro, D. Crosstalk of tight junction components with signaling pathways. *Biochimica et biophysica acta* **1778**, 729-756 (2008).
116. Abu Taha, A. & Schnittler, H.-J. Dynamics between actin and the VE-cadherin/catenin complex. *Cell adhesion & migration* **8**, 125-135 (2014).
117. Huveneers, S. & de Rooij, J. Mechanosensitive systems at the cadherin-F-actin interface. *Journal of cell science* **126**, 403-413 (2013).
118. Beckers, C.M., van Hinsbergh, V.W. & van Nieuw Amerongen, G.P. Driving Rho GTPase activity in endothelial cells regulates barrier integrity. *Thrombosis & Haemostasis* **19**, 40 (2010).
119. Sidibe, A. & Imhof, B. VE-cadherin phosphorylation decides: vascular permeability or diapedesis. *Nature immunology* **15**, 215-217 (2014).
120. Lampugnani, M.G., *et al.* VE-cadherin regulates endothelial actin activating Rac and increasing membrane association of Tiam. *Molecular biology of the cell* **13**, 1175-1189 (2002).
121. Taddei, A., *et al.* Endothelial adherens junctions control tight junctions by VE-cadherin-mediated upregulation of claudin-5. *Nature cell biology* **10**, 923-934 (2008).
122. Dejana, E. Endothelial cell-cell junctions: happy together. *Nature reviews. Molecular cell biology* **5**, 261-270 (2004).
123. Pollard, T.D., Blanchoin, L. & Mullins, R.D. Molecular mechanisms controlling actin filament dynamics in nonmuscle cells. *Annual review of biophysics and biomolecular structure* **29**, 545-576 (2000).
124. Goley, E.D. & Welch, M.D. The ARP2/3 complex: an actin nucleator comes of age. *Nature reviews. Molecular cell biology* **7**, 713-726 (2006).
125. Craig, S.W. & Chen, H. Lamellipodia Protrusion: Moving Interactions of Vinculin and Arp2/3. *Current Biology* **13**, R236-R238 (2003).
126. Abu Taha, A., Taha, M., Seebach, J. & Schnittler, H.J. ARP2/3-mediated junction-associated lamellipodia control VE-cadherin-based cell junction dynamics and maintain monolayer integrity. *Molecular biology of the cell* **25**, 245-256 (2014).
127. Rajput, C., *et al.* N-WASP mediated p120-catenin interaction with Arp2-actin stabilizes endothelial adherens junctions. *Journal of Biological Chemistry*, jbc. M112.

- 440396 (2012).
128. Lampugnani, M.G., *et al.* The molecular organization of endothelial cell to cell junctions: differential association of plakoglobin, beta-catenin, and alpha-catenin with vascular endothelial cadherin (VE-cadherin). *The Journal of cell biology* **129**, 203-217 (1995).
 129. Schnittler, H., *et al.* Actin filament dynamics and endothelial cell junctions: the Ying and Yang between stabilization and motion. *Cell and tissue research* **355**, 529-543 (2014).
 130. Carmeliet, P. Angiogenesis in life, disease and medicine. *Nature* **438**, 932-936 (2005).
 131. Schmid, B., *et al.* Loss of ALS-associated TDP-43 in zebrafish causes muscle degeneration, vascular dysfunction, and reduced motor neuron axon outgrowth. *Proceedings of the National Academy of Sciences* **110**, 4986-4991 (2013).
 132. Lyden, D., *et al.* Impaired recruitment of bone-marrow-derived endothelial and hematopoietic precursor cells blocks tumor angiogenesis and growth. *Nature medicine* **7**, 1194-1201 (2001).
 133. Avraamides, C.J., Garmy-Susini, B. & Varnier, J.A. Integrins in angiogenesis and lymphangiogenesis. *Nature Reviews Cancer* **8**, 604-617 (2008).
 134. Adams, R.H. & Alitalo, K. Molecular regulation of angiogenesis and lymphangiogenesis. *Nature reviews. Molecular cell biology* **8**, 464-478 (2007).
 135. Schmid, M.C. & Varnier, J.A. Myeloid cell trafficking and tumor angiogenesis. *Cancer letters* **250**, 1-8 (2007).
 136. Lin, E.Y. & Pollard, J.W. Tumor-associated macrophages press the angiogenic switch in breast cancer. *Cancer research* **67**, 5064-5066 (2007).
 137. Targeting Critical Pathways in Oncology Co Chairs: David Gandara, MD; Carlos Arteaga, MD; Faculty: Manuel Hidalgo, MD; Roman Perez-Soler, MD; Michael Prados, MD; Roy S. Herbst, MD; Herbert Hurwitz, MD.
 138. Shibuya, M. Involvement of Flt-1 (VEGF receptor-1) in cancer and preeclampsia. *Proceedings of the Japan Academy, Series B* **87**, 167-178 (2011).
 139. Ferrara, N. & Kerbel, R.S. Angiogenesis as a therapeutic target. *Nature* **438**, 967-974 (2005).
 140. Tan, C., *et al.* Regulation of tumor angiogenesis by integrin-linked kinase (ILK). *Cancer cell* **5**, 79-90 (2004).
 141. Markovic, D., *et al.* Gliomas induce and exploit microglial MT1-MMP expression for tumor expansion. *Proceedings of the National Academy of Sciences* **106**, 12530-12535 (2009).
 142. DeAngelis, L.M. Brain tumors. *New England Journal of Medicine* **344**, 114-123 (2001).

Fehler! Verwenden Sie die Registerkarte 'Start', um Überschrift 1;Ü 1 dem Text zuzuweisen, der hier angezeigt werden soll.

143. Legler, J.M., *et al.* Brain and other central nervous system cancers: recent trends in incidence and mortality. *Journal of the National Cancer Institute* **91**, 1382-1390 (1999).
144. Group, G.M.-a.T.G. Chemotherapy in adult high-grade glioma: a systematic review and meta-analysis of individual patient data from 12 randomised trials. *The Lancet* **359**, 1011-1018 (2002).
145. Szatmári, T., *et al.* Detailed characterization of the mouse glioma 261 tumor model for experimental glioblastoma therapy. *Cancer science* **97**, 546-553 (2006).
146. Walchli, T., *et al.* Quantitative assessment of angiogenesis, perfused blood vessels and endothelial tip cells in the postnatal mouse brain. *Nat Protoc* **10**, 53-74 (2015).
147. Eichmann, A. & Thomas, J.-L. Molecular parallels between neural and vascular development. *Cold Spring Harbor perspectives in medicine* **3**, a006551 (2013).
148. Ruhrberg, C. & Bautsch, V.L. Neurovascular development and links to disease. *Cellular and molecular life sciences : CMLS* **70**, 1675-1684 (2013).
149. Walchli, T., *et al.* Wiring the Vascular Network with Neural Cues: A CNS Perspective. *Neuron* **87**, 271-296 (2015).
150. Zlokovic, B.V. The blood-brain barrier in health and chronic neurodegenerative disorders. *Neuron* **57**, 178-201 (2008).
151. Engelhardt, B. & Sorokin, L. The blood-brain and the blood-cerebrospinal fluid barriers: function and dysfunction. *Seminars in immunopathology* **31**, 497-511 (2009).
152. Obermeier, B., Daneman, R. & Ransohoff, R.M. Development, maintenance and disruption of the blood-brain barrier. *Nature medicine* **19**, 1584-1596 (2013).
153. Winkler, E.A., *et al.* Blood–spinal cord barrier breakdown and pericyte reductions in amyotrophic lateral sclerosis. *Acta neuropathologica* **125**, 111-120 (2013).
154. Broeck, L.V., Callaerts, P. & Dermaut, B. TDP-43-mediated neurodegeneration: towards a loss-of-function hypothesis? *Trends in molecular medicine* **20**, 66-71 (2014).
155. Janssens, J. & Van Broeckhoven, C. Pathological mechanisms underlying TDP-43 driven neurodegeneration in FTLD–ALS spectrum disorders. *Human Molecular Genetics* **22**, R77-R87 (2013).
156. Chiang, P.-M., *et al.* Deletion of TDP-43 down-regulates Tbc1d1, a gene linked to obesity, and alters body fat metabolism. *Proceedings of the National Academy of Sciences* **107**, 16320-16324 (2010).
157. Ayala, Y.M., *et al.* TDP-43 regulates its mRNA levels through a negative feedback loop. *The EMBO journal* **30**, 277-288 (2011).

Fehler! Verwenden Sie die Registerkarte 'Start', um Überschrift 1;Ü 1 dem Text zuzuweisen, der hier angezeigt werden soll.

158. Avendano-Vazquez, S.E., *et al.* Autoregulation of TDP-43 mRNA levels involves interplay between transcription, splicing, and alternative polyA site selection. *Genes & development* **26**, 1679-1684 (2012).
159. Kabashi, E., *et al.* TARDBP mutations in individuals with sporadic and familial amyotrophic lateral sclerosis. *Nature genetics* **40**, 572-574 (2008).
160. Lambrechts, D., *et al.* VEGF is a modifier of amyotrophic lateral sclerosis in mice and humans and protects motoneurons against ischemic death. *Nature genetics* **34**, 383-394 (2003).
161. Kisanuki, Y.Y., *et al.* Tie2-Cre transgenic mice: a new model for endothelial cell-lineage analysis in vivo. *Dev Biol* **230**, 230-242 (2001).
162. Wang, Y., *et al.* Ephrin-B2 controls VEGF-induced angiogenesis and lymphangiogenesis. *Nature* **465**, 483-486 (2010).
163. Tata, M., Ruhrberg, C. & Fantin, A. Vascularisation of the central nervous system. *Mechanisms of development* **138 Pt 1**, 26-36 (2015).
164. Fantin, A., Vieira, J.M., Plein, A., Maden, C.H. & Ruhrberg, C. The embryonic mouse hindbrain as a qualitative and quantitative model for studying the molecular and cellular mechanisms of angiogenesis. *Nature Protocols* **8**, 418-429 (2013).
165. Mancuso, M.R., Kuhnert, F. & Kuo, C.J. Developmental angiogenesis of the central nervous system. *Lymphatic research and biology* **6**, 173-180 (2008).
166. Fruttiger, M. Development of the retinal vasculature. *Angiogenesis* **10**, 77-88 (2007).
167. Stahl, A., *et al.* The mouse retina as an angiogenesis model. *Investigative ophthalmology & visual science* **51**, 2813-2826 (2010).
168. Holzgreve, A., *et al.* Monitoring of Tumor Growth with [18F]-FET PET in a Mouse Model of Glioblastoma: SUV Measurements and Volumetric Approaches. *Frontiers in Neuroscience* **10**, 260 (2016).
169. Staley, J., *et al.* Growth of melanoma brain tumors monitored by photoacoustic microscopy. *Journal of biomedical optics* **15**, 040510-040510-040513 (2010).
170. Pitulescu, M.E., Schmidt, I., Benedito, R. & Adams, R.H. Inducible gene targeting in the neonatal vasculature and analysis of retinal angiogenesis in mice. *Nat Protoc* **5**, 1518-1534 (2010).
171. Ridley, A.J., *et al.* Cell migration: integrating signals from front to back. *Science* **302**, 1704-1709 (2003).
172. Zaidel-Bar, R., Milo, R., Kam, Z. & Geiger, B. A paxillin tyrosine phosphorylation switch regulates the assembly and form of cell-matrix adhesions. *Journal of cell science* **120**, 137-148 (2007).
173. Small, J.V., Stradal, T., Vignat, E. & Rottner, K. The lamellipodium: where motility

Fehler! Verwenden Sie die Registerkarte 'Start', um Überschrift 1;Ü 1 dem Text zuzuweisen, der hier angezeigt werden soll.

- begins. *Trends in cell biology* **12**, 112-120 (2002).
174. Mitra P, K.C., Giaver I. Electric measurements can be used to monitor the attachment and spreading of cells in tissue culture. *Biotechniques* **11**, 504-510 (1991).
175. Cavey, M. & Lecuit, T. Molecular bases of cell-cell junctions stability and dynamics. *Cold Spring Harbor perspectives in biology* **1**, a002998 (2009).
176. Riedl, J., *et al.* Lifeact: a versatile marker to visualize F-actin. *Nature methods* **5**, 605-607 (2008).
177. Bentley, K., *et al.* The role of differential VE-cadherin dynamics in cell rearrangement during angiogenesis. *Nature cell biology* **16**, 309-321 (2014).
178. Tanjore, H., Zeisberg, E.M., Gerami-Naini, B. & Kalluri, R. Beta1 integrin expression on endothelial cells is required for angiogenesis but not for vasculogenesis. *Developmental dynamics : an official publication of the American Association of Anatomists* **237**, 75-82 (2008).
179. Di Russo, J., *et al.* Endothelial basement membrane laminin 511 is essential for shear stress response. *The EMBO journal*, e201694756 (2016).
180. Wang, Y., *et al.* Integrins regulate VE-cadherin and catenins: dependence of this regulation on Src, but not on Ras. *Proceedings of the National Academy of Sciences of the United States of America* **103**, 1774-1779 (2006).
181. Su, G., *et al.* Absence of integrin α v β 3 enhances vascular leak in mice by inhibiting endothelial cortical actin formation. *American journal of respiratory and critical care medicine* **185**, 58-66 (2012).
182. van Geemen, D., *et al.* F-Actin–anchored focal adhesions distinguish endothelial phenotypes of human arteries and veins. *Arteriosclerosis, thrombosis, and vascular biology* **34**, 2059-2067 (2014).
183. Geyer, H., Geyer, R., Odenthal-Schnittler, M. & Schnittler, H.-J. Characterization of human vascular endothelial cadherin glycans. *Glycobiology* **9**, 915-925 (1999).
184. Breslin, J.W., Zhang, X.E., Worthylake, R.A. & Souza-Smith, F.M. Involvement of local lamellipodia in endothelial barrier function. *PLoS one* **10**, e0117970 (2015).
185. Huvneers, S., *et al.* Vinculin associates with endothelial VE-cadherin junctions to control force-dependent remodeling. *The Journal of cell biology* **196**, 641-652 (2012).
186. DeMali, K.A., Barlow, C.A. & Burridge, K. Recruitment of the Arp2/3 complex to vinculin: coupling membrane protrusion to matrix adhesion. *The Journal of cell biology* **159**, 881-891 (2002).
187. Malan, D., *et al.* Endothelial beta1 integrins regulate sprouting and network formation during vascular development. *Development* **137**, 993-1002 (2010).
188. Raimondi, C., *et al.* Imatinib inhibits VEGF-independent angiogenesis by targeting

Fehler! Verwenden Sie die Registerkarte 'Start', um Überschrift 1;Ü 1 dem Text zuzuweisen, der hier angezeigt werden soll.

- neuropilin 1-dependent ABL1 activation in endothelial cells. *The Journal of experimental medicine* **211**, 1167-1183 (2014).
189. Karaköse, E., *et al.* The focal adhesion protein PINCH-1 associates with EPLIN at integrin adhesion sites. *Journal of cell science* **128**, 1023-1033 (2015).
190. Zhang, Y., Chen, K., Tu, Y. & Wu, C. Distinct roles of two structurally closely related focal adhesion proteins, alpha-parvins and beta-parvins, in regulation of cell morphology and survival. *The Journal of biological chemistry* **279**, 41695-41705 (2004).
191. Armulik, A., *et al.* Pericytes regulate the blood-brain barrier. *Nature* **468**, 557-561 (2010).
192. Siegenthaler, J.A., Sohet, F. & Daneman, R. 'Sealing off the CNS': Cellular and molecular regulation of blood-brain barrierogenesis. *Current opinion in neurobiology* **23**, 1057-1064 (2013).
193. Phng, L.K., *et al.* Nrarp coordinates endothelial Notch and Wnt signaling to control vessel density in angiogenesis. *Developmental cell* **16**, 70-82 (2009).
194. Lange, C., *et al.* Relief of hypoxia by angiogenesis promotes neural stem cell differentiation by targeting glycolysis. *The EMBO journal* **35**, 924-941 (2016).
195. Dermietzel, R., Krause, D., Kremer, M., Wang, C. & Stevenson, B. Pattern of glucose transporter (Glut 1) expression in embryonic brains is related to maturation of blood-brain barrier tightness. *Developmental dynamics* **193**, 152-163 (1992).
196. Pugh, C.W. & Ratcliffe, P.J. Regulation of angiogenesis by hypoxia: role of the HIF system. *Nature medicine* **9**, 677-684 (2003).
197. Shi, X. Cochlear pericyte responses to acoustic trauma and the involvement of hypoxia-inducible factor-1 α and vascular endothelial growth factor. *The American journal of pathology* **174**, 1692-1704 (2009).
198. Daneman, R., *et al.* Wnt/ β -catenin signaling is required for CNS, but not non-CNS, angiogenesis. *Proceedings of the National Academy of Sciences* **106**, 641-646 (2009).
199. Tan, C., *et al.* Inhibition of integrin linked kinase (ILK) suppresses [beta]-catenin-Lef/Tcf-dependent transcription and expression of the E-cadherin repressor, snail, in APC-/-human colon carcinoma cells. *Oncogene* **20**, 133 (2001).
200. Corada, M., *et al.* The Wnt/beta-catenin pathway modulates vascular remodeling and specification by upregulating Dll4/Notch signaling. *Developmental cell* **18**, 938-949 (2010).
201. Zhou, Y., *et al.* Canonical WNT signaling components in vascular development and barrier formation. *The Journal of clinical investigation* **124**, 3825-3846 (2014).
202. Ma, S., Kwon, H.J., Johng, H., Zang, K. & Huang, Z. Radial glial neural progenitors

Fehler! Verwenden Sie die Registerkarte 'Start', um Überschrift 1;Ü 1 dem Text zuzuweisen, der hier angezeigt werden soll.

- regulate nascent brain vascular network stabilization via inhibition of Wnt signaling. *PLoS biology* **11**, e1001469 (2013).
203. McCarty, J.H. Integrin-mediated regulation of neurovascular development, physiology and disease. *Cell adhesion & migration* **3**, 211-215 (2009).
204. Leblanc, G.G., Golanov, E., Awad, I.A. & Young, W.L. Biology of vascular malformations of the brain. *Stroke* **40**, e694-e702 (2009).
205. Riant, F., Bergametti, F., Ayrignac, X., Boulday, G. & Tournier-Lasserre, E. Recent insights into cerebral cavernous malformations: the molecular genetics of CCM. *FEBS journal* **277**, 1070-1075 (2010).
206. Fischer, A., Zalvide, J., Faurobert, E., Albiges-Rizo, C. & Tournier-Lasserre, E. Cerebral cavernous malformations: from CCM genes to endothelial cell homeostasis. *Trends in molecular medicine* **19**, 302-308 (2013).
207. Draheim, K.M., Fisher, O.S., Boggon, T.J. & Calderwood, D.A. Cerebral cavernous malformation proteins at a glance. (The Company of Biologists Ltd, 2014).
208. Storkebaum, E., Quaegebeur, A., Vikkula, M. & Carmeliet, P. Cerebrovascular disorders: molecular insights and therapeutic opportunities. *Nature neuroscience* **14**, 1390-1397 (2011).
209. Jilkova, Z.M., *et al.* CCM proteins control endothelial β 1 integrin dependent response to shear stress. *Biology open* **3**, 1228-1235 (2014).
210. Faurobert, E. & Albiges-Rizo, C. Recent insights into cerebral cavernous malformations: a complex jigsaw puzzle under construction. *FEBS journal* **277**, 1084-1096 (2010).
211. Boulday, G., *et al.* Developmental timing of CCM2 loss influences cerebral cavernous malformations in mice. *Journal of Experimental Medicine*, jem. 20110571 (2011).
212. Hirota, S., *et al.* Neuropilin 1 balances β 8 integrin-activated TGF β signaling to control sprouting angiogenesis in the brain. *Development* **142**, 4363-4373 (2015).
213. Oosthuysen, B., *et al.* Deletion of the hypoxia-response element in the vascular endothelial growth factor promoter causes motor neuron degeneration. *Nature genetics* **28**, 131-138 (2001).

6 Index of figures and tables

List of figures

Figure 1. Schematic Steps of vessel formation.....	2
Figure 2. Integrin family in mammals.....	4
Figure 3. Overview of integrin-mediated cell-ECM adhesion structures and actin cytoskeleton organization in a migrating cell.	6
Figure 4. Regulation of GTPases activity..	7
Figure 5. Schematic composition of the IPP-complex.....	8
Figure 6. Recruitment of the IPP complex to FAs.....	9
Figure 7. Structural features of (A) α -pv and (B) β -pv and their binding sites.....	10
Figure 8. Impact of gene deletions of the integrin signaling cascade on embryonic lethality in mice.	12
Figure 9. Architecture of AJs in ECs..	15
Figure 10. Schematic illustration of JAIL formation at EC junctions under subconfluent conditions.	16
Figure 11. Angiogenesis in tumor growth.	17
Figure 12. Organization of the NVU.	19
Figure 13. TDP-43 and ALS.....	20

Fehler! Verwenden Sie die Registerkarte 'Start', um Überschrift 1;Ü 1 dem Text zuzuweisen, der hier angezeigt werden soll.

Figure 14. TDP-43 KO phenotypes in zebrafish embryos.....	21
Figure 15. Schematic development of the embryonic mouse hindbrain vascularization.....	33
Figure 16. Development of the retinal vasculature..	34
Figure 17. Inoculation site of glioma cells in the mouse brain.....	35
Figure 18. Deletion of endothelial α -pv is embryonically lethal.	51
Figure 19. Loss of endothelial α -pv leads to hemorrhages and late embryonic lethality.....	52
Figure 20. Abnormal vessel morphology in α -pv ^{ΔEC} tissues.	53
Figure 21. Normal mural cell recruitment to the vessel wall in α -pv ^{ΔEC} embryos.	54
Figure 22. Impaired junction morphology in α -pv ^{ΔEC} YS vasculature.....	55
Figure 23. Subcellular localization of α -pv in HUVECs.....	56
Figure 24. Localization of α -pv in subconfluent conditions..	57
Figure 25. Deletion of α -pv in HUVECs with siRNAs.....	58
Figure 26. Pax phosphorylation is reduced in the absence of α -pv.	59
Figure 27. Rac1 activity and cell motility is decreased in α -pv deficiency.	60
Figure 28. α -pv depleted HUVECs show altered junction formation.....	63
Figure 29. Lifeact-GFP transfected HUVECs are analyzed for JAIL formation.....	64
Figure 30. Embryonic lethality and impaired vasculature of α -pv ^{ΔEC} ; β -pv ^{-/-} embryos.....	66
Figure 31. The embryonic hindbrain of α -pv ^{fl/fl} ; β -pv ^{+/+} , α -pv ^{fl/fl} ; β -pv ^{-/-} , α -pv ^{ΔEC} ; β -pv ^{+/+} , and α -pv ^{ΔEC} ; β -pv ^{-/-}	68
Figure 32. Micro aneurisms in α -pv ^{ΔEC} ; β -pv ^{-/-} embryos at E11.5.	69
Figure 33. Reduced spinal cord vascularization in α -pv ^{ΔEC} ; β -pv ^{-/-} embryos at E11.5.....	71

Fehler! Verwenden Sie die Registerkarte 'Start', um Überschrift 1;Ü 1 dem Text zuzuweisen, der hier angezeigt werden soll.

Figure 34. Bleedings in α -pv ^{ΔEC} β -pv ^{-/-} embryos.	72
Figure 35. Altered PE attachment to the vessel walls in α -pv ^{ΔEC} ; β -pv ^{-/-} hindbrains.	73
Figure 36. Altered Glut-1 expression in the vasculature of α -pv ^{ΔEC} ; β -pv ^{-/-} compared to α -pv ^{fl/fl} ; β -pv ^{-/-} hindbrains.	74
Figure 37. Similar BM/ECM components at vessels in α -pv ^{ΔEC} ; β -pv ^{-/-} and α -pv ^{fl/fl} ; β -pv ^{-/-} hindbrains.....	75
Figure 38: Impaired EC polarity and BM integrity in α -pv ^{ΔEC} ; β -pv ^{-/-} vessels.	76
Figure 39. Cell shapes in paraffin section and isolated ECs from E11.5 embryos.....	78
Figure 40. α -pv depletion in ECs reduces tumor growth and vascularization in α -pv ^{iΔEC} mice.	79
Figure 41. Endothelial-specific deletion of TDP-43 leads to vascular defects in retinal vasculature.	81
Figure 42. Loss of endothelial TDP-43 results in hyper-sprouting and increased number of filopodia.....	82
Figure 43. Ectopic expression of tip cell marker and VEcad in TDP-43 ^{iΔEC} retinas.	83
Figure 44. TDP-43 ^{iΔEC} retinas do not show increased EC proliferation.....	84
Figure 45. Altered apical/basal orientation in TDP-43 ^{iΔEC} retinal vasculature.	84
Figure 46. Comparison of the different outcomes of parvin depletions..	89

7 List of Abbreviations

AJ	adherens junction
AD	Alzheimer's disease
ALS	Amyotrophic lateral sclerosis
ALS-FTLD	clinical presentation with similarly strong signs of ALS and FTLD
APS	ammonium persulfate
Arp2/3	actin-related protein-2/3
BBB	blood brain barrier
BCA	bicinchoninic acid assay
β -cat	β -catenin
BM	basal membrane
bp	base pair
BRP	blood retina barrier
BSA	bovine serum albumin
CCM	cerebral cavernous malformation
CH	calponin homology
Cre	cre recombinase
Col-IV	collagen IV
CNS	central nervous system
DII	delta-like
DZNE	Deutsches Zentrum für neurodegenerative Erkrankungen
DMEM	dulbecco's modified eagle's medium
DMSO	dimethyl sulfoxide
DNA	deoxyribonucleic acid

Fehler! Verwenden Sie die Registerkarte 'Start', um Überschrift 1;Ü 1 dem Text zuzuweisen, der hier angezeigt werden soll.

dNTP	deoxynucleotide triphosphate
E	embryonic day
EB	embryoid bodies
EC	endothelial cell
ECGM	endothelial cell growth medium
ECM	extracellular matrix
EDTA	ethylenediaminetetraacetic acid
ESM1	EC-specific molecule 1
EZ	Endothelzellen
EZM	Extrazelluläre Matrix
FA	focal adhesion
FCS	fetal calf serum
Flox	loxP-flanked
FN	fibronectin
FX	focal complex
GAP	GTPase-activating protein
GAPDH	glyceraldehyd-3-phosphat-Dehydrogenase
GEF	guanine exchange factor
GFP	green fluorescent protein
GRR	glycine-rich C-terminal region
H&E stain	hematoxylin and eosin stain
HUVEC	human umbilical vein endothelial cell
ICAM-1	intercellular adhesion molecule-1
ILK	integrin linked kinase
IPP	integrin PINCH parvin
JAIL	junction associated intermitted lamellipodia
kDa	kilo-Dalton
MMP	matrix metalloproteinase
MT1-MMP	membrane type 1 MMP
mRNA	messenger ribonucleic acid
MS	Multiple Sclerosis
NICD	Notch intracellular domain

Fehler! Verwenden Sie die Registerkarte 'Start', um Überschrift 1;Ü 1 dem Text zuzuweisen, der hier angezeigt werden soll.

NLS	nuclear localization site
NVU	neurovascular unit
ON	overnight
P	postnatal day
Pax	Paxillin
PBS	phosphate buffered saline
PCR	polymerase Chain Reaction
PDGF	platelet derived growth factor
PE	perycyte
PFA	paraformaldehyde
PINCH	particularly interesting Cys-His-rich protein
PNVP	perineural vascular plexus
PODXL	podocalyxin
pv	parvin
RNA	ribonucleic acid
ROCK	Rho-kinase
RRM	RNA recognition motif
RT	room temperature
RTK	receptor tyrosin kinase
SDS	sodium dodecyl sulfate
SDS-Page	sodium dodecyl sulfate-polyacrylamide gel electrophoresis
SEM	standard error of the mean
siRNA	small interfering RNA
SMA	smooth muscle actin
SRF	serum response factor
SVP	subventricular vascular plexus
TAE buffer	tris-acetic acid-EDTA buffer
TARDBP	TAR DNA-binding protein (human gene name)
<i>Tardbp</i>	TAR DNA-binding protein (zebrafish orthologue)
<i>Tardbpl</i>	TAR DNA-binding protein like (zebrafish orthologue)
TBST	tris-buffered saline with Tween
TDP-43	TAR DNA-binding protein of 43kDa

Fehler! Verwenden Sie die Registerkarte 'Start', um Überschrift 1;Ü 1 dem Text zuzuweisen, der hier angezeigt werden soll.

(protein name used here for human and zebrafish proteins)

TE buffer	tris-EDTA buffer
TEER	transendothelial electric resistance
TEMED	tetramethylethylenediamine
UV	ultra violet
VE-cadherin	vascular endothelial-cadherin
VEGF	vascular endothelial growth factor
VEGFR	vascular endothelial growth factor receptor
Vinc	Vinculin
vSMC	vascular smooth muscle cells
YS	yolk sac

8 Publications

Endothelial alpha-parvin controls integrity of developing vasculature and is required for maintenance of cell-cell junctions. Fraccaroli A*, **Pitter B***, Taha AA, Seebach J, Huveneers S, Kirsch J, Casaroli-Marano RP, Zahler S, Pohl U, Gerhardt H, Schnittler HJ, Montanez E. *Circ Res.* 2015 Jun 19;117(1):29-40. doi: 10.1161/CIRCRESAHA.117.305818. Epub 2015 Apr 29. PMID: 25925587, (* equal contribution)

VEGF-A/Notch-Induced Podosomes Proteolyse Basement Membrane Collagen-IV during Retinal Sprouting Angiogenesis. Spuul P, Daubon T, **Pitter B**, Alonso F, Fremaux I, Kramer I, Montanez E, Génot E. *Cell Rep.* 2016 Oct 4;17(2):484-500. doi: 10.1016/j.celrep.2016.09.016. PMID: 27705796

F-actin-rich contractile endothelial pores prevent vascular leakage during leukocyte diapedesis through local RhoA signalling. Heemskerk N, Schimmel L, Oort C, van Rijssel J, Yin T, Ma B, van Unen J, **Pitter B**, Huveneers S, Goedhart J, Wu Y, Montanez E, Woodfin A, van Buul JD. *Nat Commun.* 2016 Jan 27;7:10493. doi: 10.1038/ncomms10493. PMID: 26814335

Prevalence of Lymphatic Filariasis and Treatment Effectiveness of Albendazole/ Ivermectin in Individuals with HIV Co-infection in Southwest-Tanzania. Kroidl I, Saathof E, Maganga L, Clowes P, Maboko L, Hoerauf A, Makunde WH, Haule A, Mviombo P, **Pitter B**, Mgeni N, Mabuye J, Kowuor D, Mwingira U, Malecela MN, Löscher T, Hoelscher M. *PLoS Negl Trop Dis.* 2016 Apr 12;10(4):e0004618. doi: 10.1371/journal.pntd.0004618. eCollection 2016 Apr. PMID: 27070786

9 Danksagung

Viele Menschen haben zu dieser Doktorarbeit maßgeblich beigetragen. Allen voran steht hier mein Betreuer und direkter Chef Dr. Eloi Montanez, der mich die ganze Zeit über hervorragend betreut und gefördert hat, und immer für meine Fragen und für fachliche Diskussionen Zeit hatte. Ein herzlicher Dank geht auch an Herrn Prof. Dr. Pohl, meinen Doktorvater. Er hat mir eine angenehme Arbeitsumgebung ermöglicht und mir sehr freie Hand bei der Arbeit gelassen, und mir dennoch bei Bedarf stets fachliche Ratschläge und Unterstützung geboten.

Des Weiteren möchte ich hier die gute Zusammenarbeit im Labor mit allen Doktoranden, PIs, TAs und Tierpflegern erwähnen. Sie alle haben viel zum erfolgreichen Arbeiten beigetragen. Weiter bedanke ich mich bei meiner Arbeitsgruppe, die mir stets Zeit und Spontaneität entgegengebracht hat und somit eine große Unterstützung für mich war. Hier möchte ich Ann-Cathrin Werner, Brigitte Bergner, Miriam Singer, Alessia Fraccaroli und Matthias Semisch nennen.

Nicht nur die großartige Mithilfe in der Arbeit, sondern auch Unterstützung, Beistand und viel Verständnis habe ich von meinen Freunden, Familie und Eltern erfahren. Vielen Dank auch an meinen Mann Peter.

Ihnen allen ein herzliches Dankeschön.